



Alert Geomaterials



Advanced multiphysics of geomaterials: multiscale approaches and heterogeneities

ALERT OZ / EURAD GAS & HITEC Summer School
28 August – 01 September 2023 • Liège (Belgium)

Pierre BÉSUELLE, Frédéric COLLIN,
Anne-Catherine DIEUDONNÉ, Sebastia OLIVELLA



The project leading to this application has received funding from the European Union's Horizon 2020 research and innovation programme under grant agreement n° 847593.



Alert Geomaterials



Advanced multiphysics of geomaterials: Multiscale modelling of gas flow

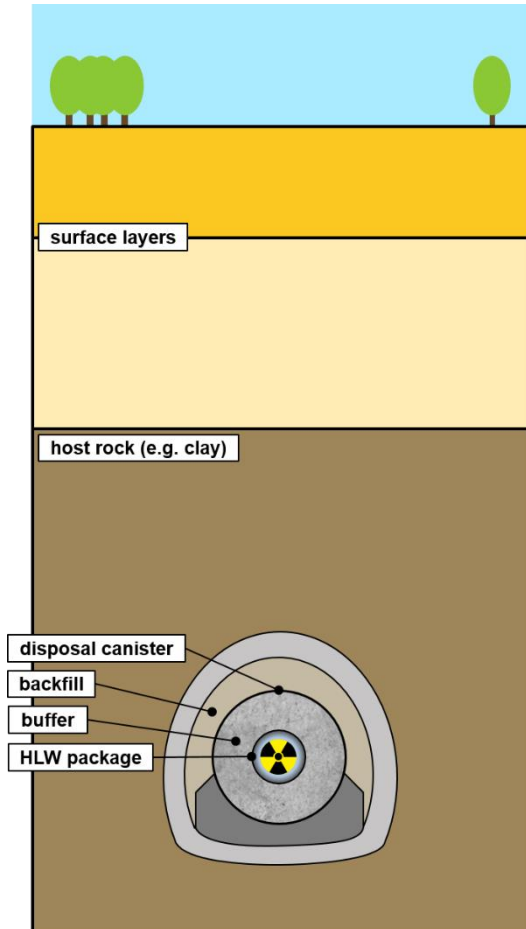
ALERT OZ / EURAD GAS & HITEC Summer School
28 August – 01 September 2023 • Liège (Belgium)

Gilles Corman, Frédéric COLLIN



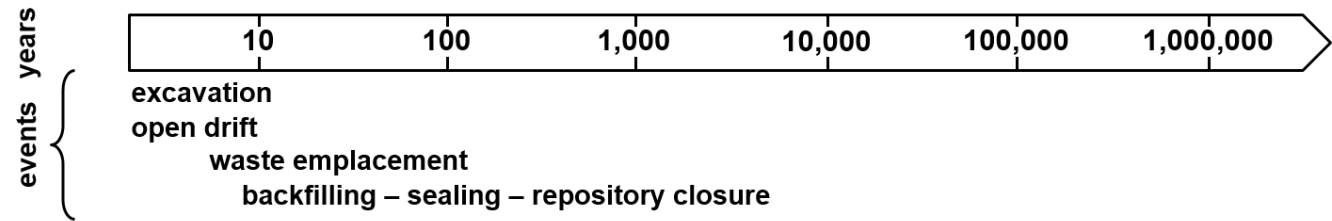
The project leading to this application has received funding from the European Union's Horizon 2020 research and innovation programme under grant agreement n° 847593.

Context

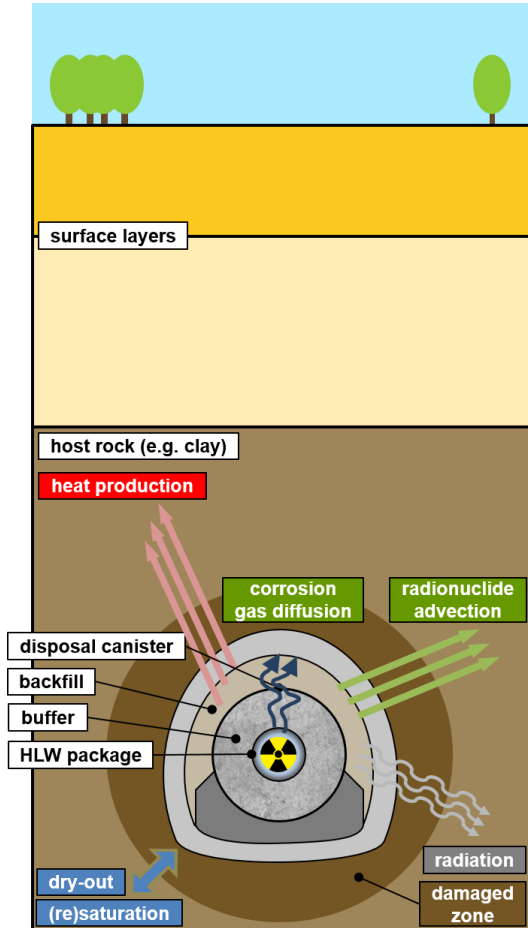


Conceptual scheme of a deep geological repository.

Geological disposal of radioactive wastes



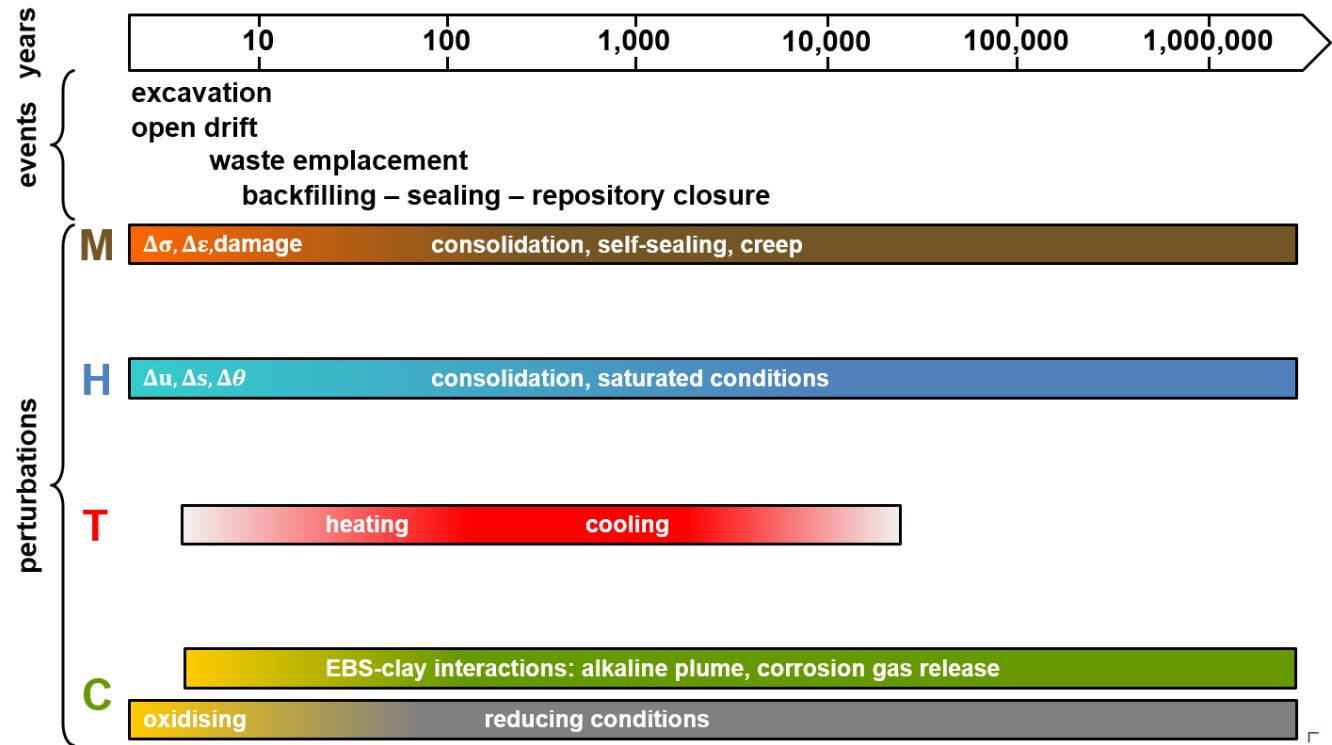
Context



Conceptual scheme of a deep geological repository.

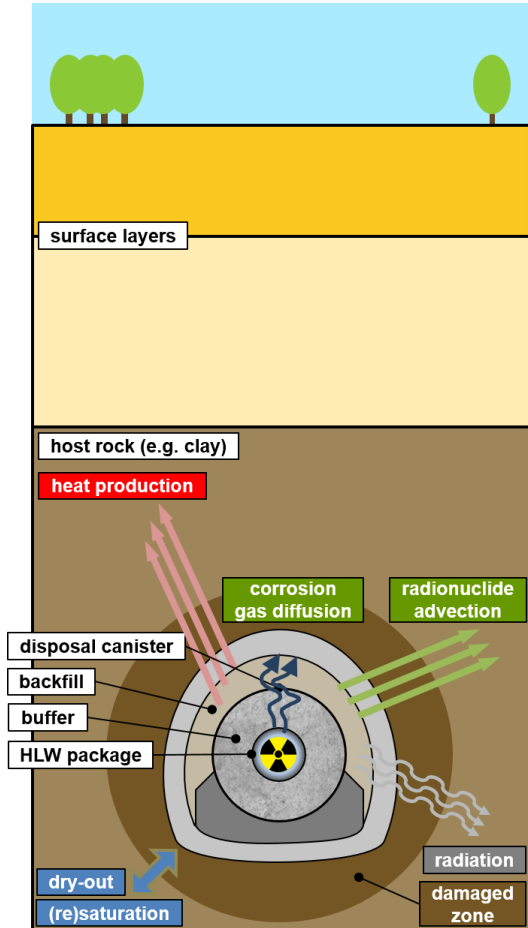
Geological disposal of radioactive wastes

- ▶ Complex multi-physical (THMC) processes



Major perturbations of the host rock over the lifetime of a geological repository, adapted from *Sillen (2012)*.

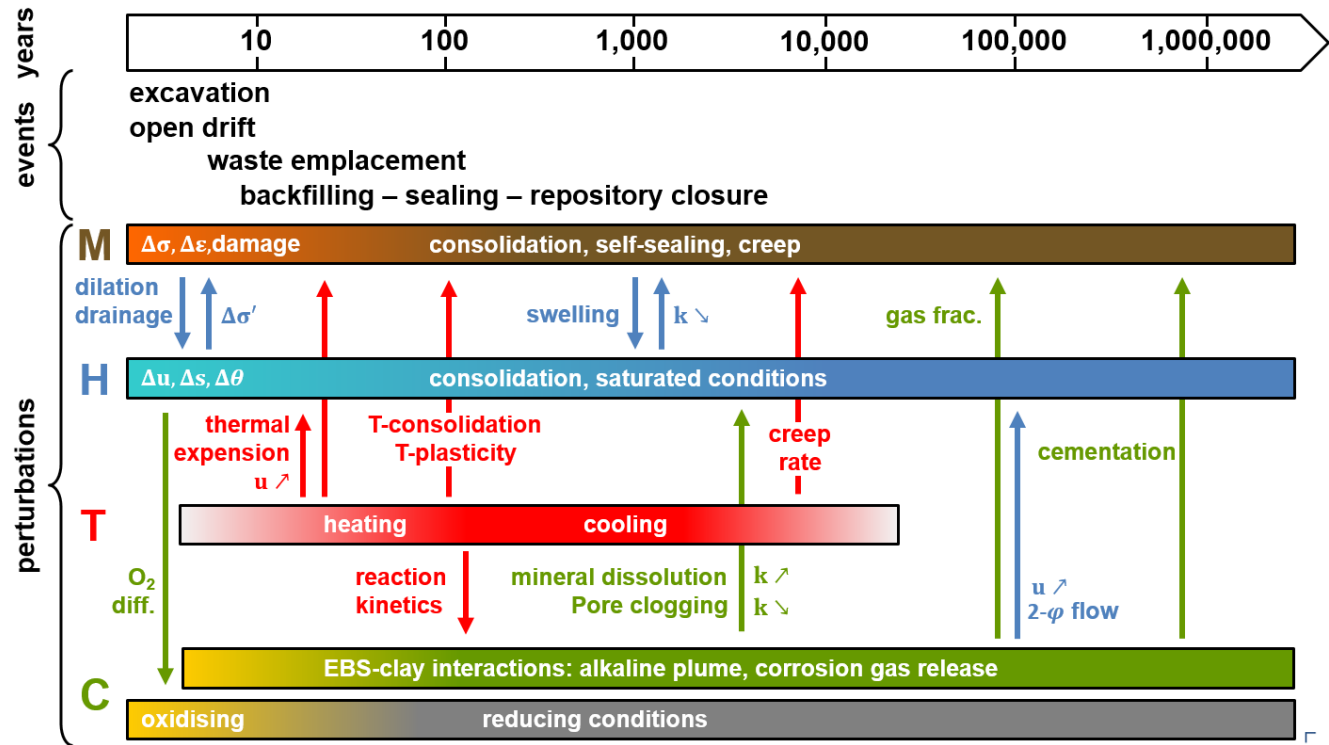
Context



Conceptual scheme of a deep geological repository.

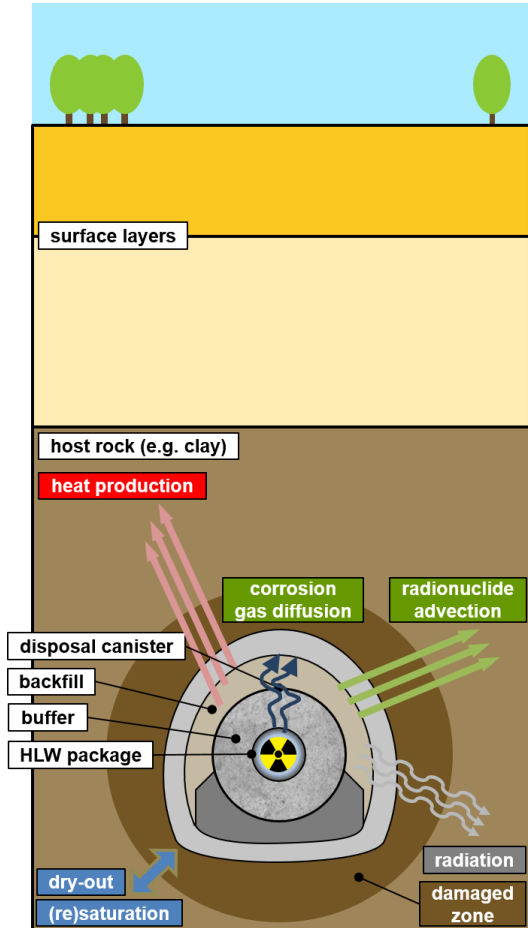
Geological disposal of radioactive wastes

- ▶ Complex multi-physical (THMC) processes
- ▶ Interactions between processes



Major perturbations of the host rock over the lifetime of a geological repository, adapted from *Sillen (2012)*.

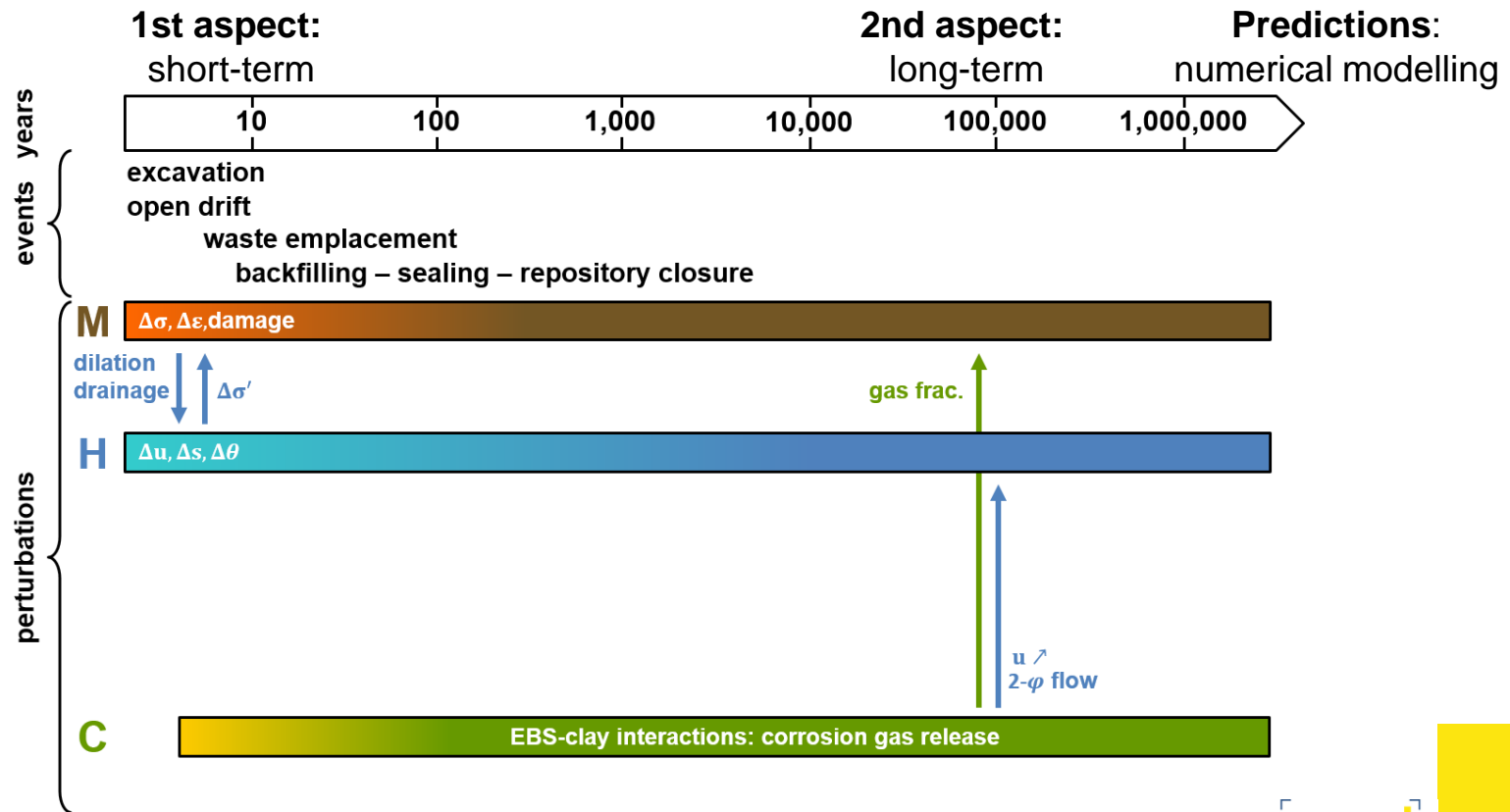
Context



Conceptual scheme of a deep geological repository.

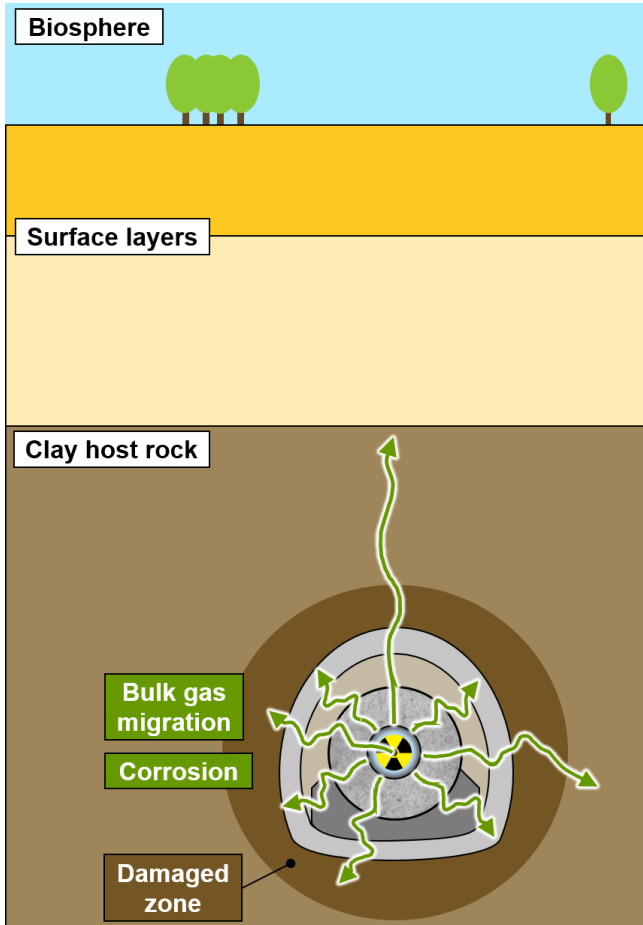
Geological disposal of radioactive wastes

- ▶ Complex multi-physical (THMC) processes
- ▶ Interactions between processes



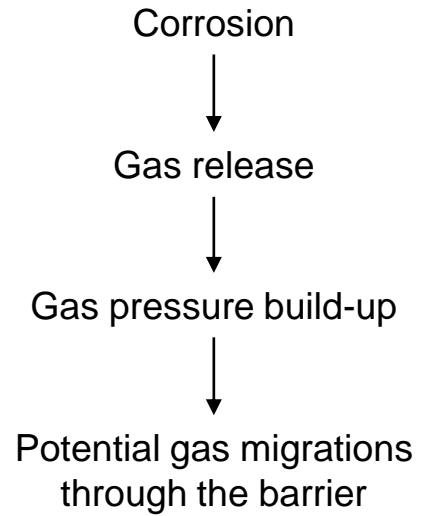
Major perturbations of the host rock over the lifetime of a geological repository, adapted from *Sillen (2012)*.

Context

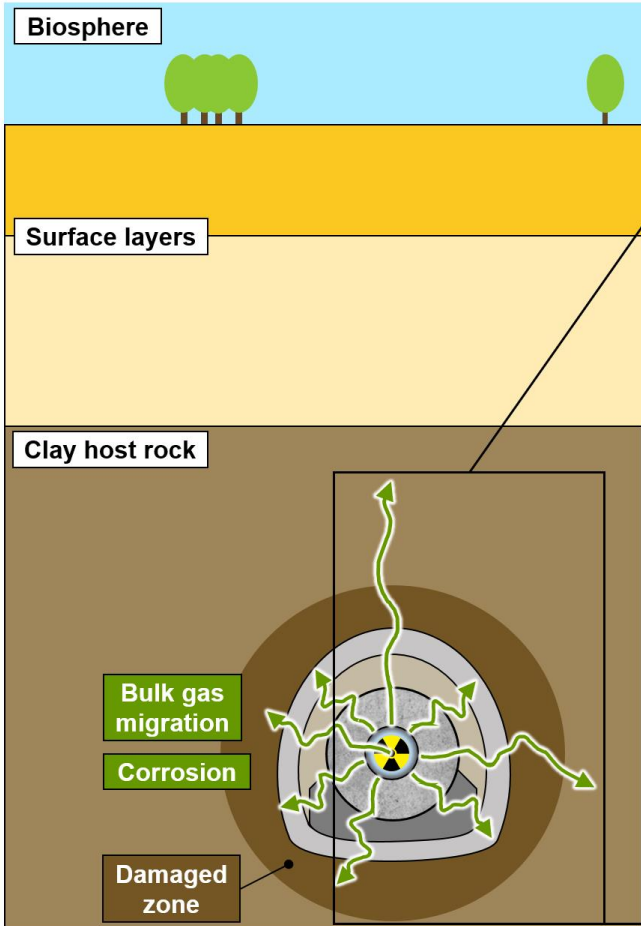


Conceptual scheme of a deep geological repository focussing on the gas generation process.

Gas migration issue

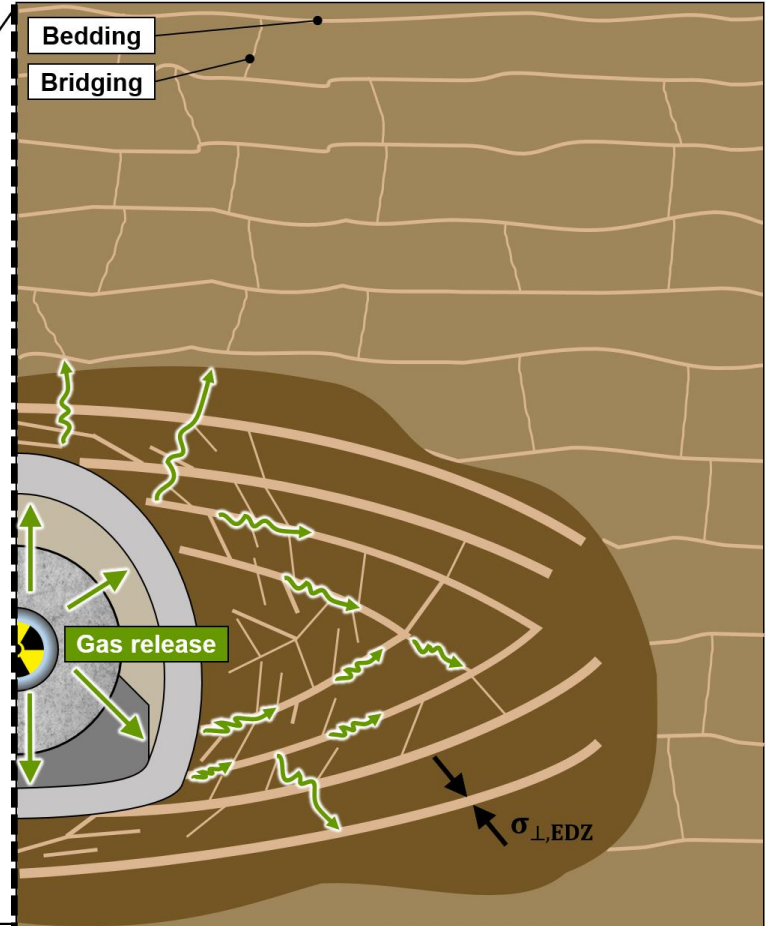


Context



Conceptual scheme of a deep geological repository focussing on the gas generation process.

Gas migration issue

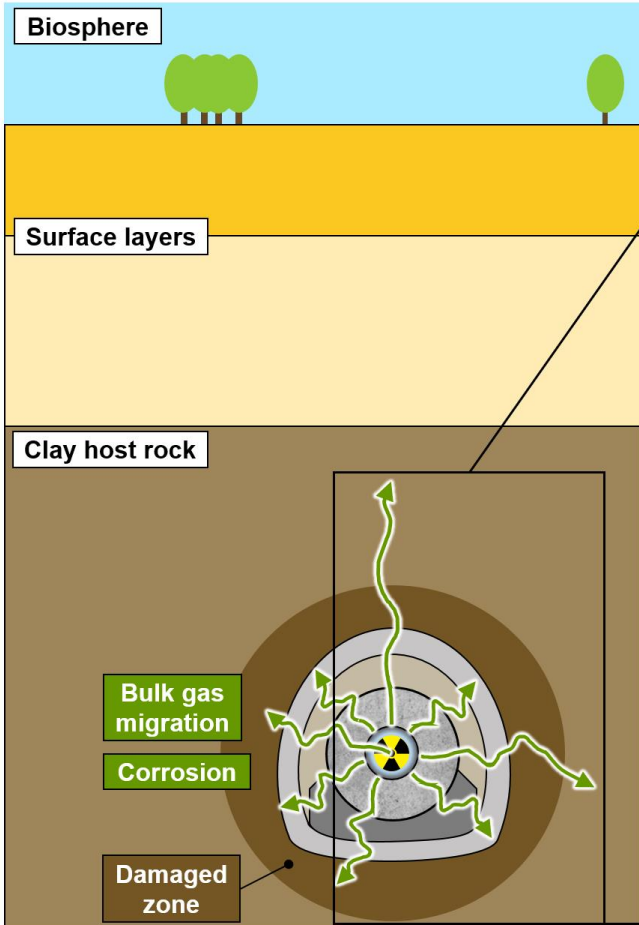


Expected gas transport modes in the EDZ and the sound rock, from ONDRAF/NIRAS (2016).

Excavation damaged zone (EDZ)

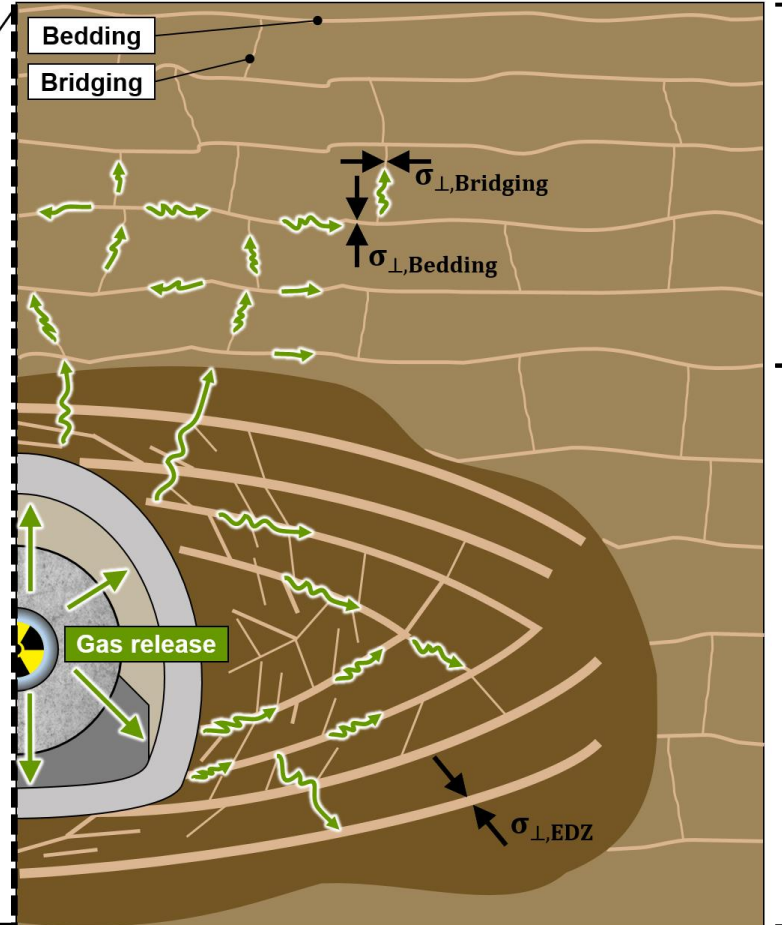
- Governed by the hydraulic properties modifications induced by fracturation

Context



Conceptual scheme of a deep geological repository focussing on the gas generation process.

Gas migration issue



Expected gas transport modes in the EDZ and the sound rock, from ONDRAF/NIRAS (2016).

Sound rock layers

- ▶ Governed by the rock structure at a micro-level
- ▶ Multi-Scale Model

Excavation damaged zone (EDZ)

- ▶ Governed by the hydraulic properties modifications induced by fracturation

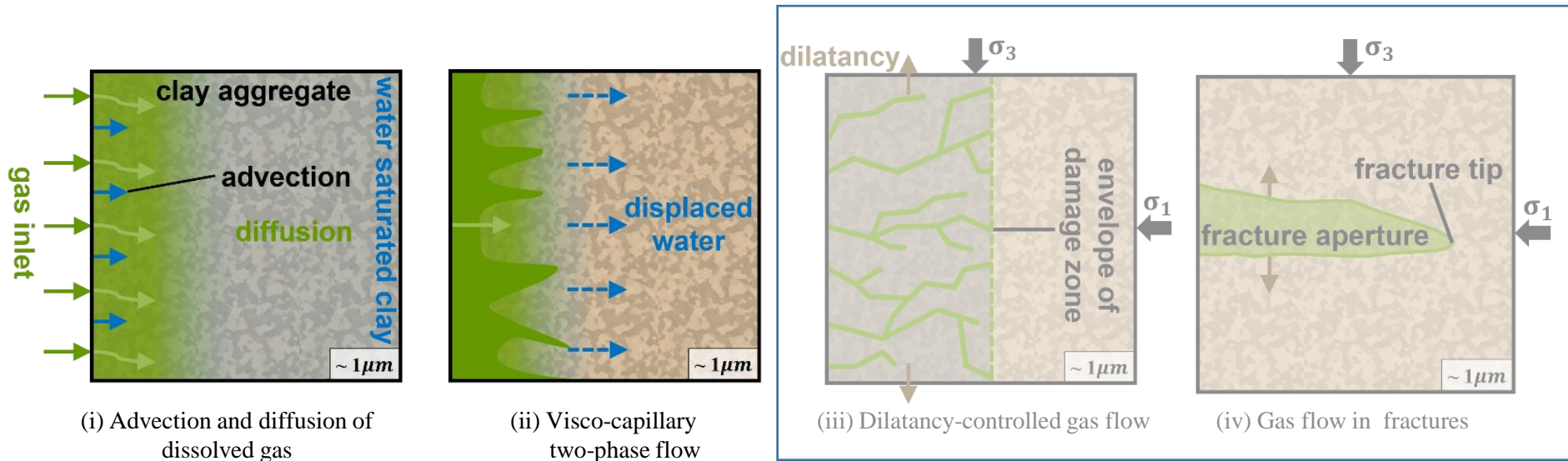


Content

- ① Context
- ② From experimental evidence to modelling
- ③ Multi-scale modelling approach
- ④ Preliminary modelling
- ⑤ Modelling gas injection experiment
- ⑥ Conclusions

From experimental evidence to modelling

Background

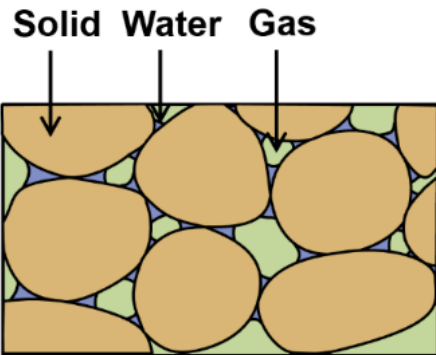


Phenomenological description of the gas transport processes relevant to low-permeable clayey rocks, adapted from Marschall et al. (2005).

Classical HM two-phase flow models

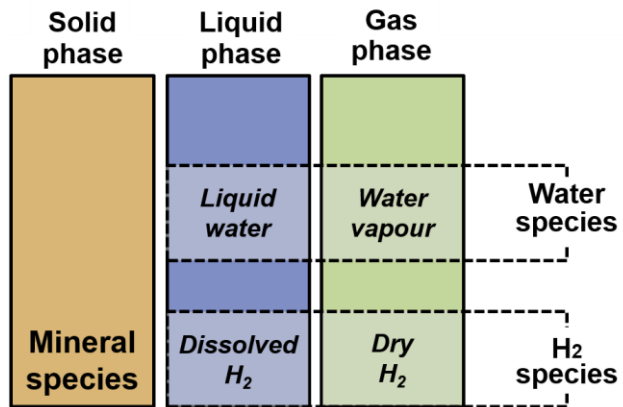
From experimental evidence to modelling

Classical HM two-phase flow models



Triphasic porous medium

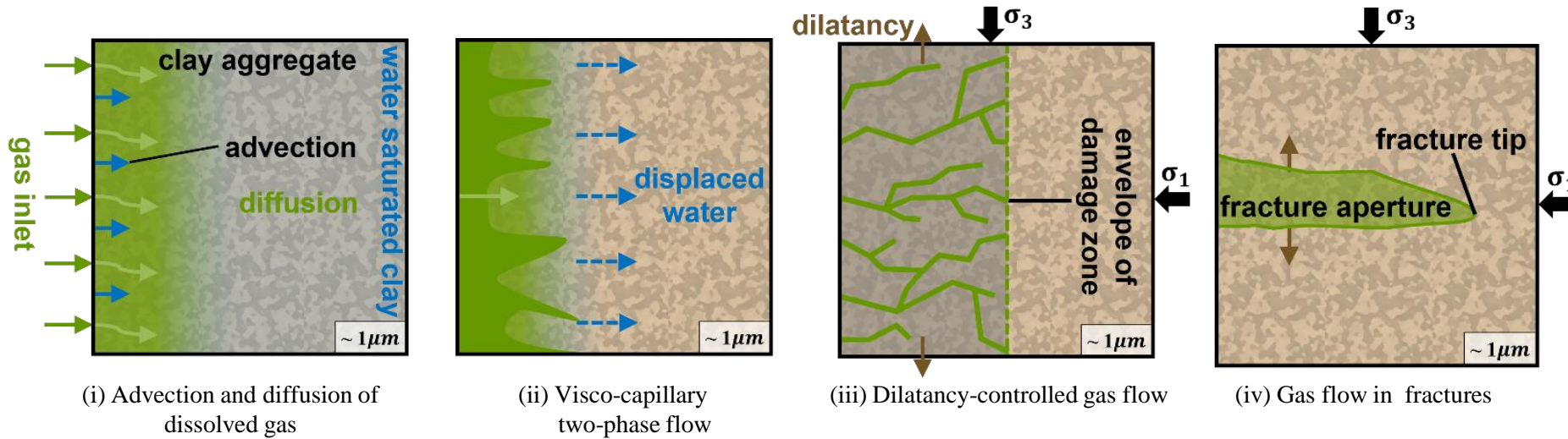
Bright, Aster, Lagamine, OpenGEOSys, Though2/3



Phases and species

From experimental evidence to modelling

Background



Phenomenological description of the gas transport processes relevant to low-permeable clayey rocks, adapted from Marschall et al. (2005).

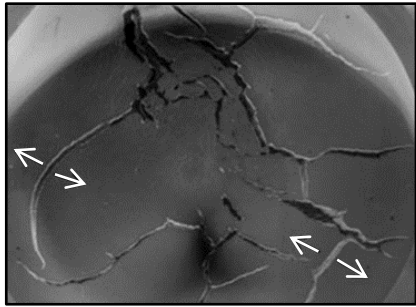
Classical HM two-phase flow models

Supported by experimental data

From experimental evidence to modelling

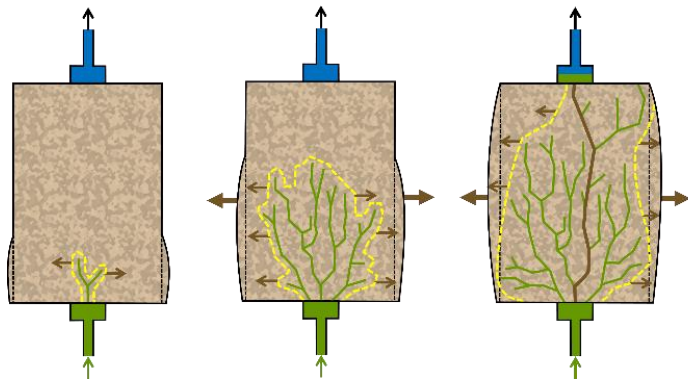
Laboratory experiments

Clay-rich material



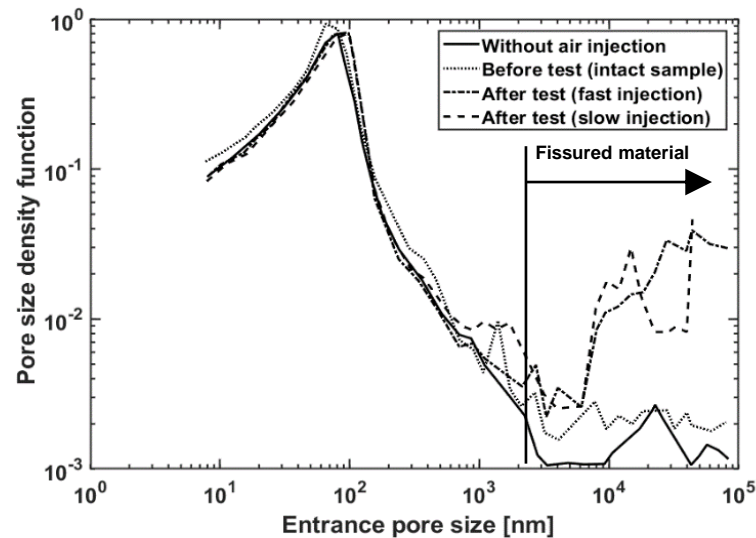
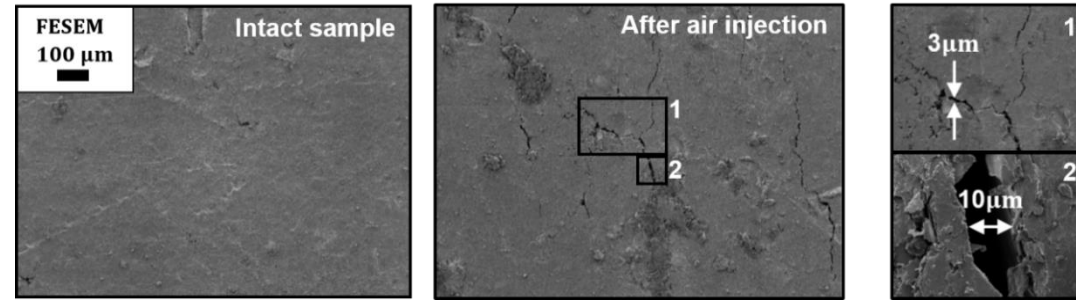
Gas-induced fracturing, *Wiseall et al. (2015)*

Callovo-Oxfordian claystone



Onset of gas flow, modified after *Cuss et al. (2014)*

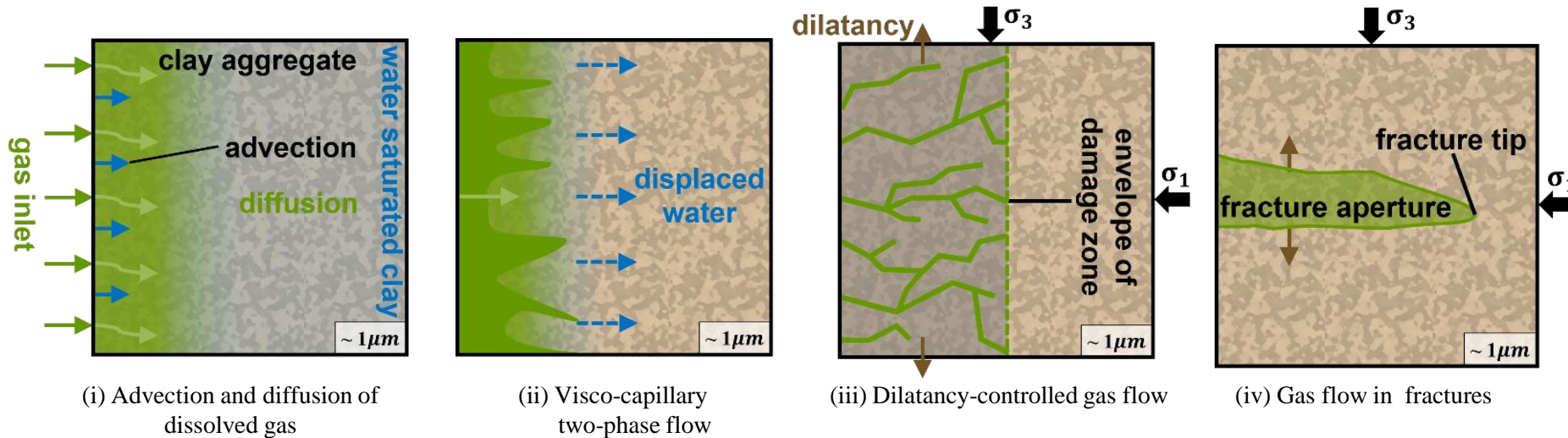
Boom Clay



Changes in Boom Clay pore size distribution after air injection, and corresponding FESEM images with zooms on the detected fissures, modified after *Gonzalez-Blanco et al. (2022)*

From experimental evidence to modelling

Background



Phenomenological description of the gas transport processes relevant to low-permeable clayey rocks, adapted from Marschall et al. (2005).

Classical HM two-phase flow models

Supported by experimental data

- Natural heterogeneities represent preferred weaknesses for the process of opening discrete gas-filled pathway
- Introduce stronger coupling between gas flow and mechanical behaviour into the models.

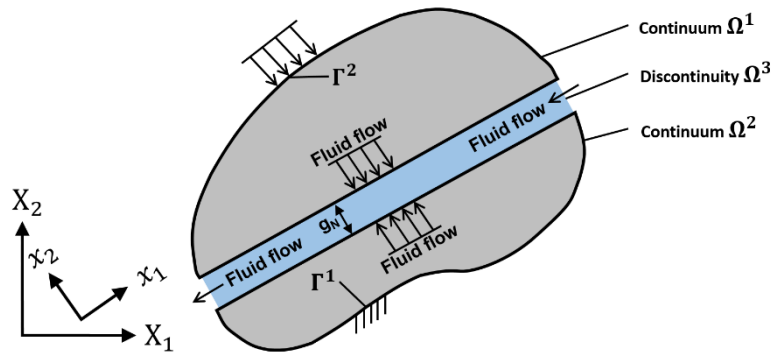
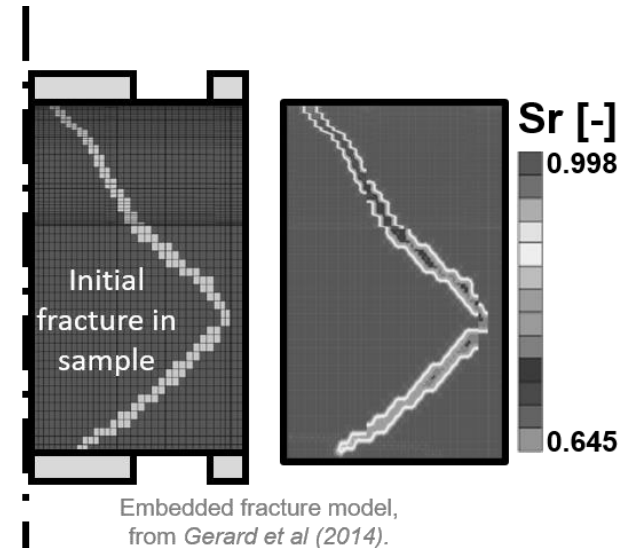
► Advanced HM models

From experimental evidence to modelling

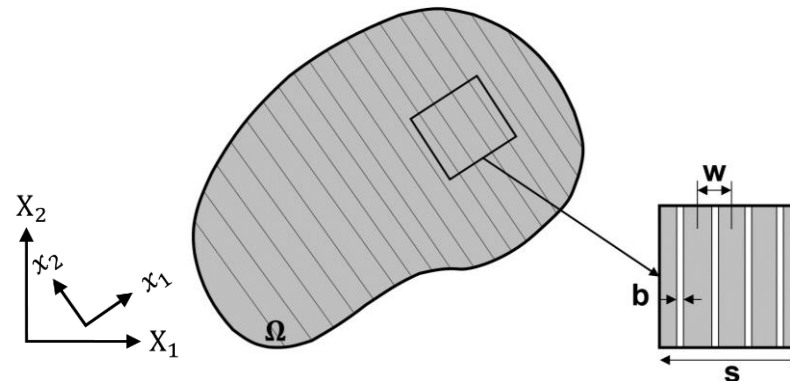
Advanced HM models

Macroscopic models

- ▶ No direct representation of local phenomena
- ▶ Enriched with micromechanical effects
- ▶ Examples:
 - Natural heterogeneity based models Olivella and Alonso (2008)
 - Intrinsic permeability based models Pardoen et al. (2016)
 - Embedded fracture models Alonso et al. (2006)
 - Explicit fracture based models Cerfontaine et al. (2015)



Conceptual scheme of the explicit fracture based model, after Cerfontaine et al. (2015)



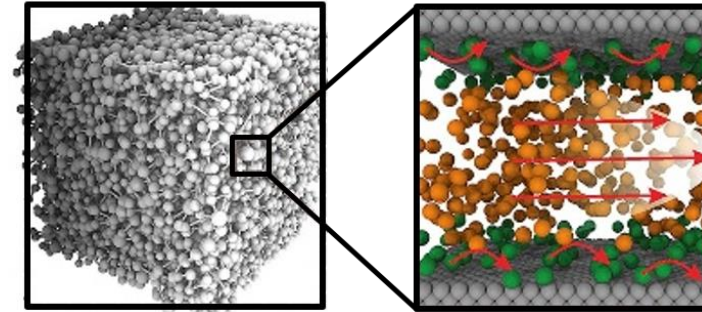
Conceptual scheme of the embedded fracture model, after Olivella et al. (2008)

From experimental evidence to modelling

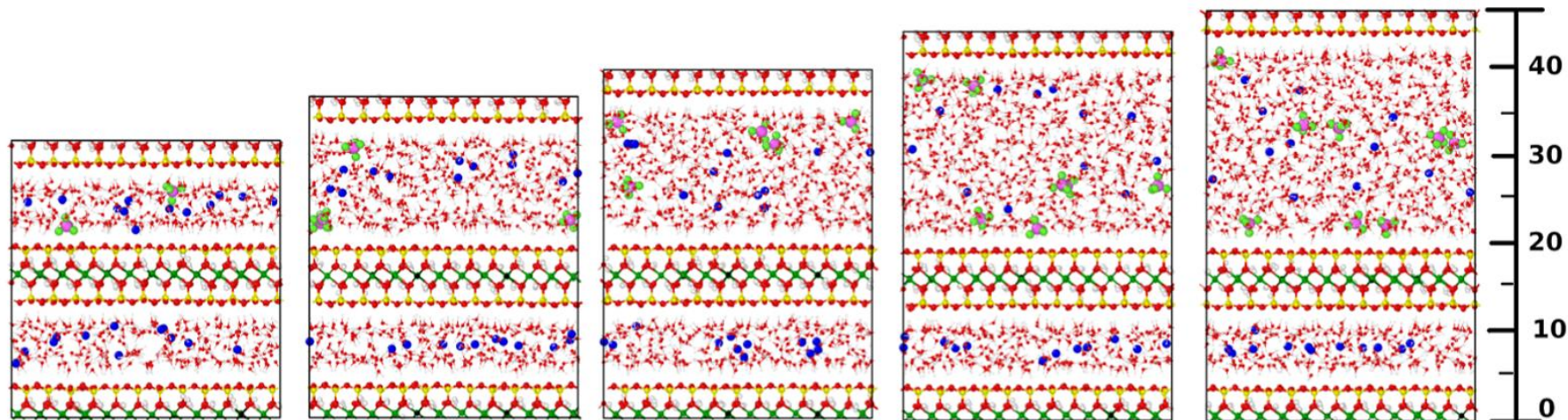
Advanced HM models

Microscopic models

- ▶ Direct modelling of all the microstructure complexity at very low scale
- ▶ Useful for modelling at the process scale
- ▶ High computational expense at the scale of a repository



From pore network to molecular model, from *Yu et al. (2019)*.



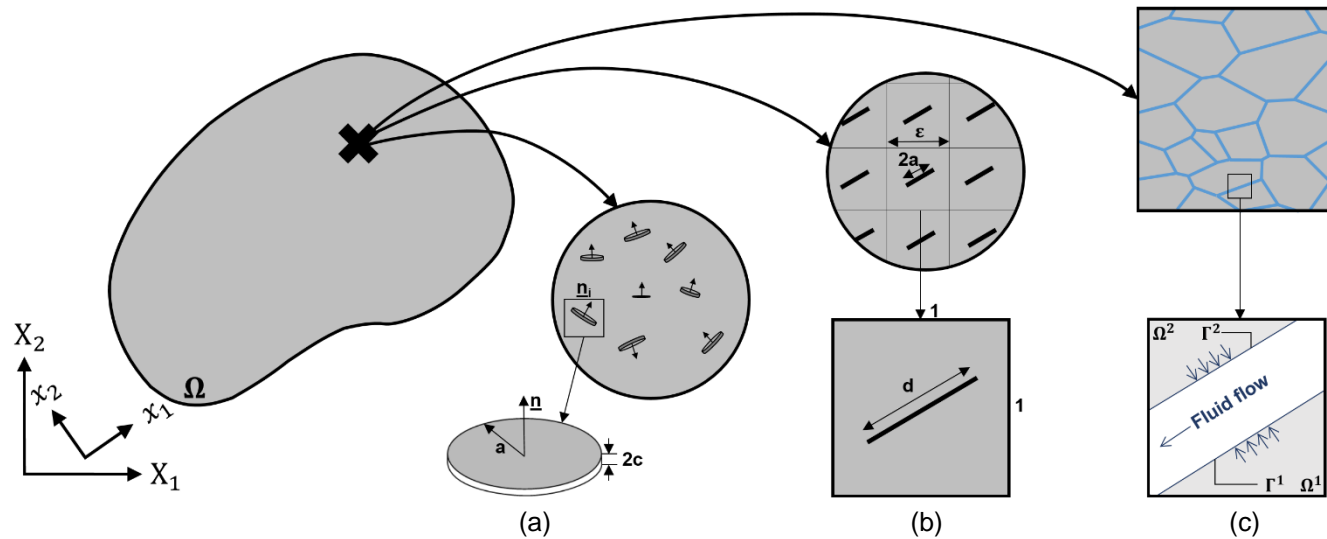
Study of the the physico-chemical properties of dissolved gases in several configurations of a hydrated clay system, from *Owusu et al. (2022)*.

From experimental evidence to modelling

Advanced HM models

Micro-macro based models

- ▶ Combines the benefits from large- and small-scale modelling strategies
- ▶ Explicit description of all the constituents on their specific length scale through a REV definition



Conceptual scheme of micro-macro based models, with microstructure definitions of a microcracked material, after (a) Levasseur (2013), (b) François (2010), and (c) van den Eijnden (2016).



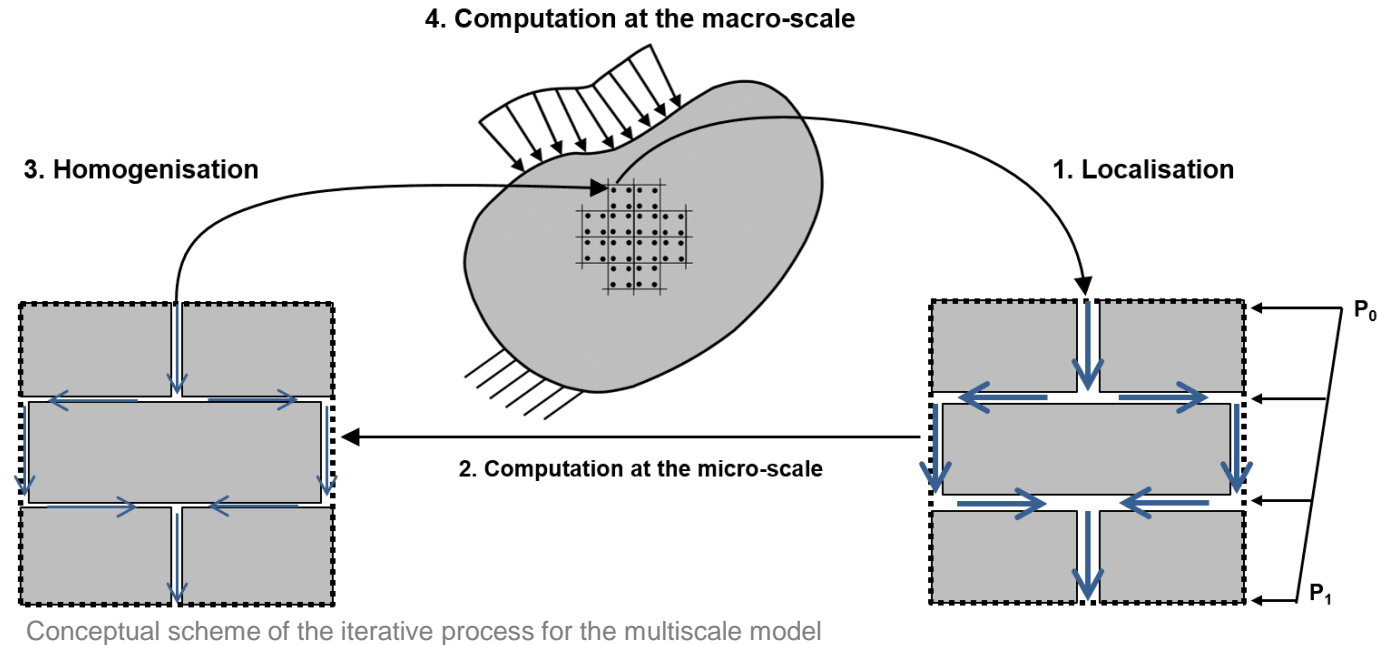
Content

- ① Context
- ② From experimental evidence to modelling
- ③ Multi-scale modelling approach
- ④ Preliminary modelling
- ⑤ Modelling gas injection experiment
- ⑥ Conclusions

Multi-scale modelling approach

Overview

- Macro-to-micro scale transition: Localisation of the macro-scale deformations to the micro-scale
- Resolution of the boundary value problem at the micro-scale
- Micro-to-macro scale transition: Homogenisation of the micro-scale stresses to compute the macroscopic quantities
- Resolution of the boundary value problem at the macro-scale



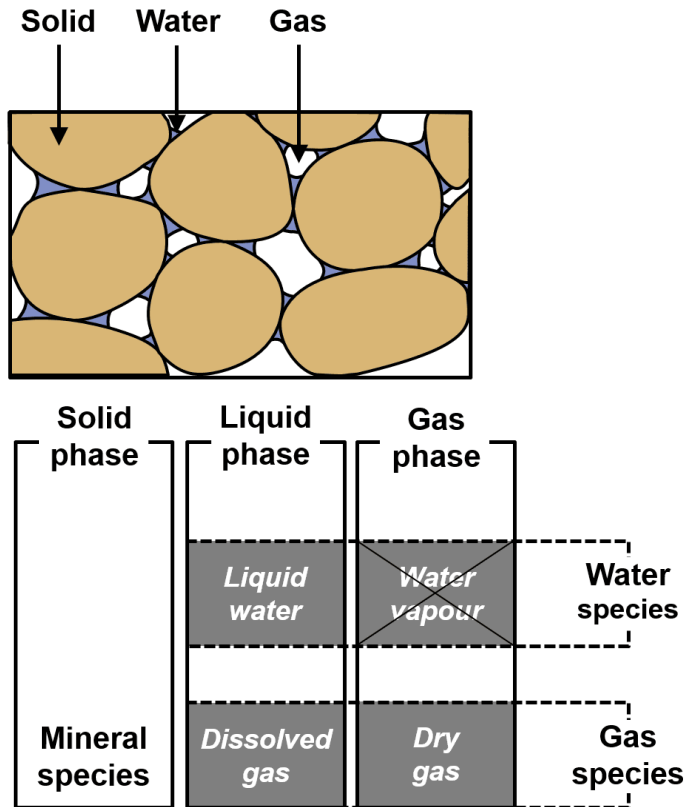
Hybrid developed tool

- Complete hydraulic system implemented and solved at the micro-scale
- Mechanical effects addressed at the macro-scale and implicitly integrated at the lower scale through HM couplings

Multi-scale modelling approach

Model formulation at the macroscopic scale

Clay material treated as a porous medium



Unsaturated triphasic porous medium and definition of phases and species

Balance equations

- Momentum

$$\frac{\partial \sigma_{ij}}{\partial x_j} + \rho g_i = 0$$

- Water

$$\underbrace{\dot{M}_w + \frac{\partial f_{w,i}}{\partial x_i}}_{\text{Liquid water}} - Q_w = 0$$

- Gas

$$\underbrace{\dot{M}_g + \frac{\partial f_{g,i}}{\partial x_i}}_{\text{Dry gas}} + \underbrace{\dot{M}_{dg} + \frac{\partial f_{dg,i}}{\partial x_i}}_{\text{Dissolved gas}} - Q_g = 0$$

Constitutive equations

- Total stress definition

$$\sigma_{ij} = \sigma'_{ij} + b_{ij} \left[S_{r_w} p_w^M + (1 - S_{r_w}) p_g^M \right] \delta_{ij}$$

- Variation of solid density

$$\frac{\dot{\rho}_s}{\rho_s} = \frac{(b_{ij} - \phi)(S_r^w \dot{p}_w + S_r^g \dot{p}_g) + \dot{\sigma}'}{(1 - \phi)K_s}$$

Multi-scale modelling approach

Macro-to-micro scale transition: Localisation

Decomposition of the micro-kinematics:

- Macro-pressure fields (\square^M) of water and gas must be identical to the micro-quantities (\square^m) for any point of the material

$$p_w^M(\hat{P}) = p_w^m(\hat{P})$$

$$p_g^M(\hat{P}) = p_g^m(\hat{P})$$

- For any point P close to \hat{P} , at the macroscopic scale:

$$p_w^M(P) \approx p_w^M(\hat{P}) + \frac{\partial p_w^M(\hat{P})}{\partial x_j} (x_j - \hat{x}_j) \quad p_g^M(P) \approx p_g^M(\hat{P}) + \frac{\partial p_g^M(\hat{P})}{\partial x_j} (x_j - \hat{x}_j)$$

Higher-order terms neglected

at the microscopic scale:

$$p_w^m(P) \approx p_w^M(\hat{P}) + \frac{\partial p_w^M(\hat{P})}{\partial x_j} (x_j - \hat{x}_j) + p_w^f(\hat{P}) \quad p_g^m(P) \approx p_g^M(\hat{P}) + \frac{\partial p_g^M(\hat{P})}{\partial x_j} (x_j - \hat{x}_j) + p_g^f(\hat{P})$$

Fluctuation fields to replace higher-order terms

Separation of scales

- Approach restricted to situations where the variations of the macroscopic fields is large compared to the variations of micro-scale fields

$$\frac{\partial p_w^M(\hat{P})}{\partial x_j} (x_j - \hat{x}_j) + p_w^f(\hat{P}) \ll p_w^M(\hat{P})$$

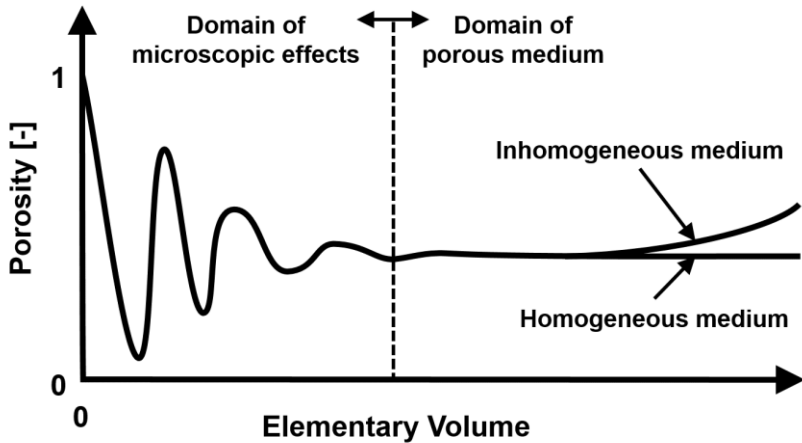
$$\frac{\partial p_g^M(\hat{P})}{\partial x_j} (x_j - \hat{x}_j) + p_g^f(\hat{P}) \ll p_g^M(\hat{P})$$

Multi-scale modelling approach

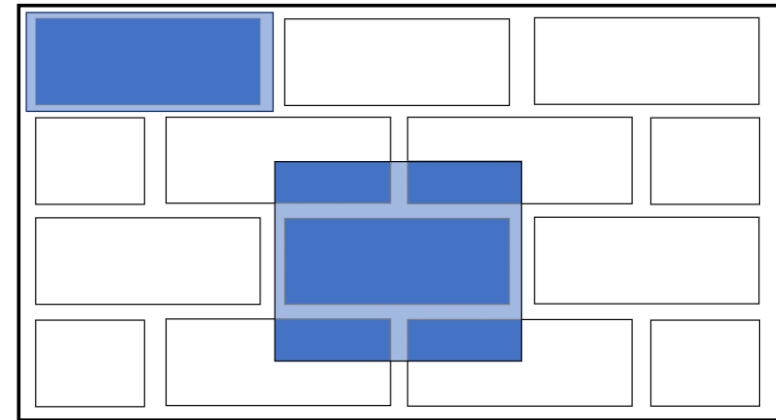
Micro-scale boundary value problem

REV generation in general

- Representative of the microstructure
 - Large enough to represent the microstructure
 - Small enough to satisfy the principle of scale separation
- Spatial repetition of a very small part of the whole microstructure
 - Relevant statistical representation of any random part of the micro-scale
 - Not a unique choice



Representativeness of an elementary volume applied to the concept of porosity, *Bear (1972)*.

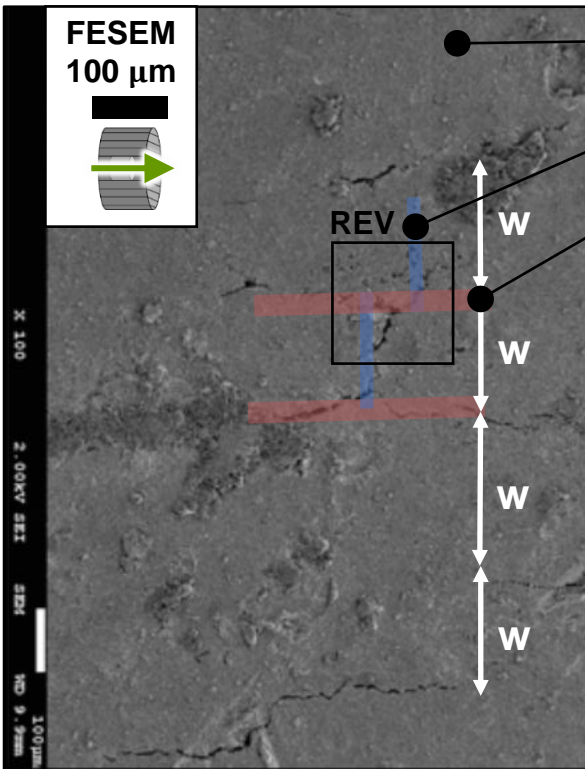
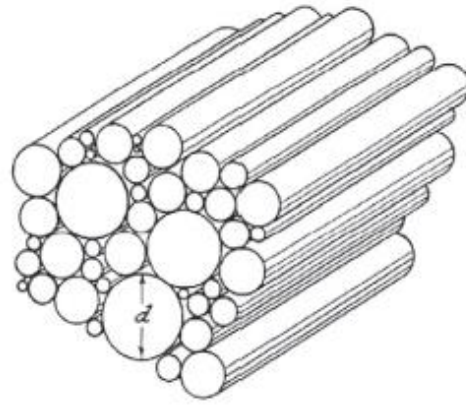


Examples of two rectangular unit cells, *Anthoine (1995)*

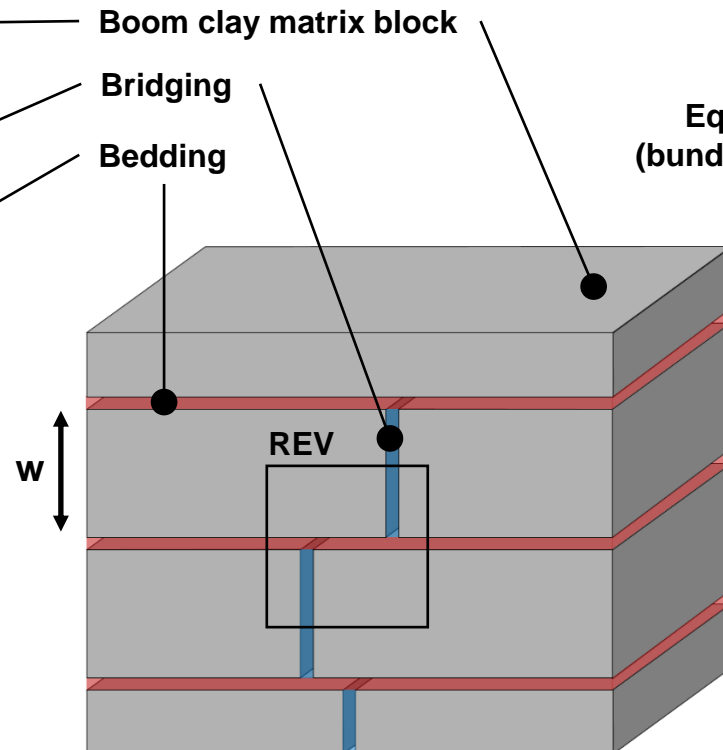
Multi-scale modelling

Micro-scale boundary value problem

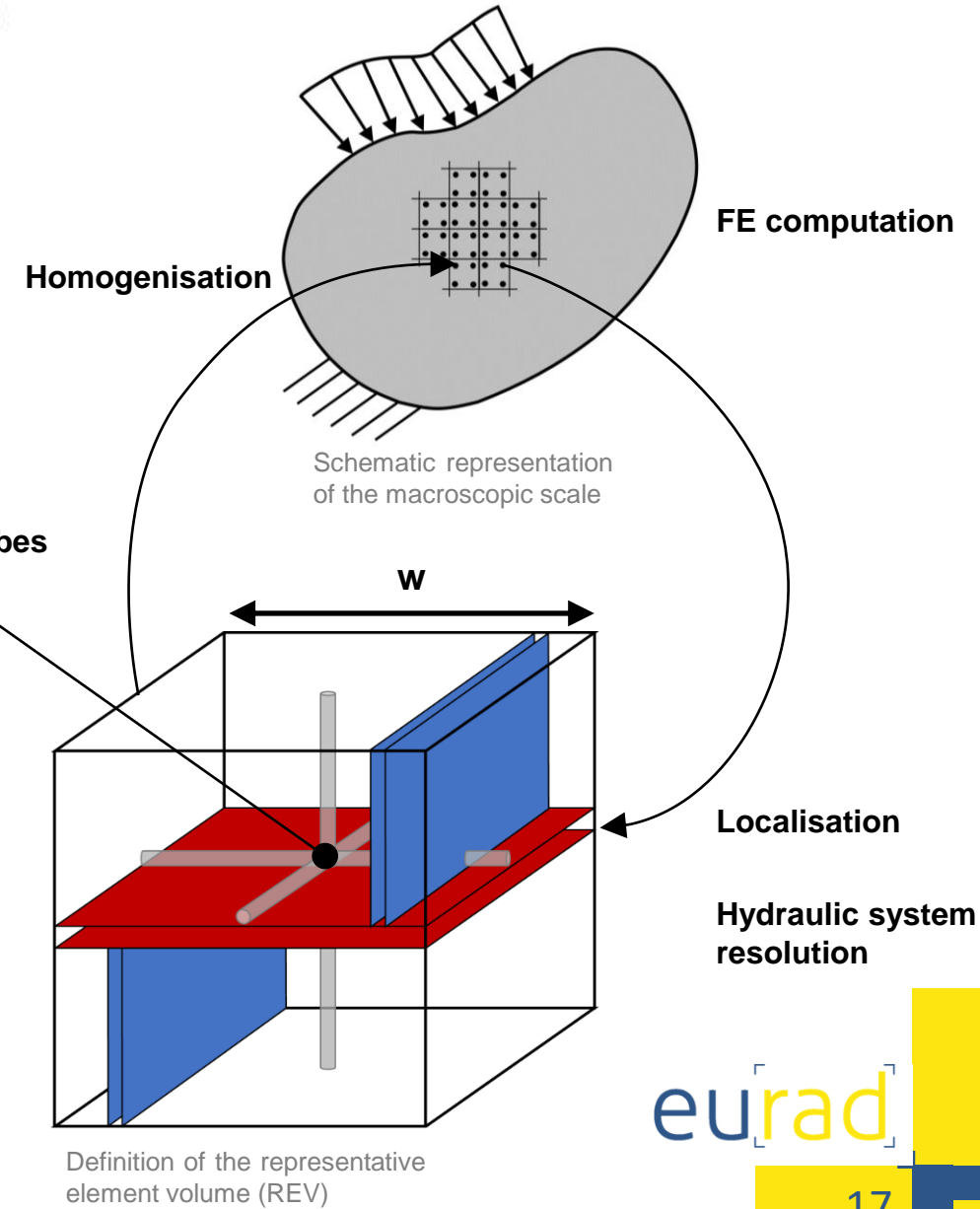
Multi-scale model supported by experimental data



Internal visualisation of a Boom Clay sample using FESEM, from Gonzalez-Blanco (2017).



Physical idealisation of the microstructure.



Multi-scale modelling approach

Micro-scale boundary value problem

Balance equations at the micro-scale

- Gas

$$\cancel{\frac{\partial f_g^m}{\partial x_i}} + \frac{\partial f_{g_i}^m}{\partial x_i} + \cancel{\frac{\partial f_g^m}{\partial x_i}} + \frac{\partial f_{dg_i}^m}{\partial x_i} = 0$$

- Water

$$\cancel{\frac{\partial f_w^m}{\partial x_i}} + \frac{\partial f_{w_i}^m}{\partial x_i} = 0$$

$\dot{M}_g^m \quad \dot{M}_{dg}^m \quad \dot{M}_w^m$ Variations of fluid contents

$$f_{w_i}^m = \rho_w q_{w_i}$$

$$f_{g_i}^m = \rho_g q_{g_i} \quad \text{Mass flows}$$

$$f_{dg_i}^m = \rho_{dg} q_{w_i} + i_{dg_i}$$

- Mechanical effects: computed at the macro-scale and transferred to the micro-scale through HM couplings

Multi-scale modelling approach

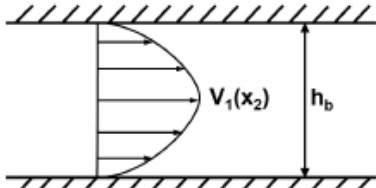
Micro-scale boundary value problem

Constitutive equations: Hydraulic problem considering a channel flow model (Navier-Stokes equations)

- Advective component:

$$q_{\alpha_i} = -\frac{k_{r\alpha}}{\mu_\alpha} \frac{1}{A} \kappa_{frac} \frac{\partial p_\alpha}{\partial x_i} = -\frac{k_{r\alpha}}{\mu_\alpha} \frac{h_b^3}{12w} \frac{\partial p_\alpha}{\partial x_i}$$

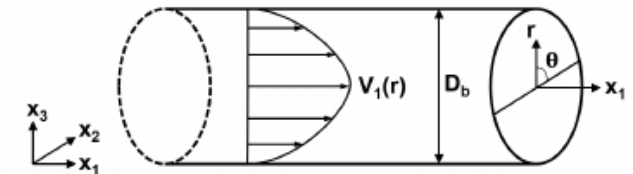
$$q_{\alpha_i} = -\frac{k_{r\alpha}}{\mu_\alpha} \frac{1}{A} \kappa_{tube} \frac{\partial p}{\partial x_i} = -\frac{k_{r\alpha}}{\mu_\alpha} \pi \frac{D^4}{128w^2} \frac{\partial p}{\partial x_i}$$



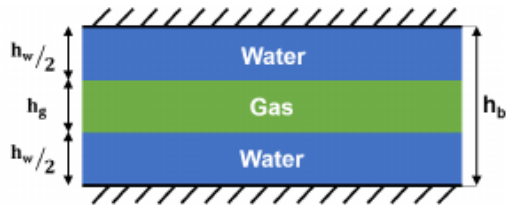
Laminar fluid flow profiles between two parallel plates

$$\kappa_{frac} = -\frac{h_b^2}{12} h_b \cdot w$$

$$\kappa_{tube} = -\pi \frac{D^4}{128}$$



Laminar fluid flow profiles in a circular pipe



Gas flow in between of water flows in a fracture space

$$k_{r_w} = \frac{S_r^2}{2} (3 - S_r)$$

$$k_{r_g} = (1 - S_r)^3$$

$$k_{r_w} = S_r^2$$

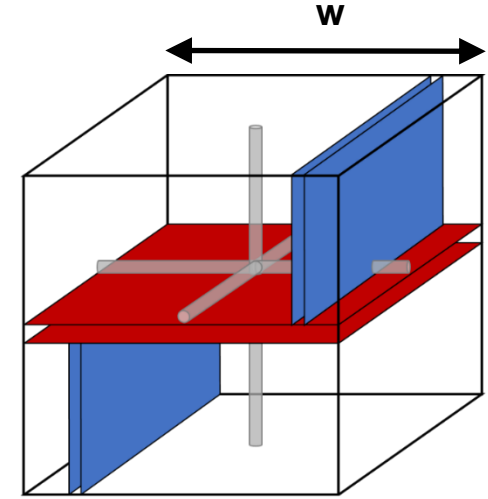
$$k_{r_g} = (1 - S_r)^2$$



Gas flow in between of water flows in a circular pipe

- Diffusive component

$$i_{dgi} = -S_{r_w} \bar{\tau} D_{dg/w} \rho_w \frac{\partial}{\partial x_i} \left(\frac{\rho_{dg}}{\rho_w} \right)$$



Multi-scale modelling approach

Micro-scale boundary value problem

Constitutive equations: Hydro-mechanical couplings

- Stress-dependent evolution of micro-elements aperture

$$\Delta\sigma' = K_n \Delta h$$

$$K_n = \frac{K_n^0}{\left(1 + \frac{\Delta h}{h_0}\right)^2}$$

$$\Delta\sigma' = K \Delta D_b$$

$$K = \frac{2G}{D_0}$$

- Stress-dependent formulation of the transmissivity and the entry pressure of micro-elements

$$\kappa_{frac} = -\frac{h_b^2}{12} h_b \cdot w$$

$$p_e = p_{e0} \left(\frac{h_{b0}}{h_b}\right)^m$$

$$p_{e0} = \frac{2\sigma_{GL} \cos\theta}{h_b}$$

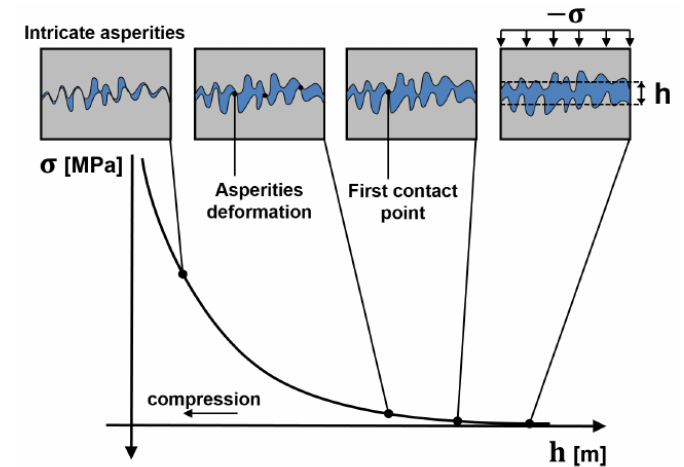
$$h_b = h_0 + h$$

$$\kappa_{tube} = -\pi \frac{D^4}{128}$$

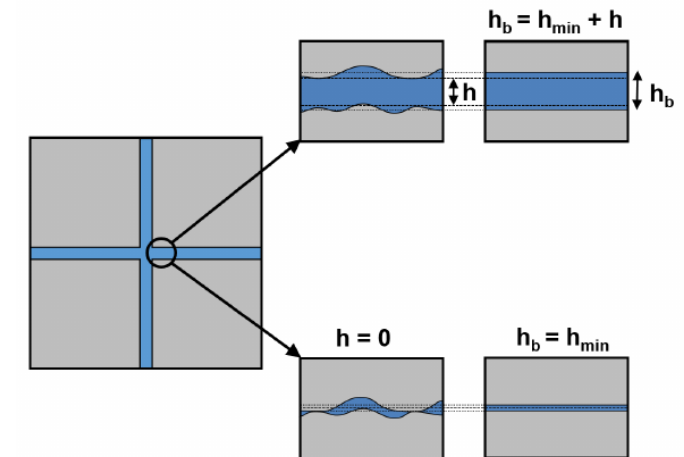
$$p_e = p_{e0} \left(\frac{D_{b0}}{D_b}\right)^m$$

$$p_{e0} = \frac{2\sigma_{GL} \cos\theta}{D_b/2}$$

$$D_b = D_0 + D$$



Constitutive law describing the normal behaviour of a rough rock joint, *Cerfontaine (2015)*



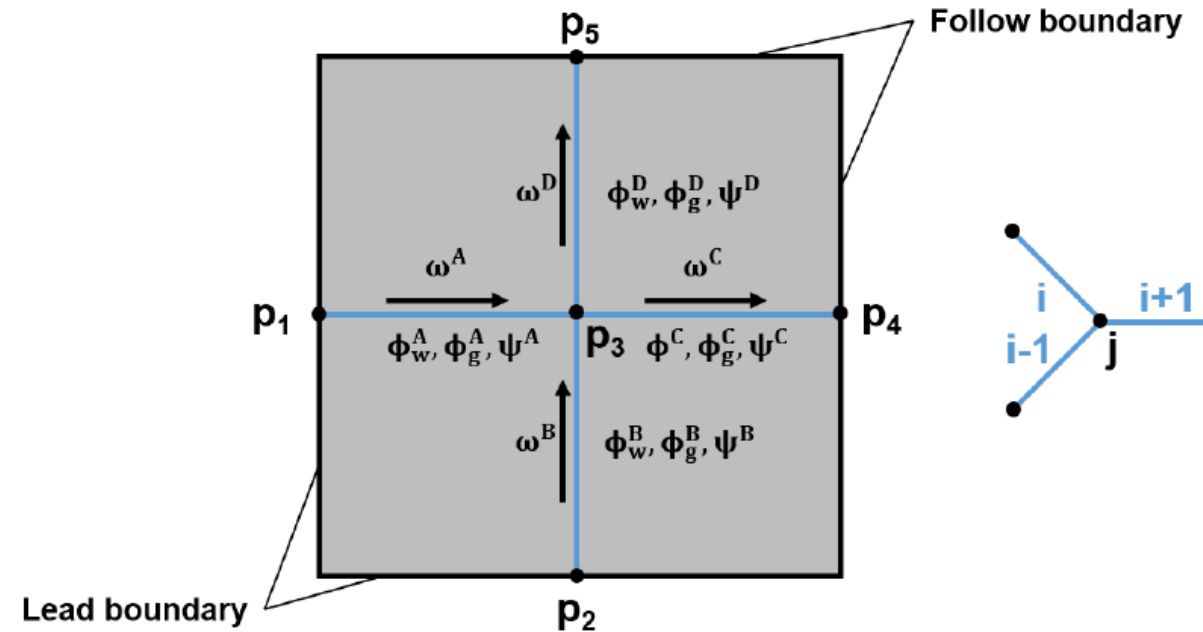
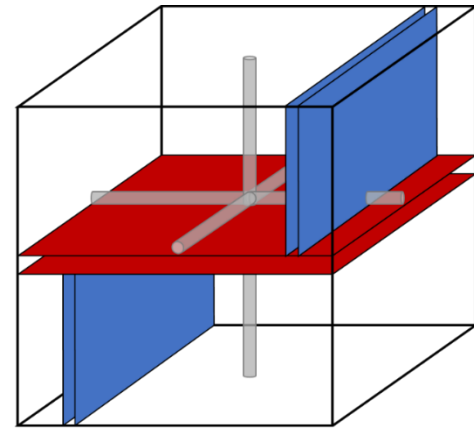
Definitions of the hydraulic and the mechanical aperture in reality (left) and in the modelling (right), *Marinelli (2016)*

Multi-scale modelling approach

Micro-scale boundary value problem

General principles for numerical resolution of the hydraulic system

- Hydraulic network respecting these conditions:
 - Anti-symmetric boundary fluxes
 - Macroscopic pressure gradient between the boundaries
- Hydraulic problem established through mass balance on each node (j)
- Hydraulic problem solved
 - For a given configuration
 - Under steady-state conditions
 - By applying the macro-pressure to one node



Example of a channel network with the mass balance on node j

Multi-scale modelling approach

Micro-scale boundary value problem

General principles for numerical resolution of the hydraulic system

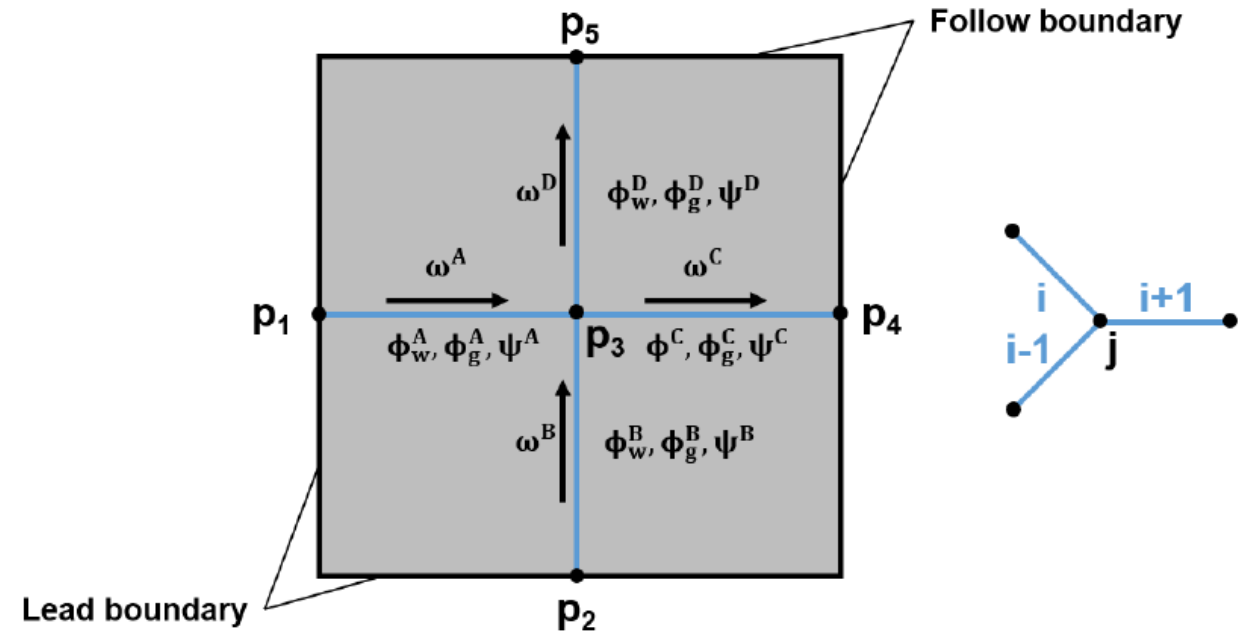
- Hydraulic network respecting these conditions:
 - Anti-symmetric boundary fluxes
 - Macroscopic pressure gradient between the boundaries

=> Channel (fracture or tube) mass fluxes of water and gas

$$\omega_w = - \underbrace{\frac{\rho_w k_{rw}}{\mu_w} \kappa \frac{\partial p_w^m}{\partial s}}_{\text{Advection of liquid water}}$$

$$\omega_g = - \underbrace{\frac{\rho_g k_{rg}}{\mu_g} \kappa \frac{\partial p_g^m}{\partial s}}_{\text{Advection of gaseous gas}} - \underbrace{H_g \frac{\rho_g k_{rw}}{\mu_w} \kappa \frac{\partial p_w^m}{\partial s}}_{\text{Advection of dissolved gas}}$$

$$- \underbrace{S_{rw} \bar{\tau} D_{dg/w} \frac{H_g}{\rho_w} \left(\frac{\rho_w \rho_{g,0}}{p_{g,0}} \frac{\partial p_g^m}{\partial s} - \frac{\rho_g \rho_{w,0}}{\chi_w} \frac{\partial p_w^m}{\partial s} \right)}_{\text{Diffusion of dissolved gas}}$$



Example of a channel network with the mass balance on node j

Multi-scale modelling approach

Micro-scale boundary value problem

General principles for numerical resolution of the hydraulic system

- Hydraulic problem established through mass balance on each node (j)
 - Mass conservation principle, *i.e.* for each node of the network, the sum of the input flows is equal to the sum of the output flows

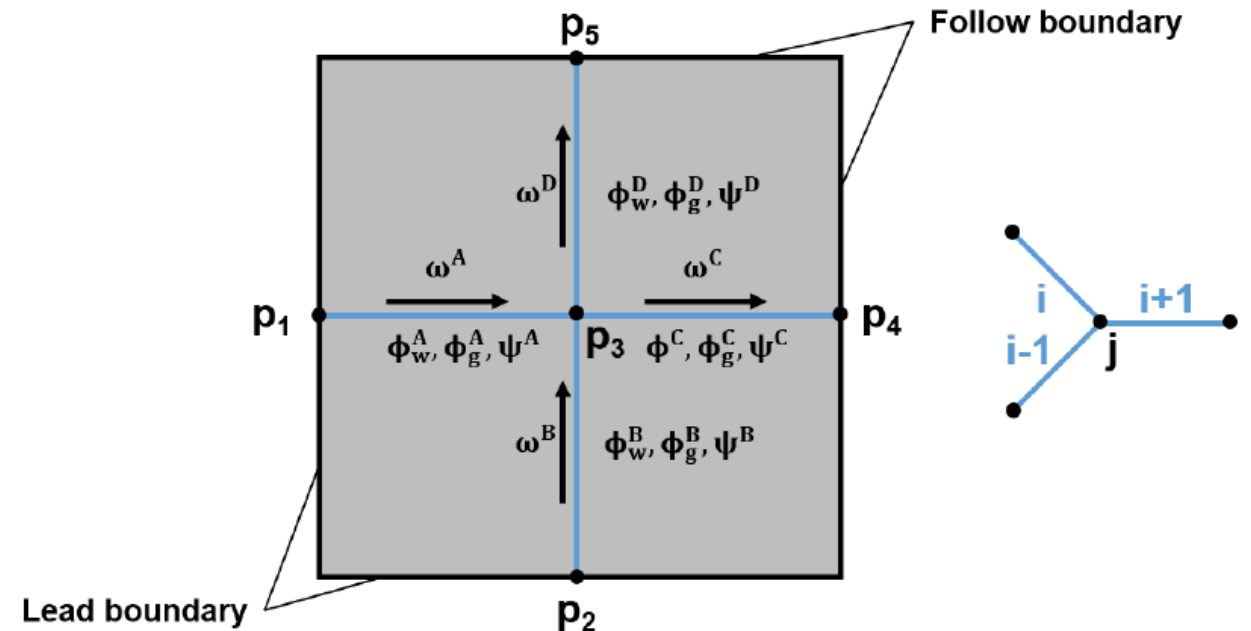
$$\frac{d\omega_\alpha^i}{ds^i} = 0 \quad \Leftrightarrow \quad \omega_\alpha^{i-1} + \omega_\alpha^i + \omega_\alpha^{i+1} = 0$$

$\alpha = w, g$ Liquid or gaseous phase

- Well-posed hydraulic system to solve

$$[G_{ww}] \{p_w^m\} = 0 \quad [G_{gg}] \{p_g^m\} + [G_{gw}] \{p_w^m\} = 0$$

- For a given configuration
- Under steady-state conditions
- By applying the macro-pressure to one node



Example of a channel network with the mass balance on node j

Multi-scale modelling approach

Micro-to-macro scale transition: Homogenisation

- Fluid fluxes

$$\begin{aligned} f_{w_i}^M \frac{\partial p_w^{*,M}}{\partial x_i} &= \frac{1}{\Omega} \int_{\Omega} f_{w_i}^m \frac{\partial p_w^{*,M}}{\partial x_i} d\Omega = \frac{1}{\Omega} \int_{\Gamma} \bar{q}_w^m p_w^{*,M} d\Gamma \\ &= \frac{1}{\Omega} \frac{\partial p_w^{*,M}}{\partial x_i} \int_{\Gamma} \bar{q}_w^m x_i d\Gamma \\ &= \frac{1}{\Omega} \int_{\Gamma} \bar{q}_w^m x_i d\Gamma \end{aligned}$$

$$f_{g_i}^M + f_{dg_i}^M = \frac{1}{\Omega} \int_{\Gamma} \bar{q}_g^m x_i d\Gamma$$

- Fluid masses: total amount of fluids inside the fractures and tubes

$$\begin{aligned} M_w^M &= \frac{1}{\Omega} \int_{\Omega_w^{int}} \rho_w d\Omega \\ &= \rho_w S_{r_w} \phi_n \end{aligned}$$

$$\begin{aligned} M_g^M &= M_g^m + M_{dg}^m \\ &= \frac{1}{\Omega} \left(\int_{\Omega_g^{int}} \rho_g d\Omega + \int_{\Omega_w^{int}} \rho_{dg} d\Omega \right) \\ &= \rho_g (1 - S_{r_w}) \phi_n + \rho_{dg} S_{r_w} \phi_n \end{aligned}$$

Multi-scale modelling approach

Macro-scale boundary value problem

- Under matrix form:

$$\begin{bmatrix} [K_{ww}^M]_{(3 \times 3)} & [K_{wg}^M]_{(3 \times 3)} \\ [K_{gw}^M]_{(3 \times 3)} & [K_{gg}^M]_{(3 \times 3)} \end{bmatrix} \begin{Bmatrix} \begin{Bmatrix} \delta \nabla p_w^M \\ \delta p_w^M \end{Bmatrix}_{(3)} \\ \begin{Bmatrix} \delta \nabla p_g^M \\ \delta p_g^M \end{Bmatrix}_{(3)} \end{Bmatrix} = \begin{Bmatrix} \begin{Bmatrix} \delta f_w^M \\ \delta \dot{M}_w^M \end{Bmatrix}_{(3)} \\ \begin{Bmatrix} \delta f_g^M \\ \delta \dot{M}_g^M \end{Bmatrix}_{(3)} \end{Bmatrix}$$

Summarized as:

$$[A^M]_{(10 \times 10)} \{\delta U^M\}_{(10)} = \{\delta \Sigma^M\}_{(10)}$$



Content

- ① Context
- ② From experimental evidence to modelling
- ③ Multi-scale modelling approach
- ④ Preliminary modelling
- ⑤ Modelling gas injection experiment
- ⑥ Conclusions

Preliminary modelling

One-element simulation

Bedding plane separation:

- $300\mu m$

Bedding plane aperture:

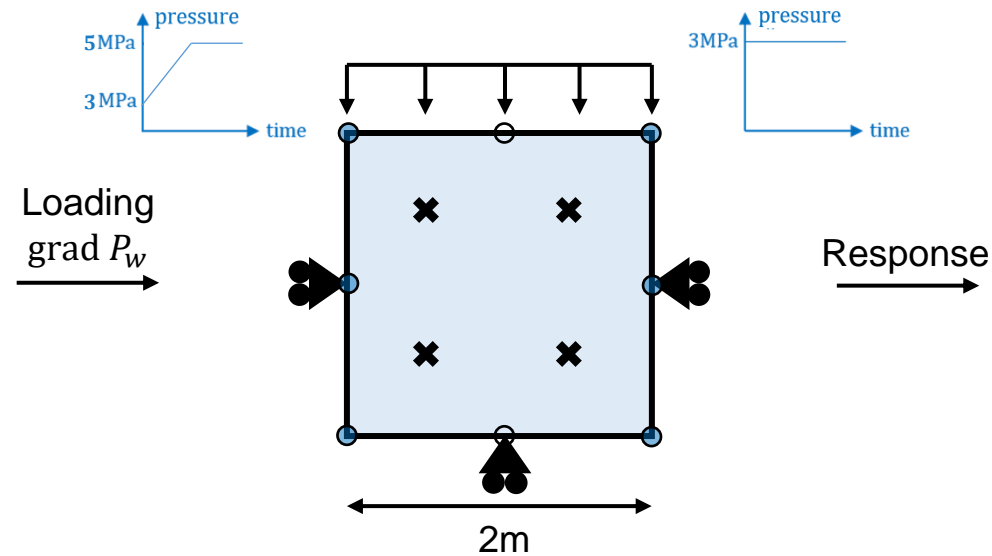
- $0.1\mu m$

Tubes diameter

→ Distribution curve

Bridging plane aperture

→ not considered

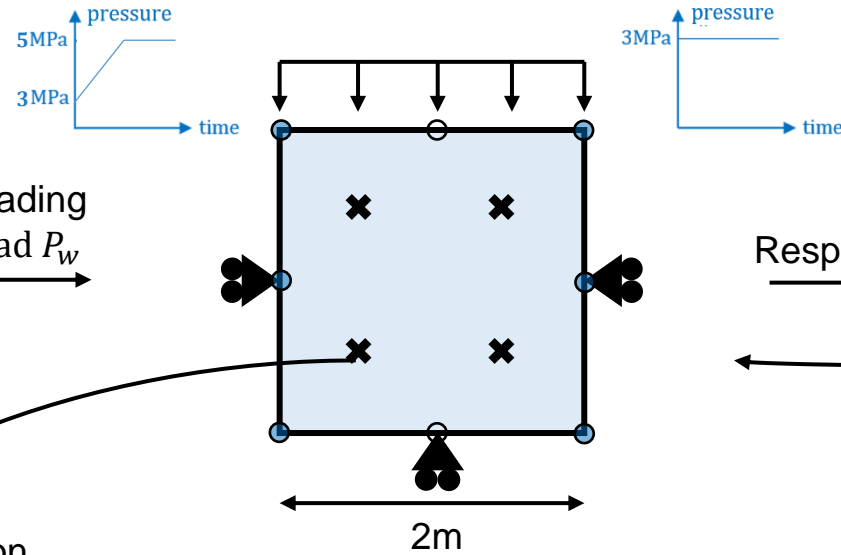


Injection test

- Mechanically blocked
- Water pressure increase
 - 3MPa to 5MPa
- Gas pressure imposed at 3MPa

Preliminary modelling

One-element simulation

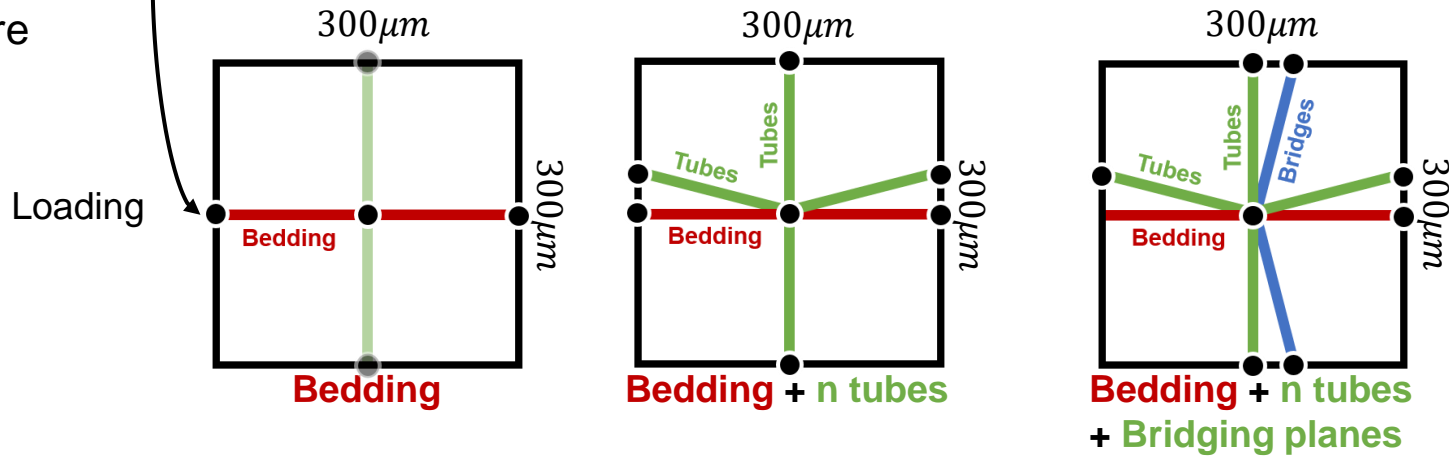


Injection test

- Mechanically blocked
- Water pressure increase from 3MPa to 5MPa
- Gas pressure imposed at 3MPa

Localisation

Homogenisation



Response

Bedding plane separation:

- $300\mu m$

Bedding plane aperture:

- $0.1\mu m$

Tubes diameter

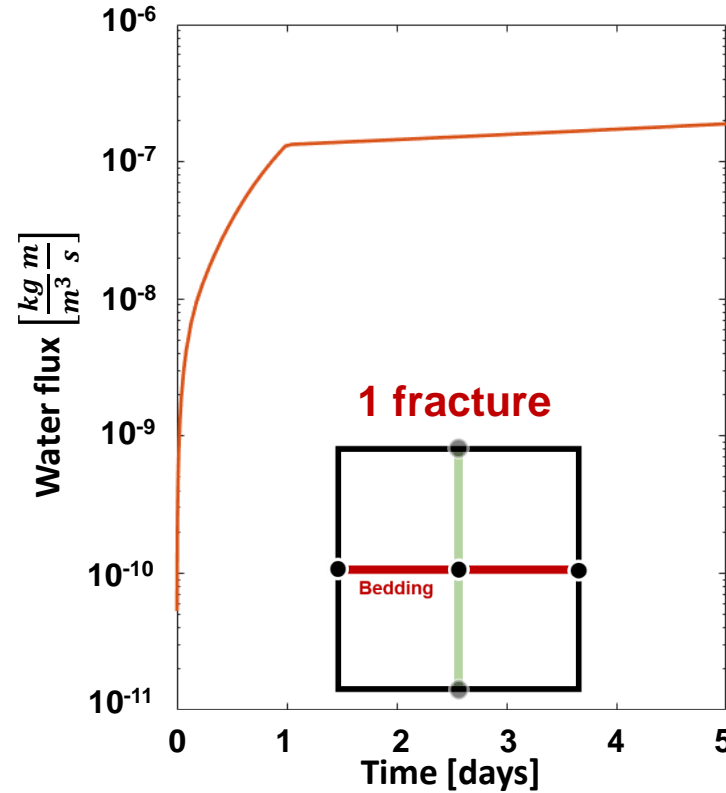
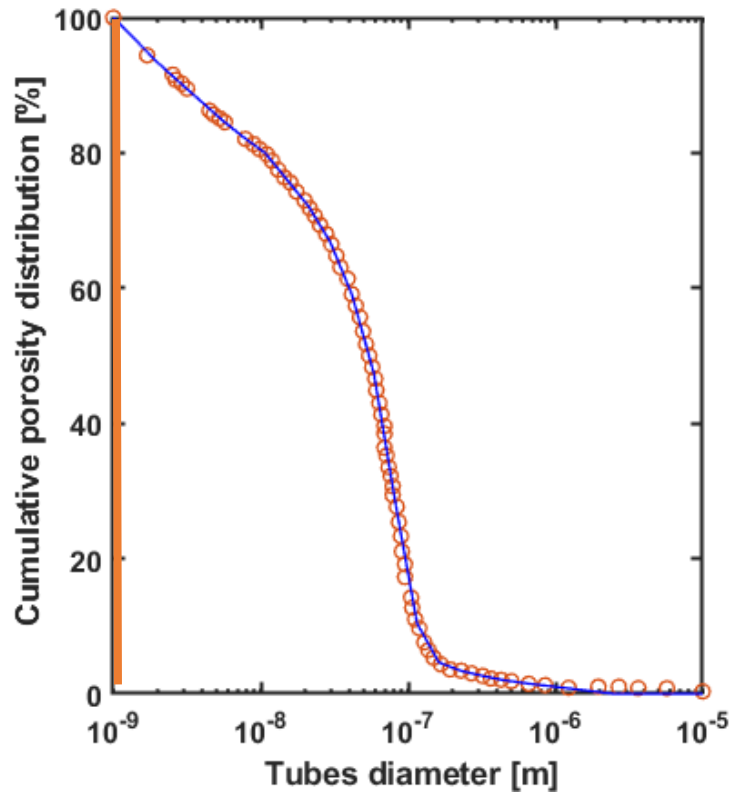
→ Distribution curve

Bridging plane aperture

→ not considered

Preliminary modelling

One-element simulation

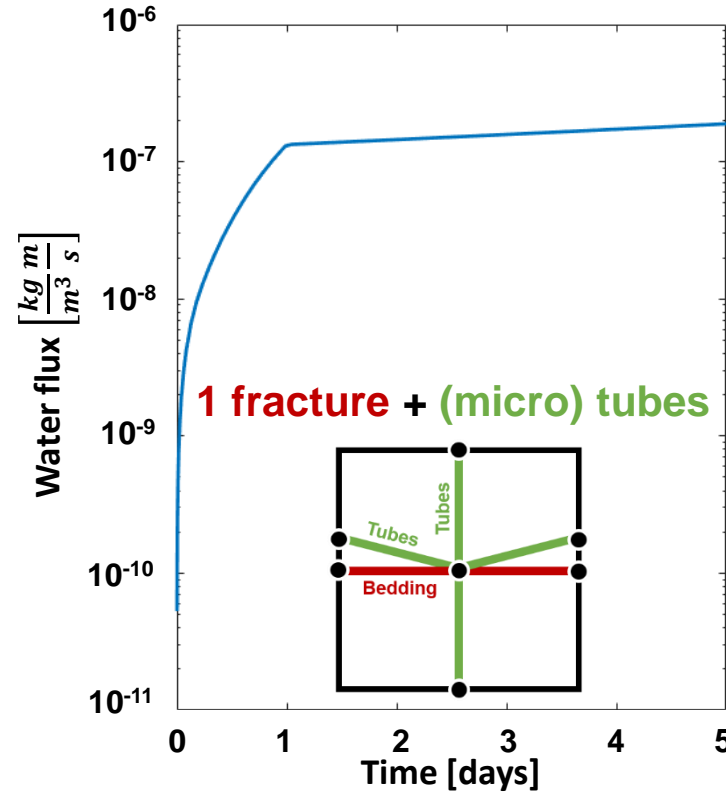
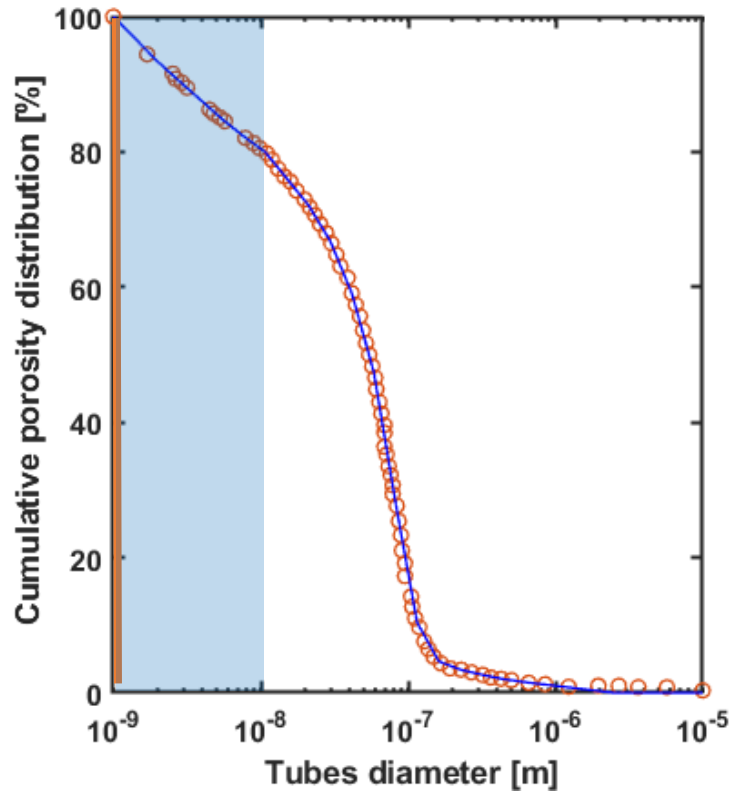


$$k_{int} = \frac{\mu_w}{\rho_w} Flux \frac{\Delta x}{\Delta p} \quad \text{with} \quad \begin{array}{l} \Delta x = 2m \\ \Delta p = 2\ MPa \\ \text{Aperture} = 2.0 \cdot 10^{-6}m \end{array}$$

Number of tubes	Flux [$\frac{kg\ m}{m^3\ s}$]	$k_{int,x}$ [m^2]
0	$1.581 \cdot 10^{-7}$	$1.581 \cdot 10^{-19}$

Preliminary modelling

One-element simulation

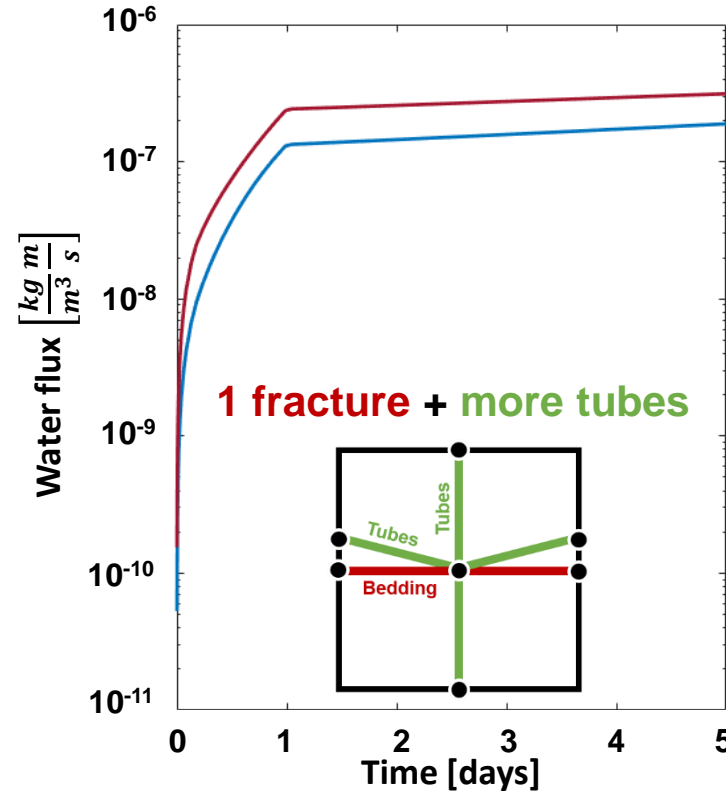
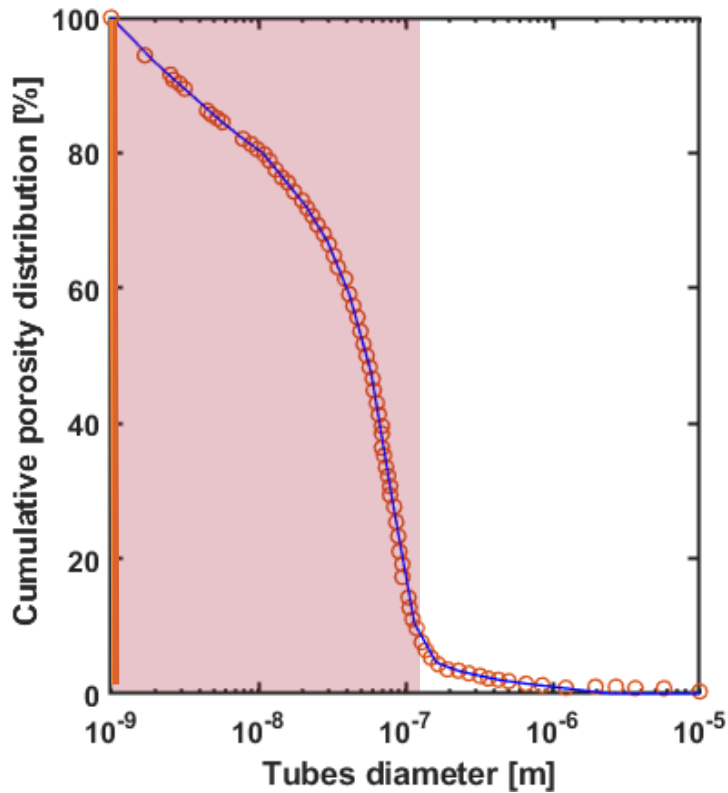


$$k_{int} = \frac{\mu_w}{\rho_w} Flux \frac{\Delta x}{\Delta p} \quad \text{with} \quad \begin{array}{l} \Delta x = 2m \\ \Delta p = 2\ MPa \\ \text{Aperture} = 2.0 \cdot 10^{-6}m \end{array}$$

Number of tubes	Flux [$\frac{kg\ m}{m^3\ s}$]	$k_{int,x}$ [m^2]
0	$1.581 \cdot 10^{-7}$	$1.581 \cdot 10^{-19}$
770	$1.643 \cdot 10^{-7}$	$1.643 \cdot 10^{-19}$

Preliminary modelling

One-element simulation



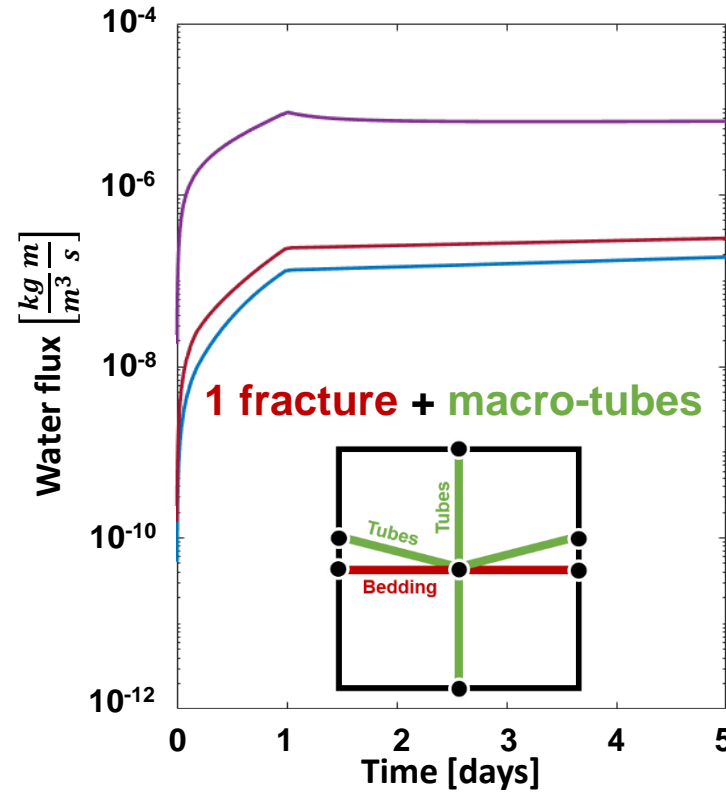
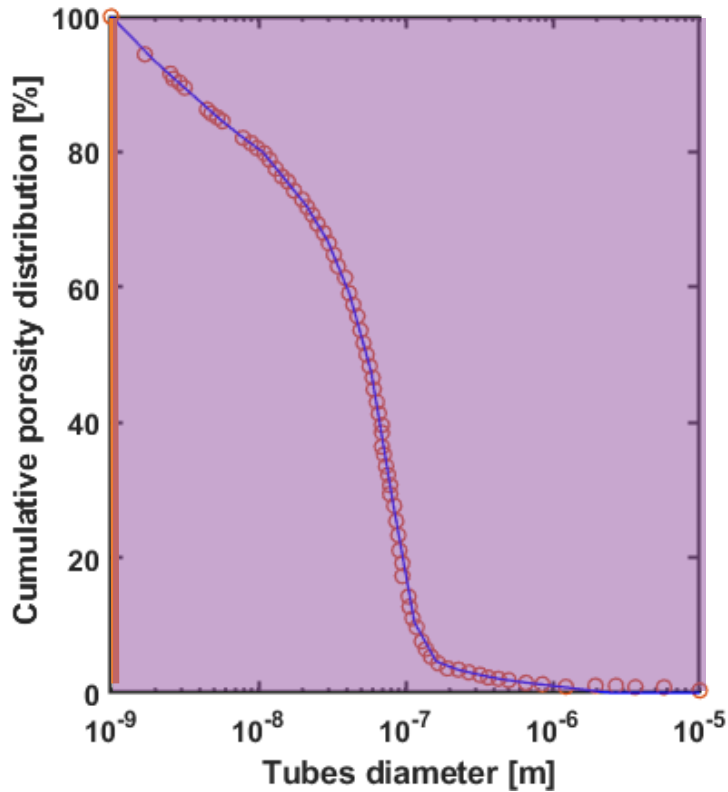
$$k_{int} = \frac{\mu_w}{\rho_w} Flux \frac{\Delta x}{\Delta p} \quad \text{with} \quad \begin{aligned} \Delta x &= 2m \\ \Delta p &= 2\ MPa \\ \text{Aperture} &= 2.0 \cdot 10^{-6}m \end{aligned}$$

Number of tubes	Flux [$\frac{kg\ m}{m^3\ s}$]	$k_{int,x}$ [m^2]
0	$1.581 \cdot 10^{-7}$	$1.581 \cdot 10^{-19}$
770	$1.643 \cdot 10^{-7}$	$1.643 \cdot 10^{-19}$
6394	$3.057 \cdot 10^{-7}$	$3.057 \cdot 10^{-19}$

Fracture-controlled flow

Preliminary modelling

One-element simulation



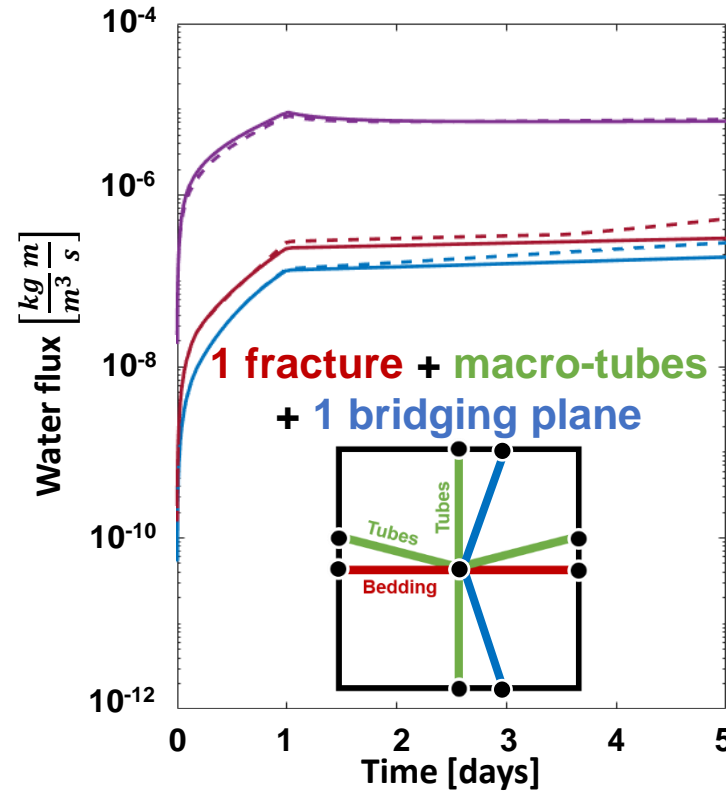
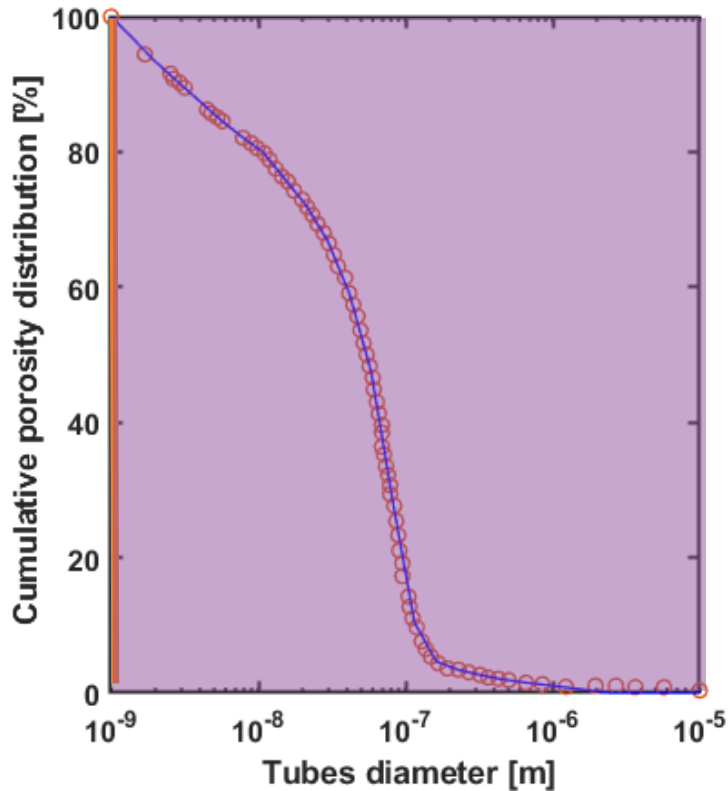
$$k_{int} = \frac{\mu_w}{\rho_w} Flux \frac{\Delta x}{\Delta p} \quad \text{with} \quad \begin{aligned} \Delta x &= 2m \\ \Delta p &= 2\ MPa \\ \text{Aperture} &= 2.0 \cdot 10^{-6}m \end{aligned}$$

Number of tubes	Flux [$\frac{kg\ m}{m^3\ s}$]	$k_{int,x}$ [m^2]
0	$1.581 \cdot 10^{-7}$	$1.581 \cdot 10^{-19}$
770	$1.643 \cdot 10^{-7}$	$1.643 \cdot 10^{-19}$
6394	$3.057 \cdot 10^{-7}$	$3.057 \cdot 10^{-19}$
Fracture-controlled flow		
9995	$7.200 \cdot 10^{-6}$	$7.200 \cdot 10^{-18}$

Effect of large pores

Preliminary modelling

One-element simulation



$$k_{int} = \frac{\mu_w}{\rho_w} Flux \frac{\Delta x}{\Delta p} \quad \text{with} \quad \begin{aligned} \Delta x &= 2m \\ \Delta p &= 2\ MPa \\ \text{Aperture} &= 2.0 \cdot 10^{-6}m \end{aligned}$$

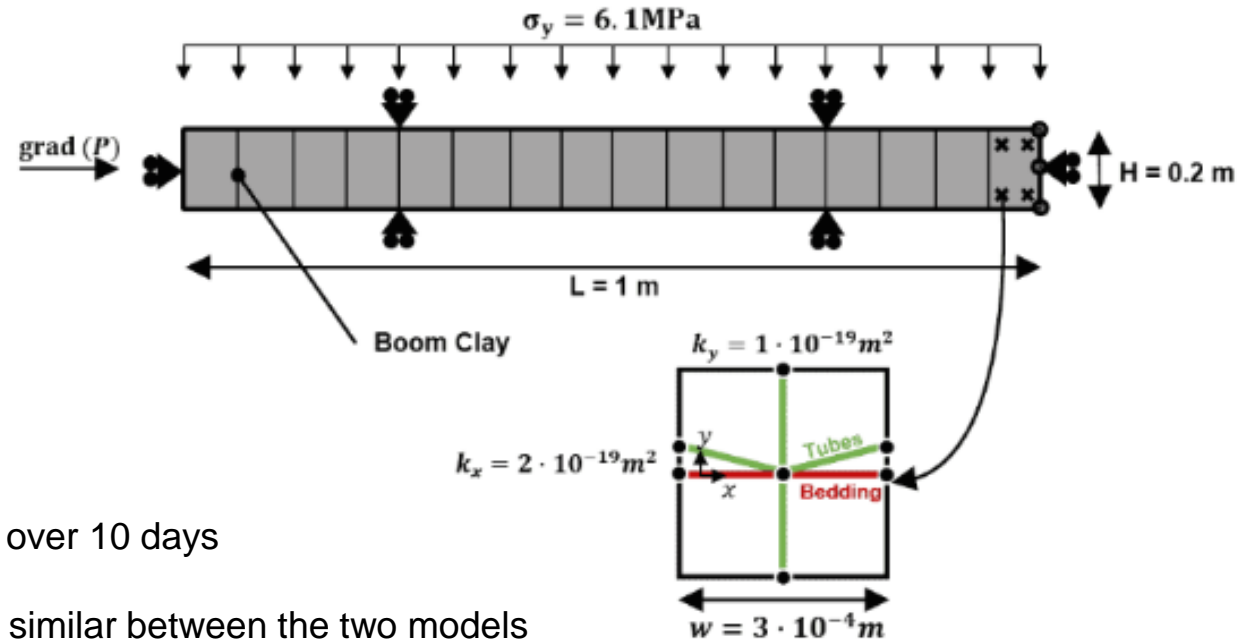
Number of tubes	Flux [$\frac{kg\ m}{m^3\ s}$]	$k_{int,x}$ [m^2]
0	$1.581 \cdot 10^{-7}$	$1.581 \cdot 10^{-19}$
770	$1.643 \cdot 10^{-7}$	$1.643 \cdot 10^{-19}$
6394	$3.057 \cdot 10^{-7}$	$3.057 \cdot 10^{-19}$
Fracture-controlled flow		
9995	$7.200 \cdot 10^{-6}$	$7.200 \cdot 10^{-18}$

Effect of large pores

Model verification

Comparison with a macro-scale THM coupled model

Geometry



$$P_{w0} = 0.6\text{ MPa}$$

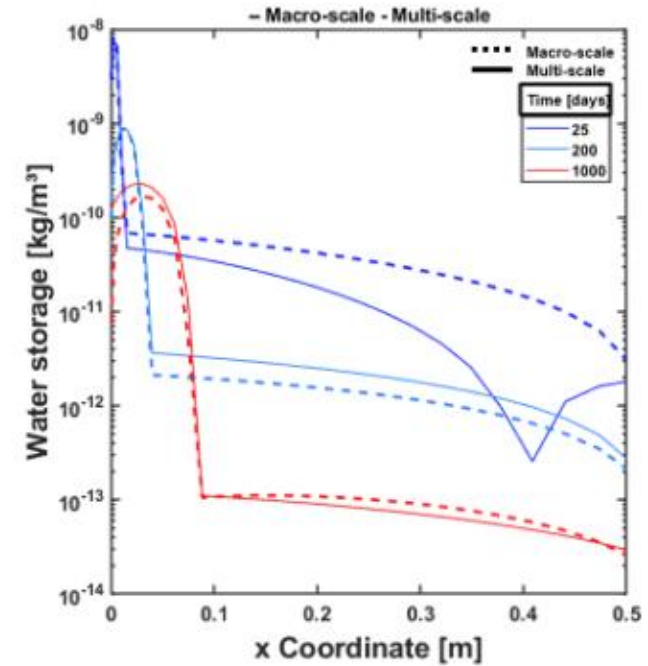
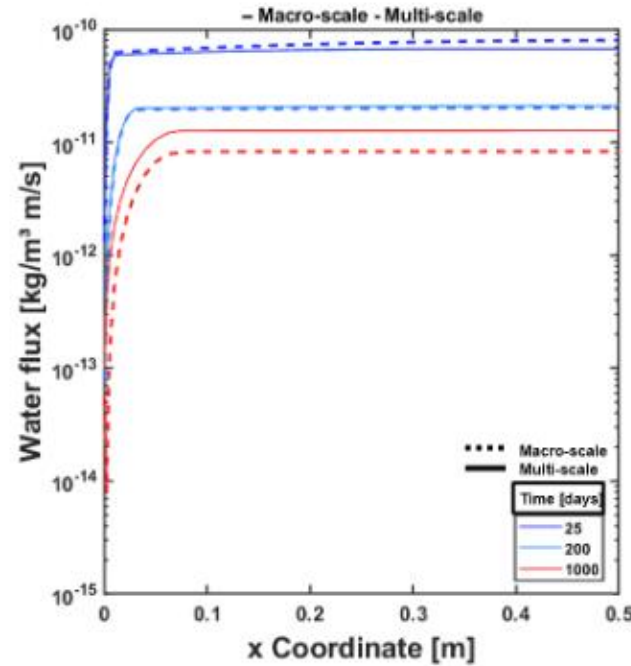
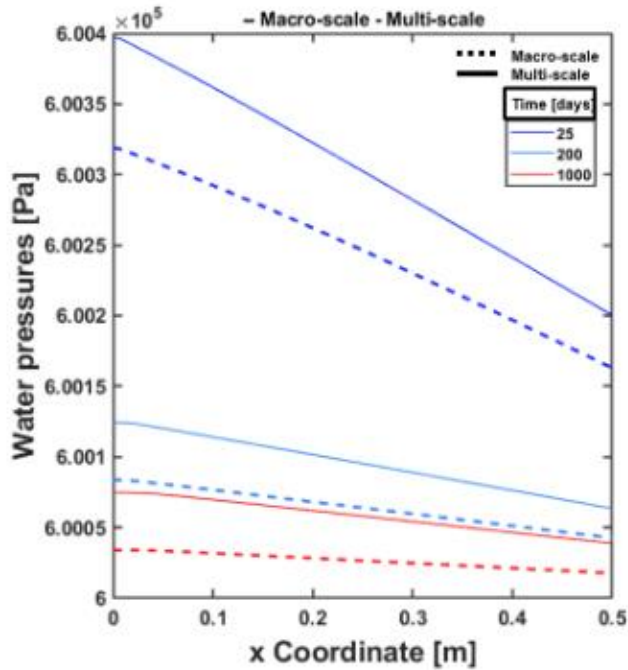
$$P_{g0} = 0.1\text{ MPa} \rightarrow P_g = 1.0\text{ MPa over 10 days}$$

All the parameters are taken similar between the two models

Model verification

Comparison with a macro-scale THM coupled model

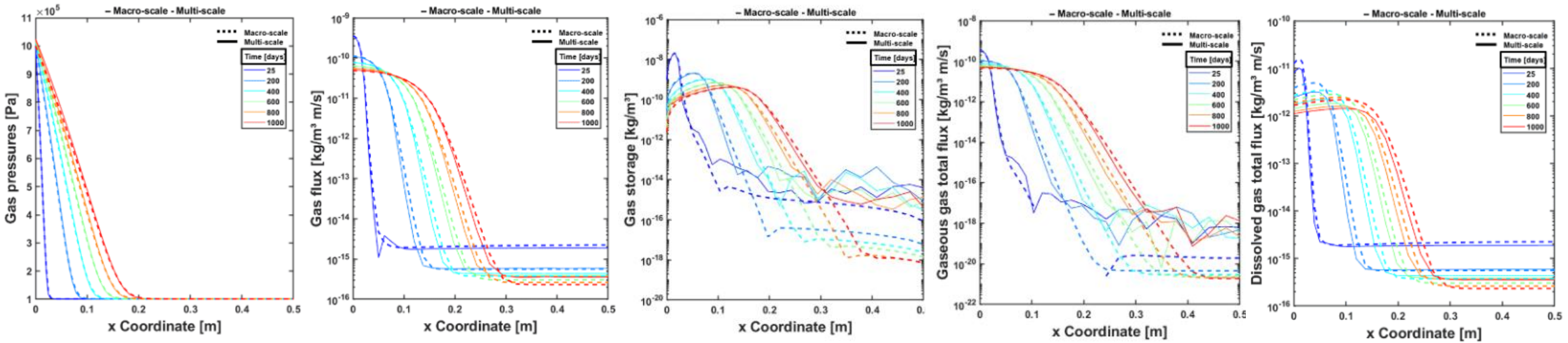
Water-related results



Model verification

Comparison with a macro-scale THM coupled model

Gas-related results





Content

- ① Context
- ② From experimental evidence to modelling
- ③ Multi-scale modelling approach
- ④ Preliminary modelling
- ⑤ Modelling gas injection experiment
- ⑥ Conclusions

Gas injection experiment

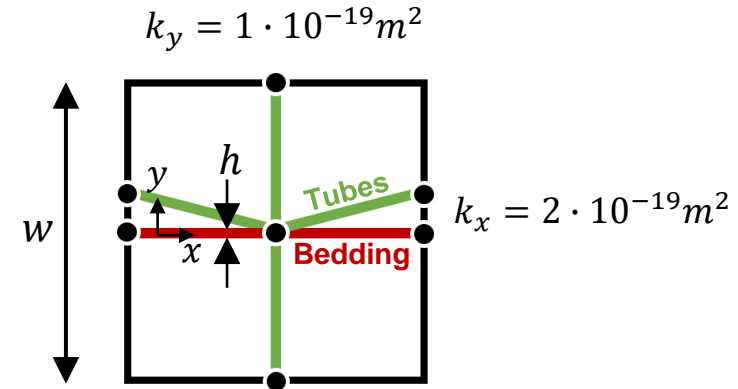
Characterisation of the microstructure parameters

► 1. Size of the REV

Bedding plane separation
 $w = 300 \mu m$

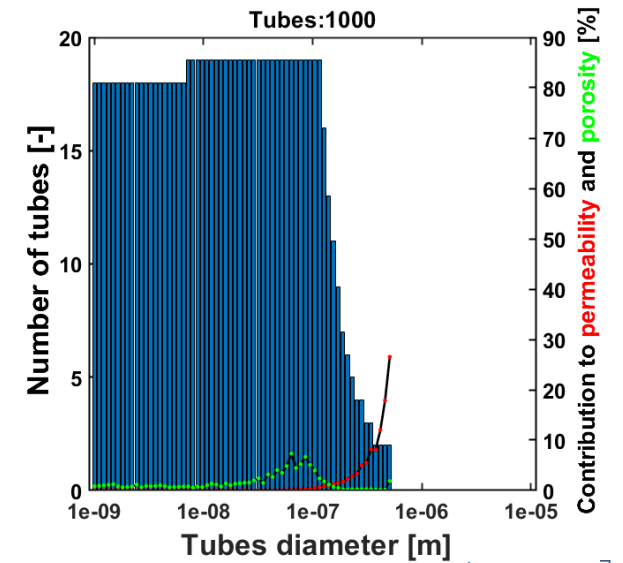
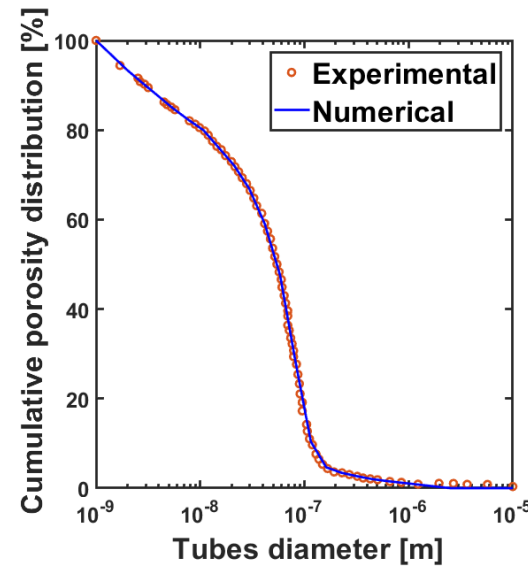
Experimental estimations of bedding plane separation,
 from *Gonzalez-Blanco (2017)*

FESEM	μ -CT
150 – 270 μm	410 – 560 μm



► 2. Macroporosity

Fitting of the pore size distribution
 Effect of small-size pores
 (Tortuosity = Calibration factor)



Gas injection experiment

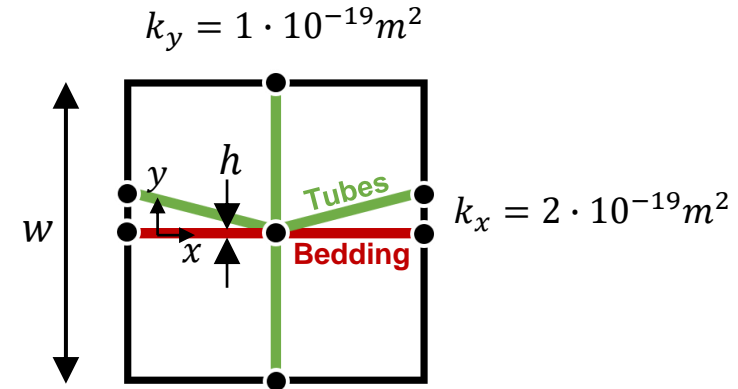
Characterisation of the microstructure parameters

► 1. Size of the REV

Bedding plane separation
 $w = 300 \mu m$

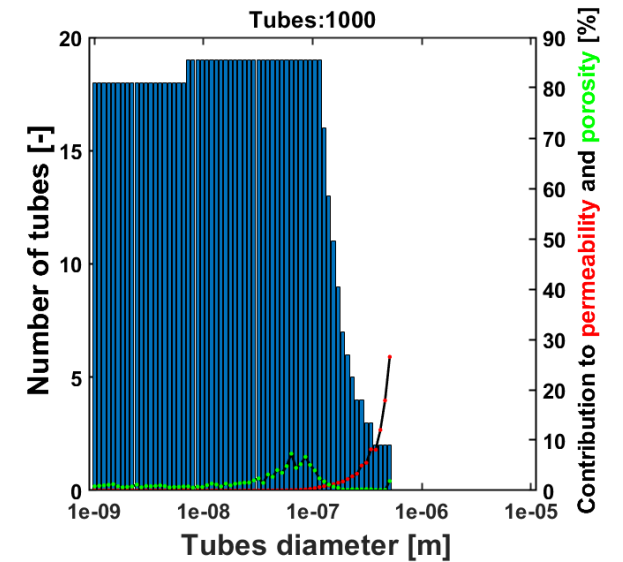
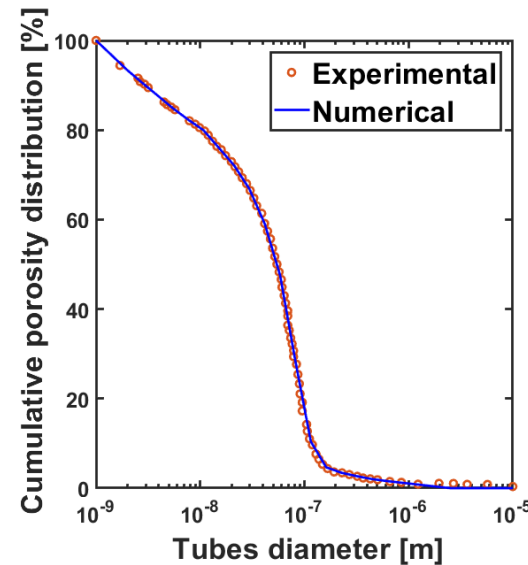
Experimental estimations of bedding plane separation,
 from Gonzalez-Blanco (2017)

FESEM	μ -CT
150 – 270 μm	410 – 560 μm



► 2. Macroporosity

Fitting of the pore size distribution
 Effect of small-size pores
 (Tortuosity = Calibration factor)



► 3. Intrinsic permeability Effect of large-size pores

Fracture aperture

$$k_{x,frac,0} = 10^{-19} m^2$$

$$\rightarrow h_0 = \sqrt[3]{12 w k}$$

Macropores

$$k_x = \frac{\pi}{8} \left(\frac{D}{2}\right)^4 \left(\frac{1}{w^2}\right) + \frac{k_{x,frac}}{12} \left(\frac{h}{w}\right)$$

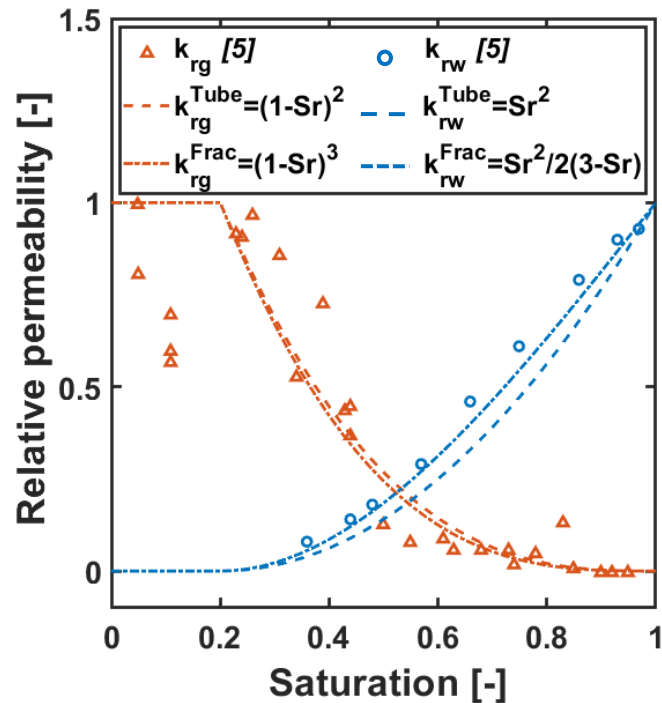
$$k_y = \frac{\pi}{8} \left(\frac{D}{2}\right)^4 \left(\frac{1}{w^2}\right)$$

Gas injection experiment

Characterisation of the microstructure parameters

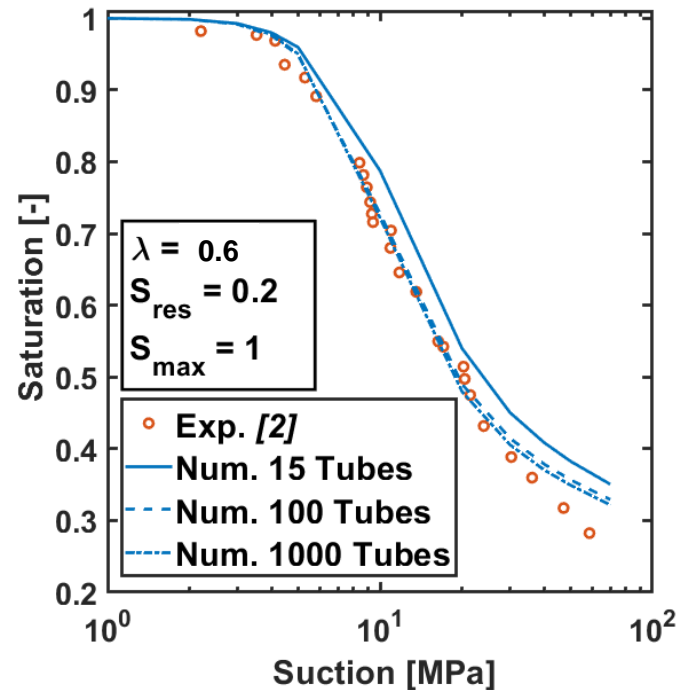
► 4. Relative permeability curves

Yuster et al. (1951)



► 5. Retention curve

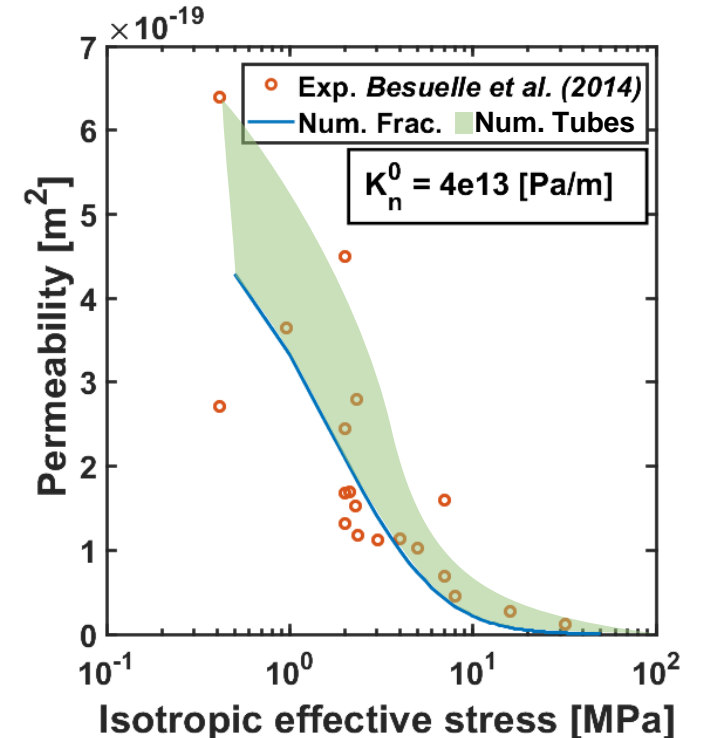
Van Genuchten (1980)



$$S_r = S_{res} + (S_{max} - S_{res}) \left(1 + \left(\frac{s}{P_e} \right)^{\frac{1}{1-\lambda}} \right)^{-\lambda}$$

► 6. Normal stiffness of the fracture

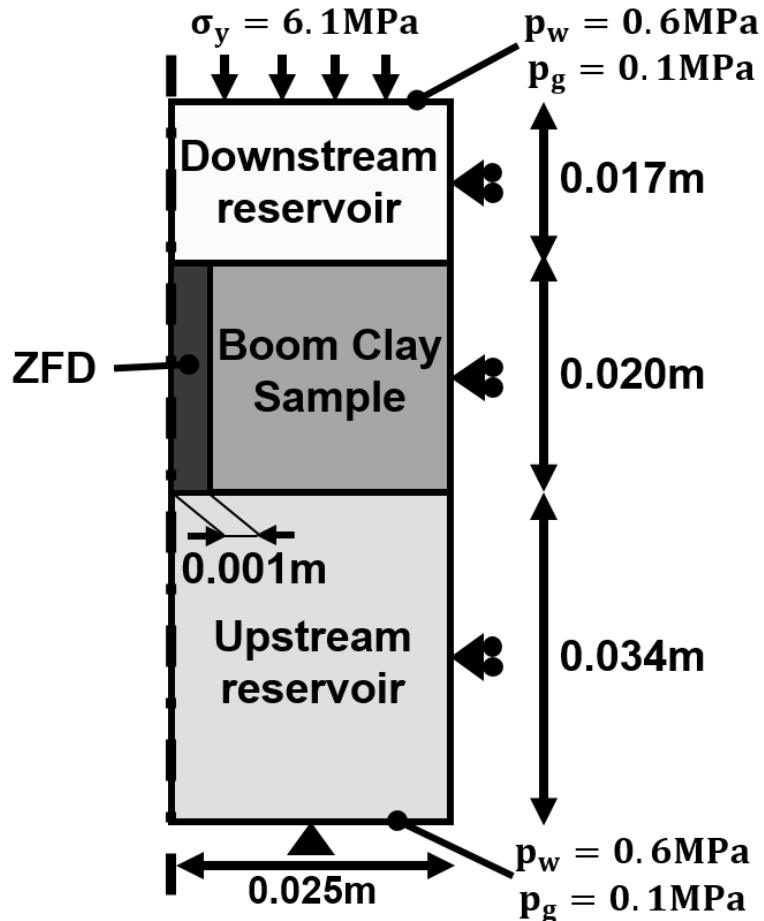
Goodman (1976)



$$\Delta\sigma' = K_n \Delta h \quad \text{with} \quad K_n = \frac{K_n^0}{\left(1 + \frac{\Delta h}{h_0}\right)^2}$$

Gas injection experiment

Geometry and boundary conditions



Parameters

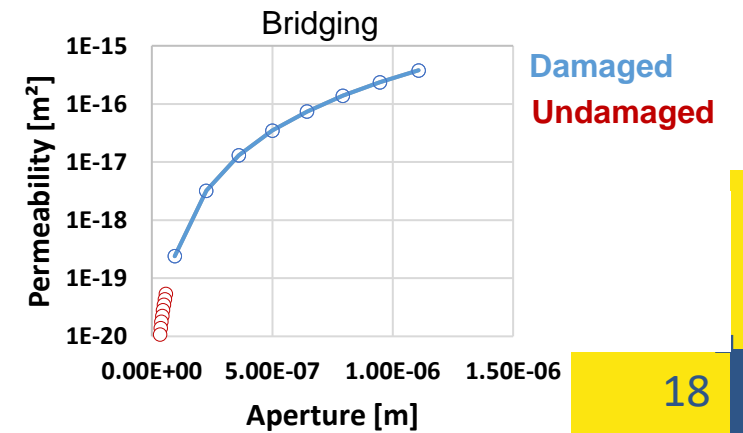
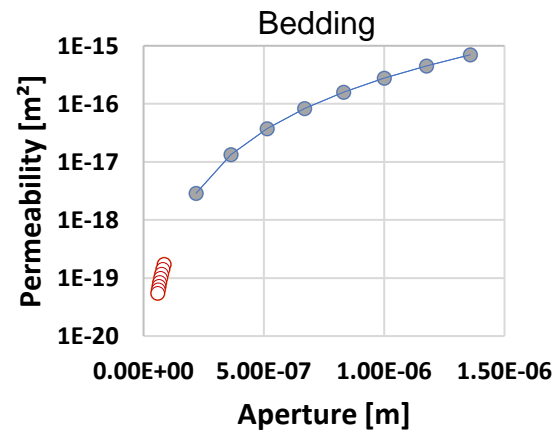
Reservoirs

- Stiff elements: $E = 10000\text{MPa}$, $\nu = 0.3$
- Highly conductive: $n = 0.5$, $k = 10^{-10}\text{m}^2$
- Flat retention curve: $P_{\text{entry}} = 0.01\text{MPa}$

Boom Clay matrix

- Mechanical: $E = 200 - 400\text{MPa}$, $\nu = 0.33$
- Hydraulic:
 - Initial aperture: $0.80 - 1.27 \cdot 10^{-7}\text{m}$
 - Initial permeability: $2.0 - 4.0 \cdot 10^{-19}\text{m}^2$
 - Initial porosity: 0.363

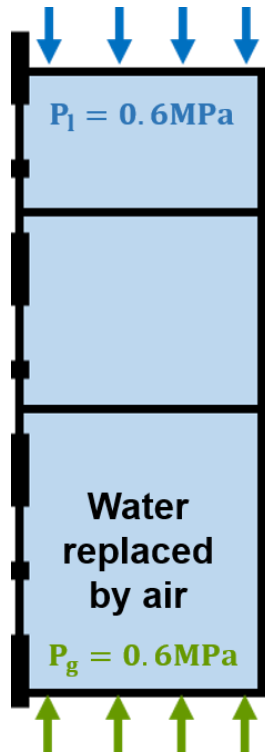
Boom Clay Zone of Fracture Development (ZFD)



Gas injection experiment

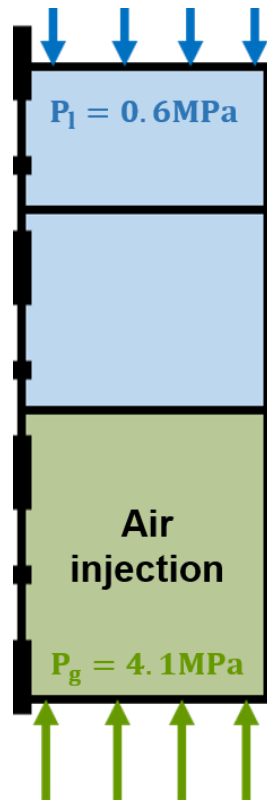
Simulation stages

Stage 1



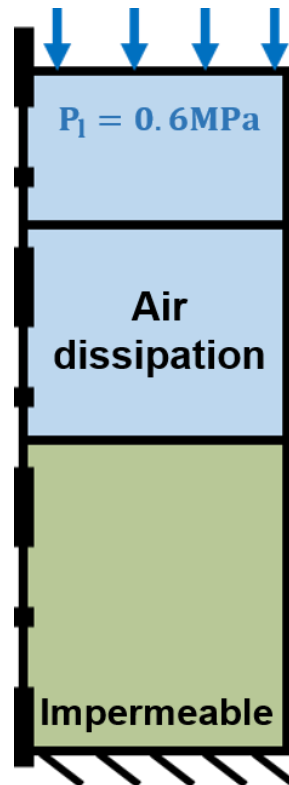
0-500 [min]

Stage 2

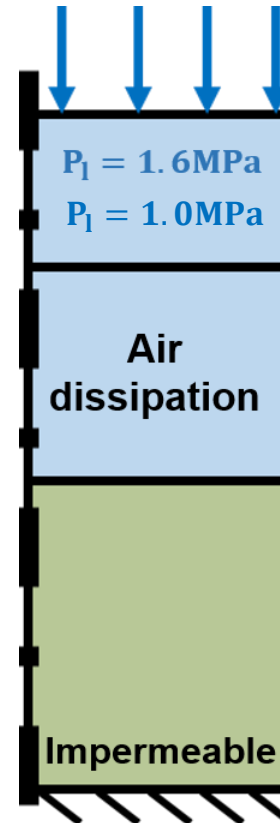


500-745 [min]

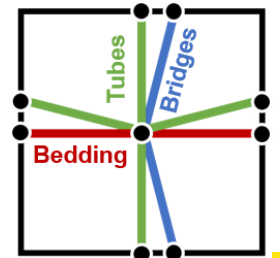
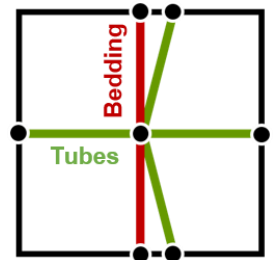
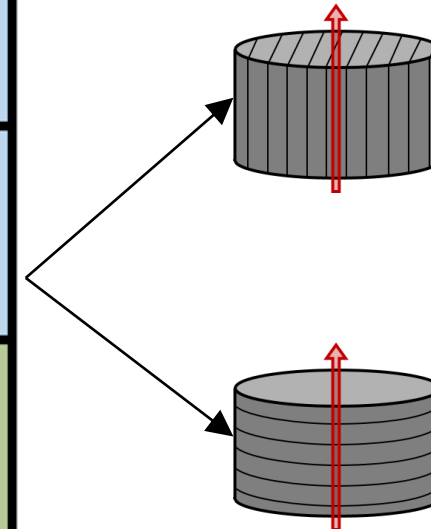
Stage 3



745-1080 [min]

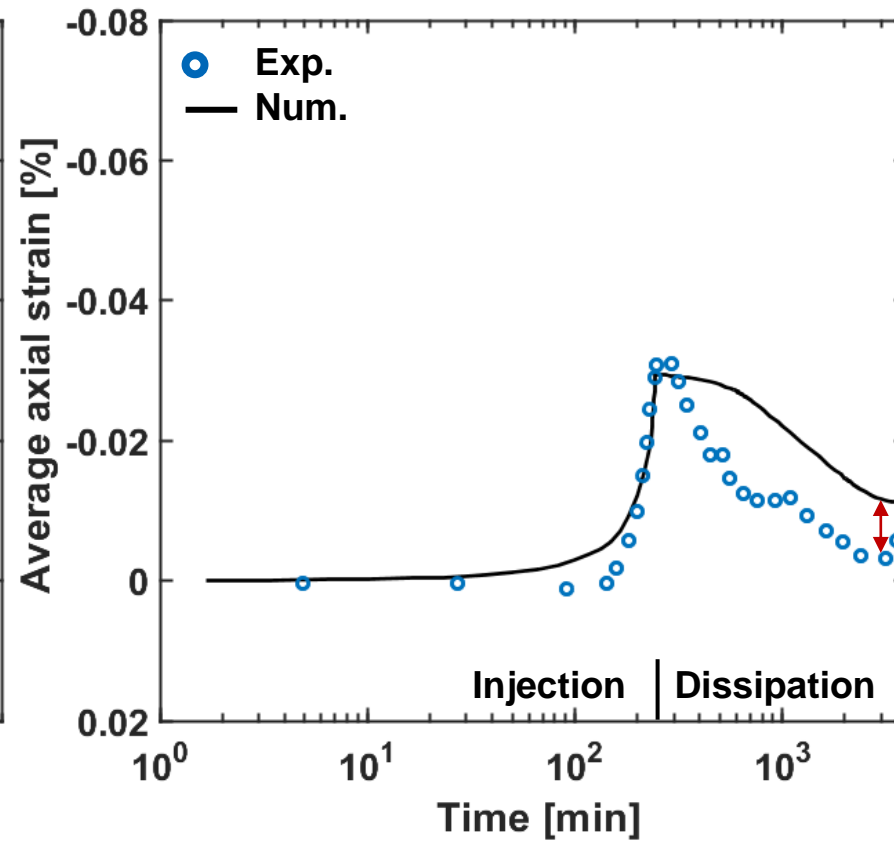
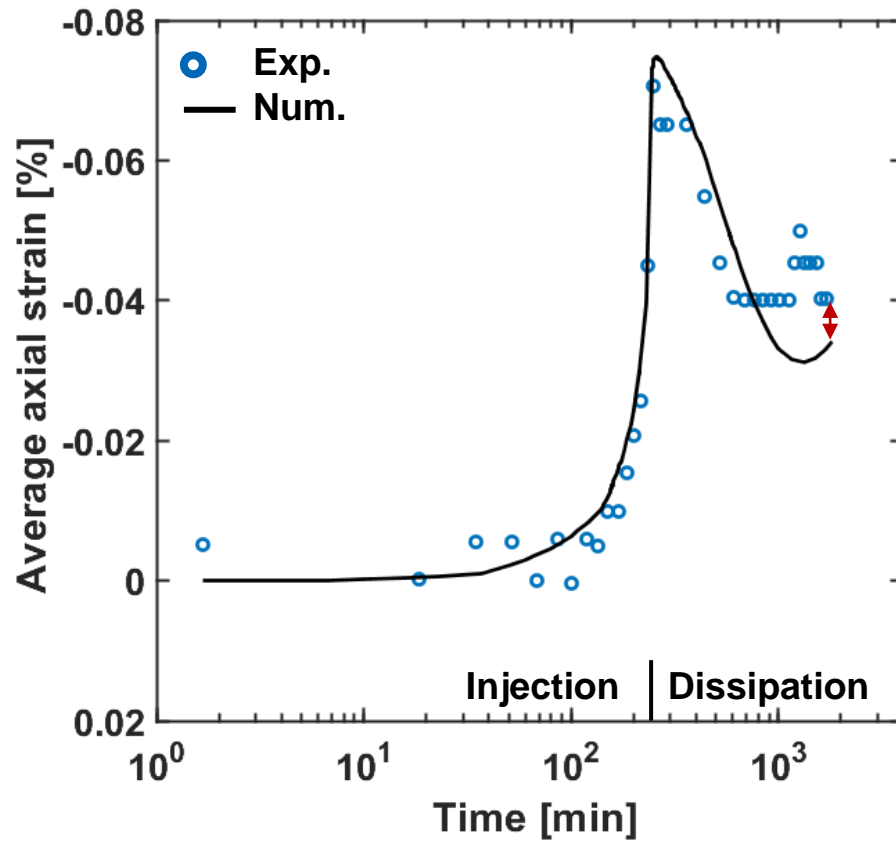
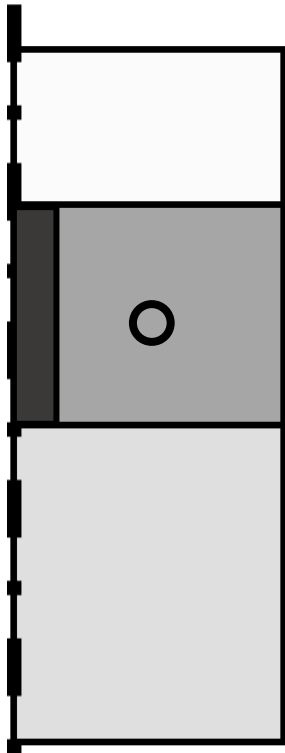
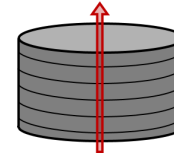
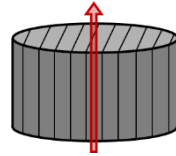


1080-2300 [min]



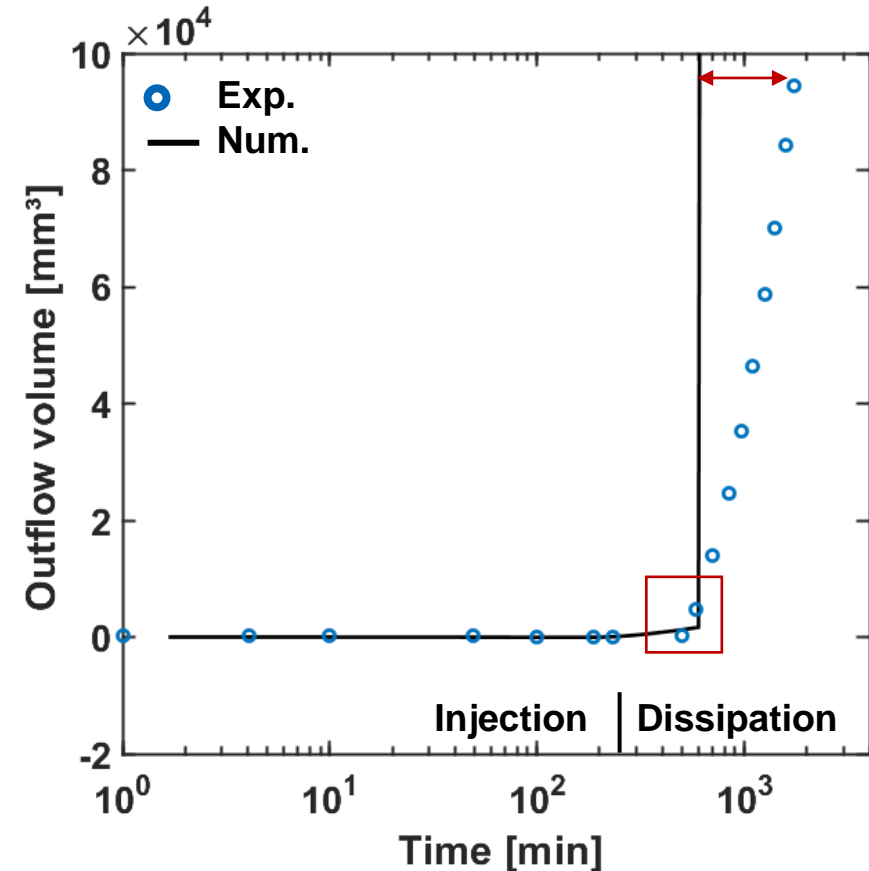
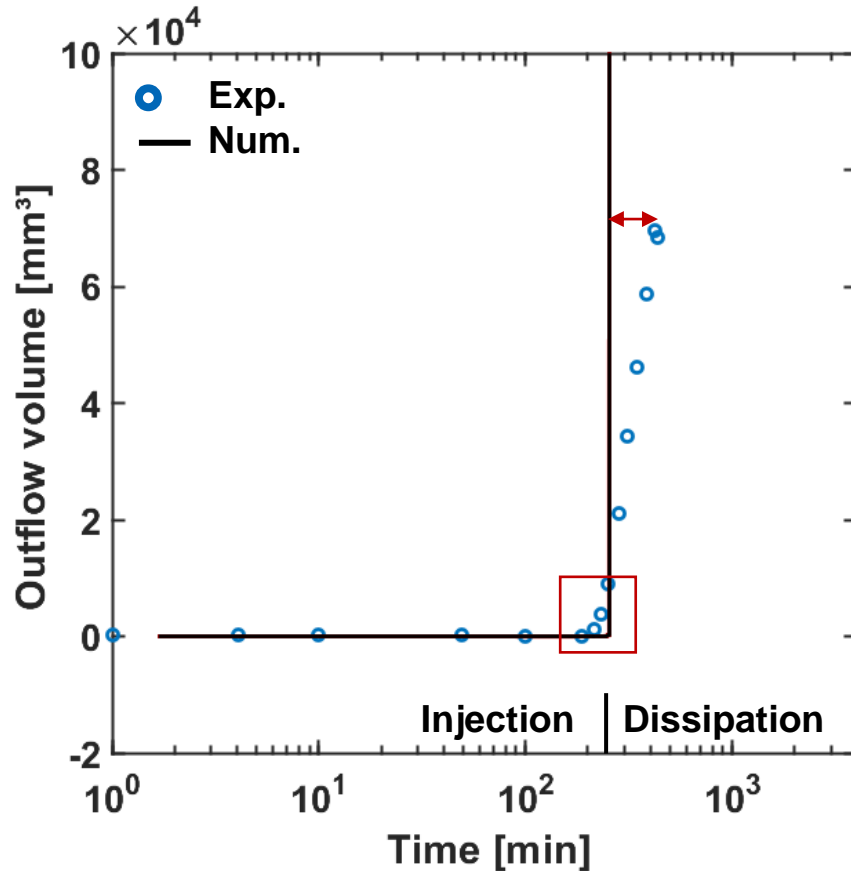
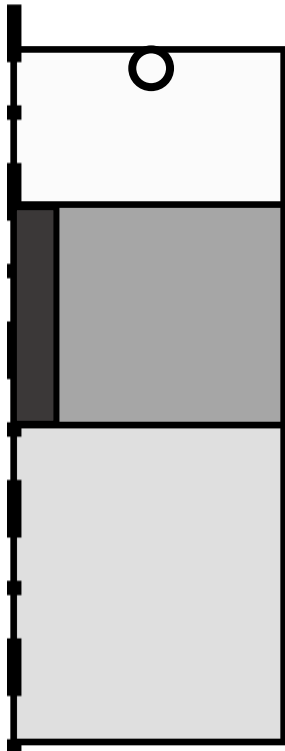
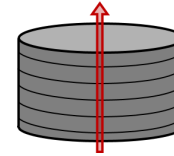
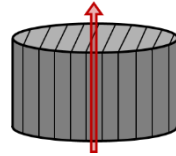
Gas injection experiment

Average axial strain



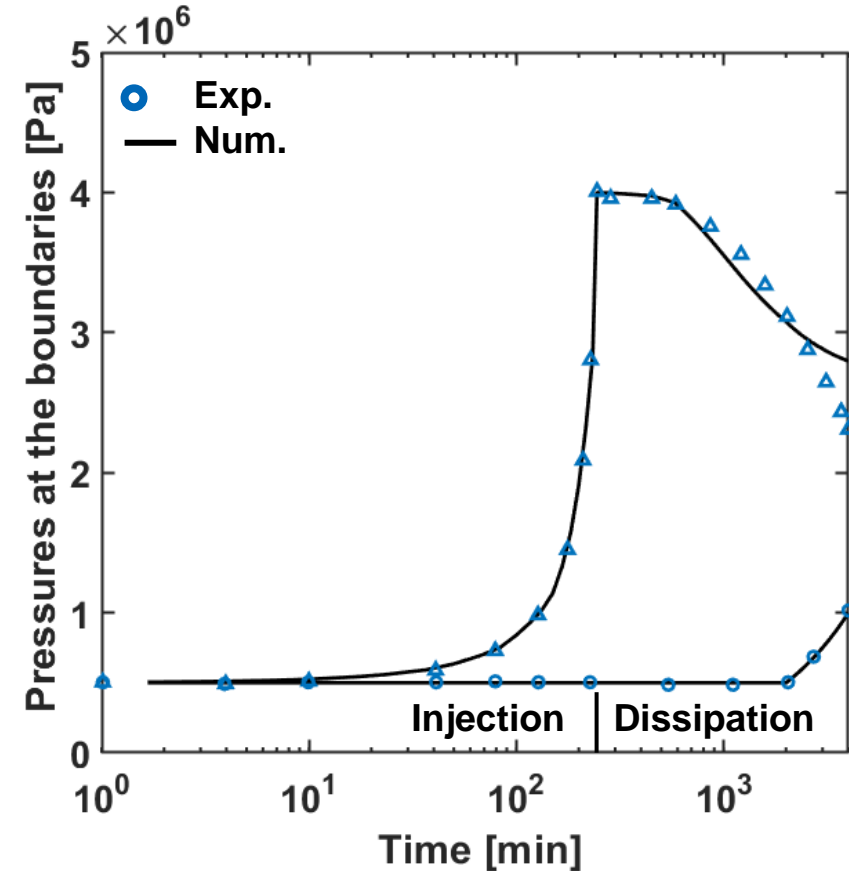
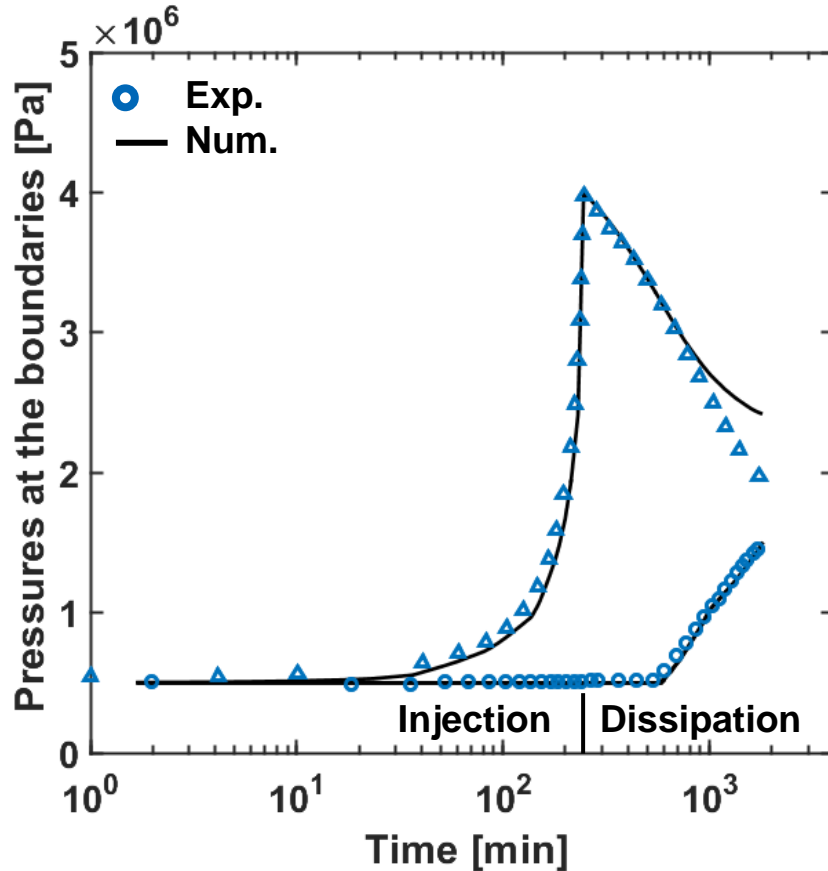
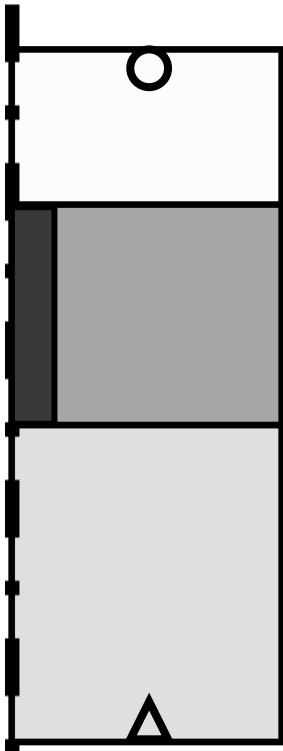
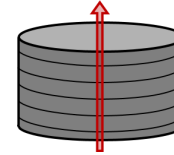
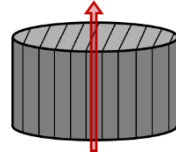
Gas injection experiment

Outflow volume



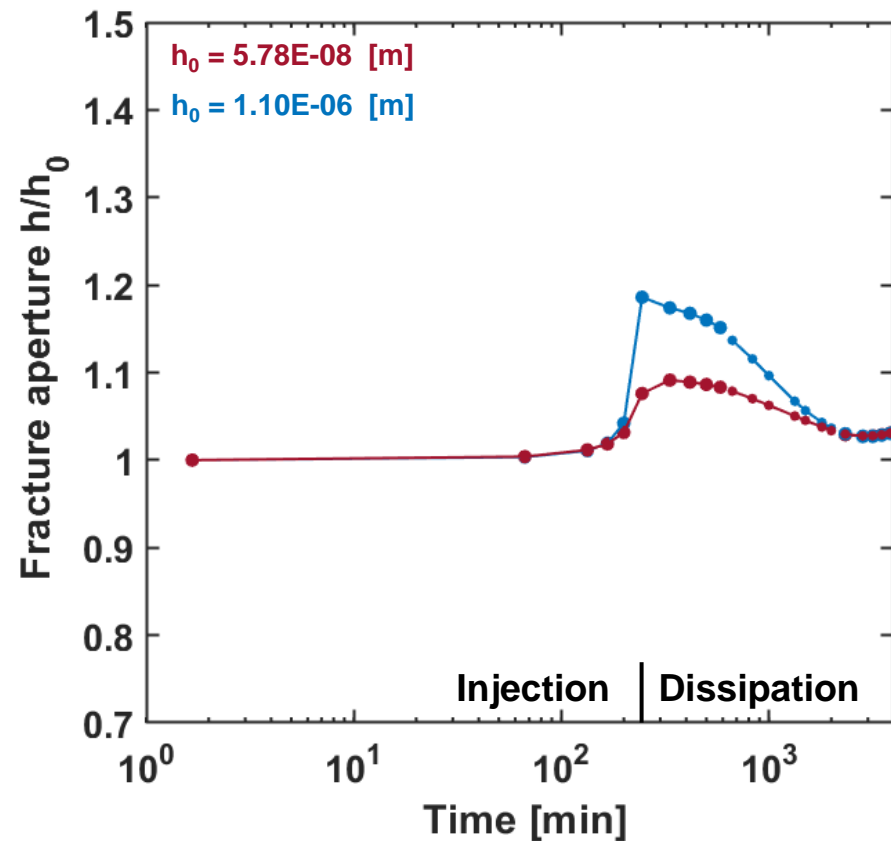
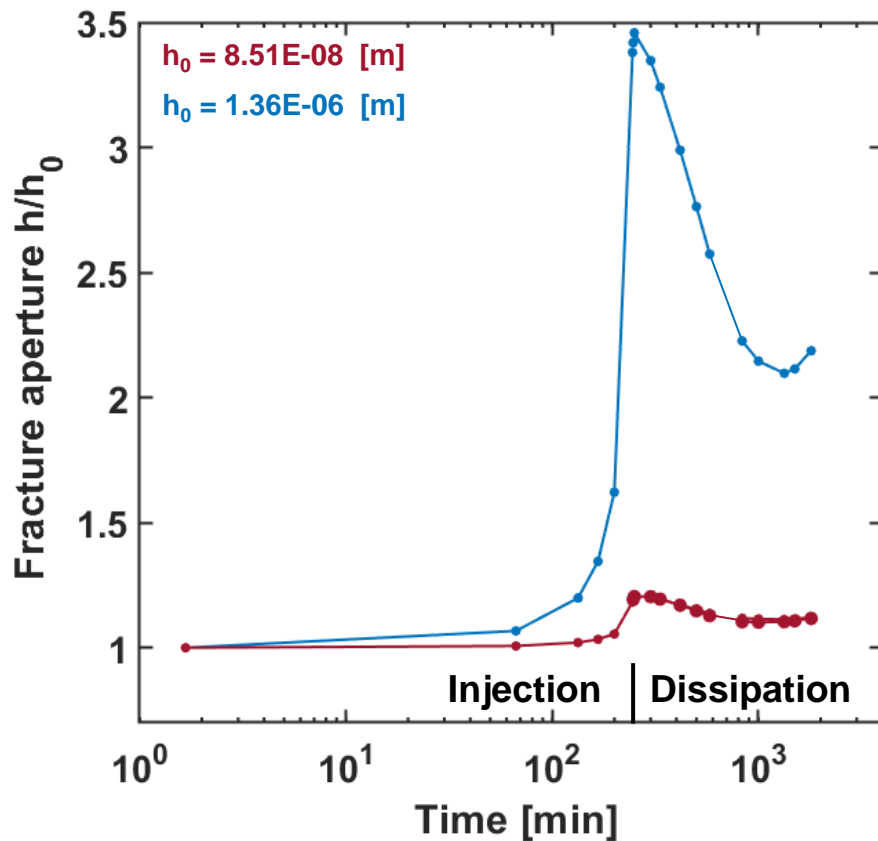
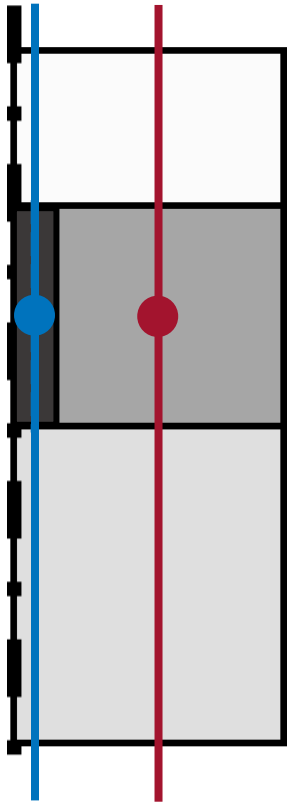
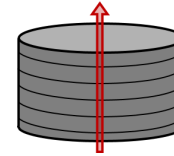
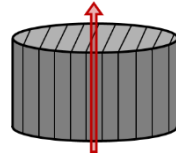
Gas injection experiment

Injection and recovery pressures



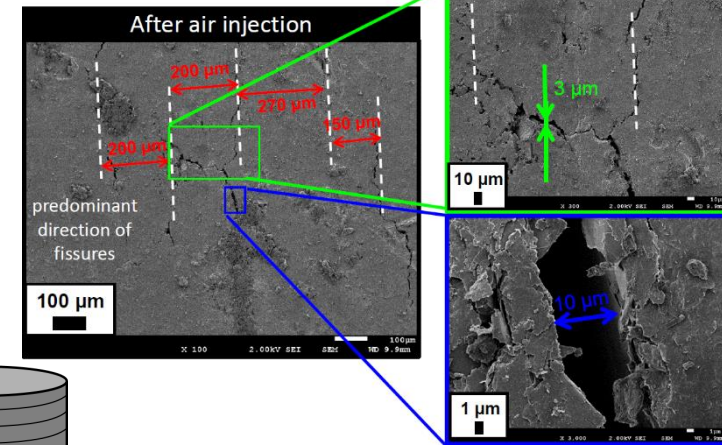
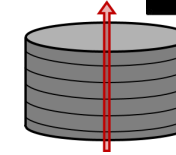
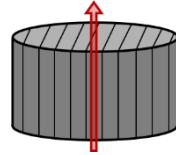
Gas injection experiment

Fracture aperture



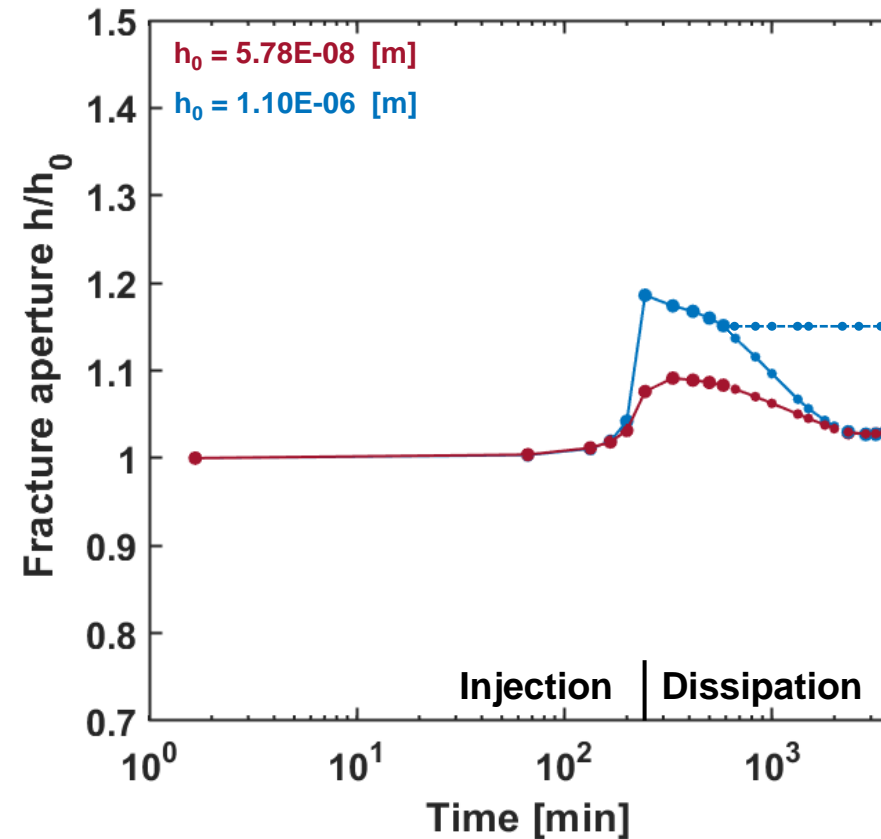
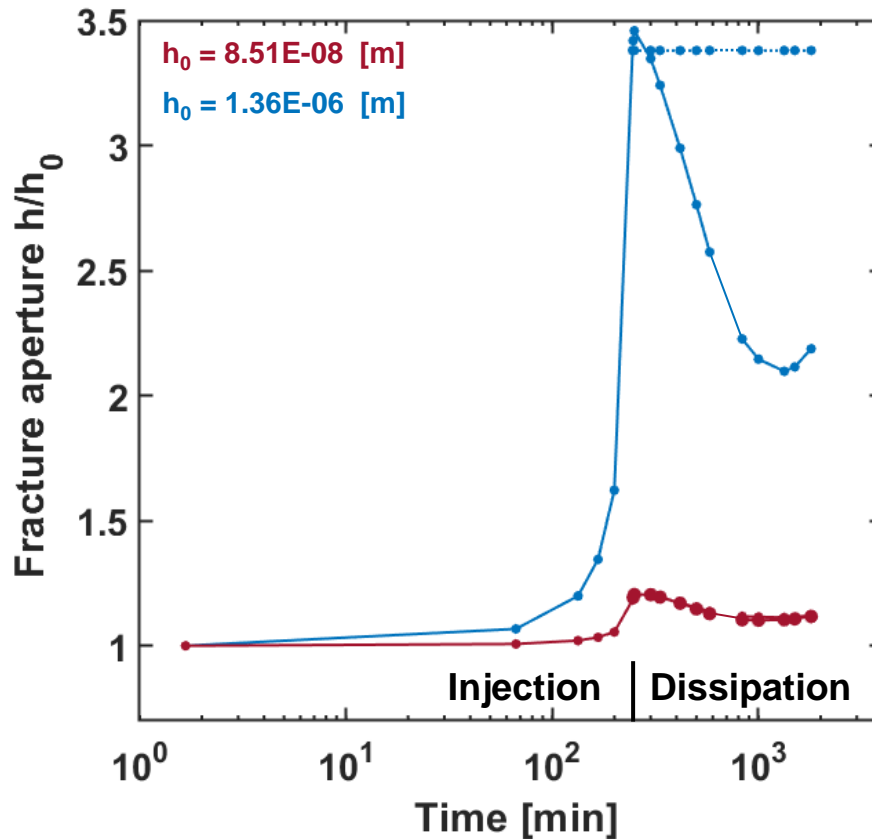
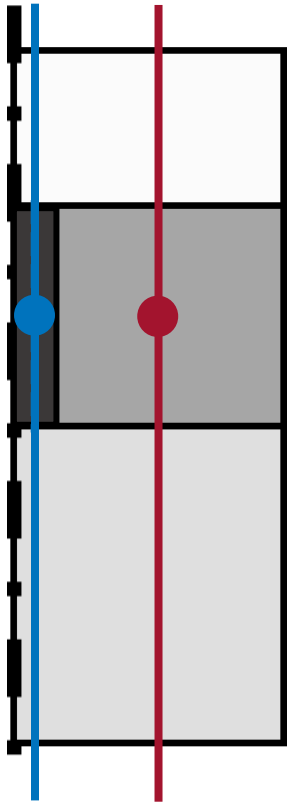
Gas injection experiment

Fracture aperture



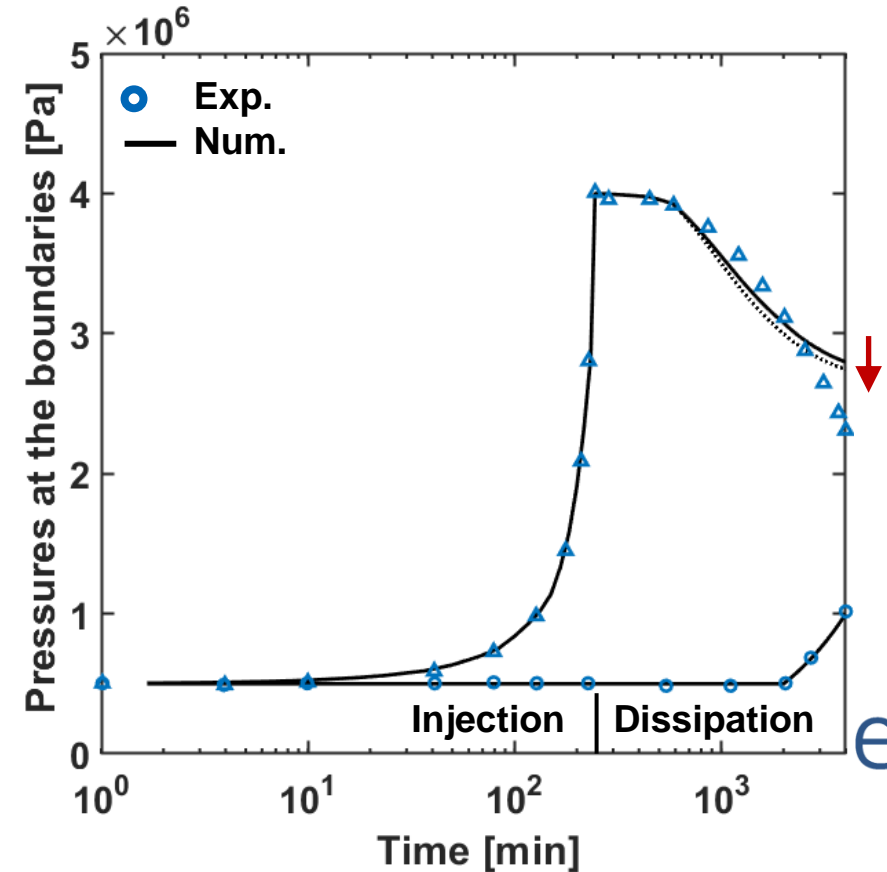
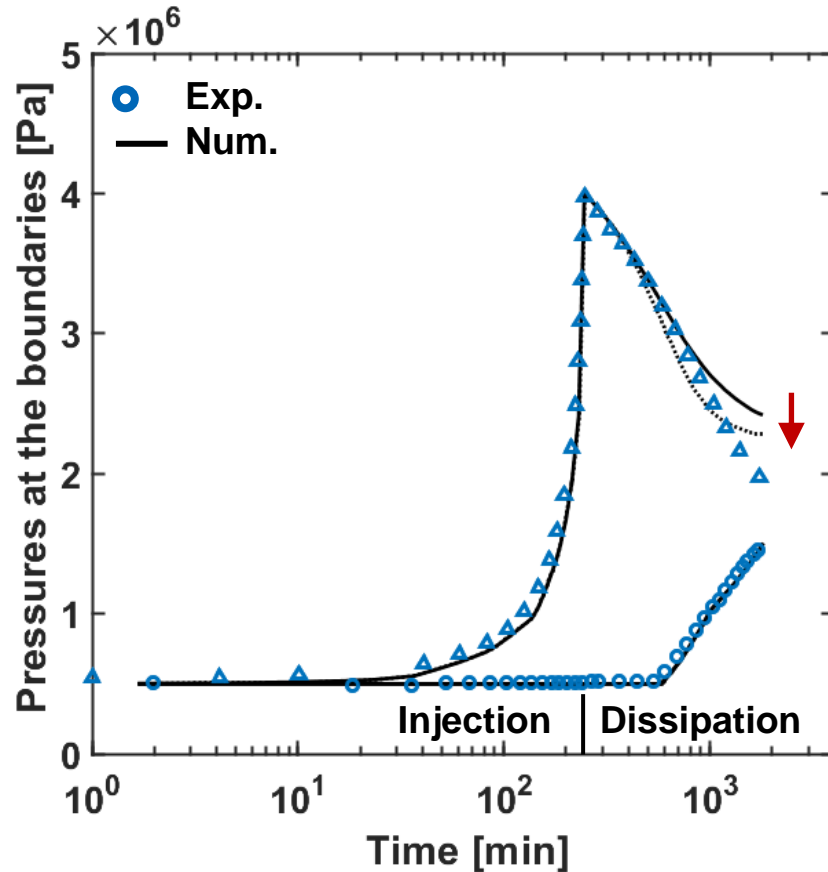
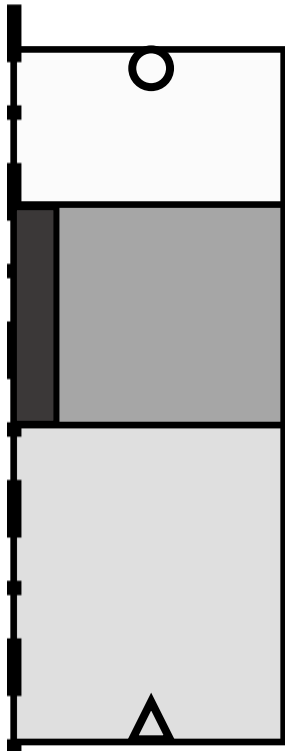
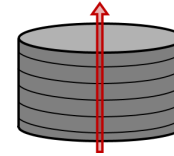
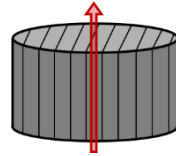
Experimental observations:
Opened fractures after injection

Gonzalez-Blanco & Romero (2022)



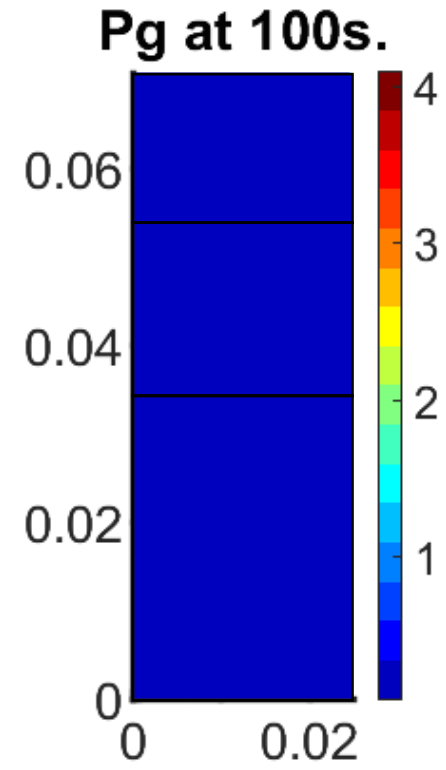
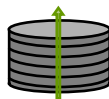
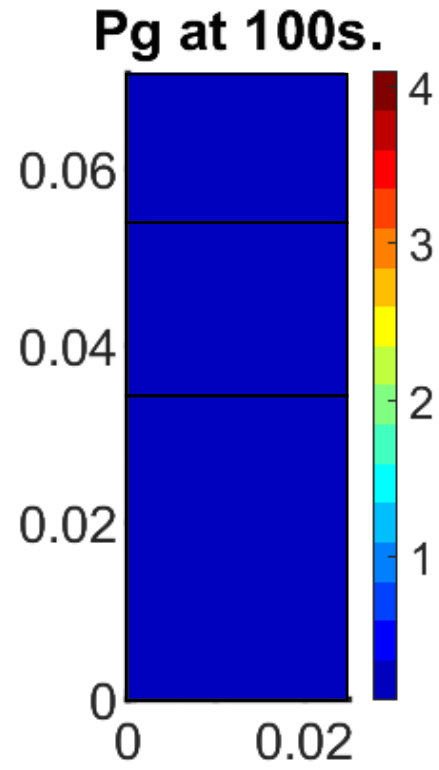
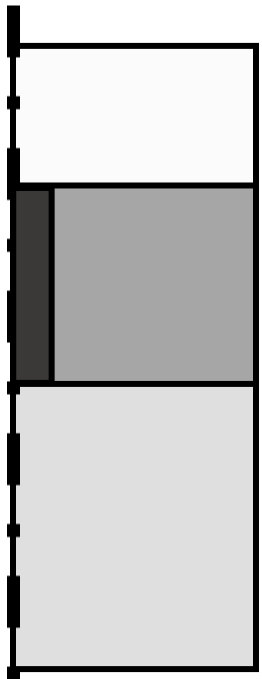
Gas injection experiment

Injection and recovery pressures



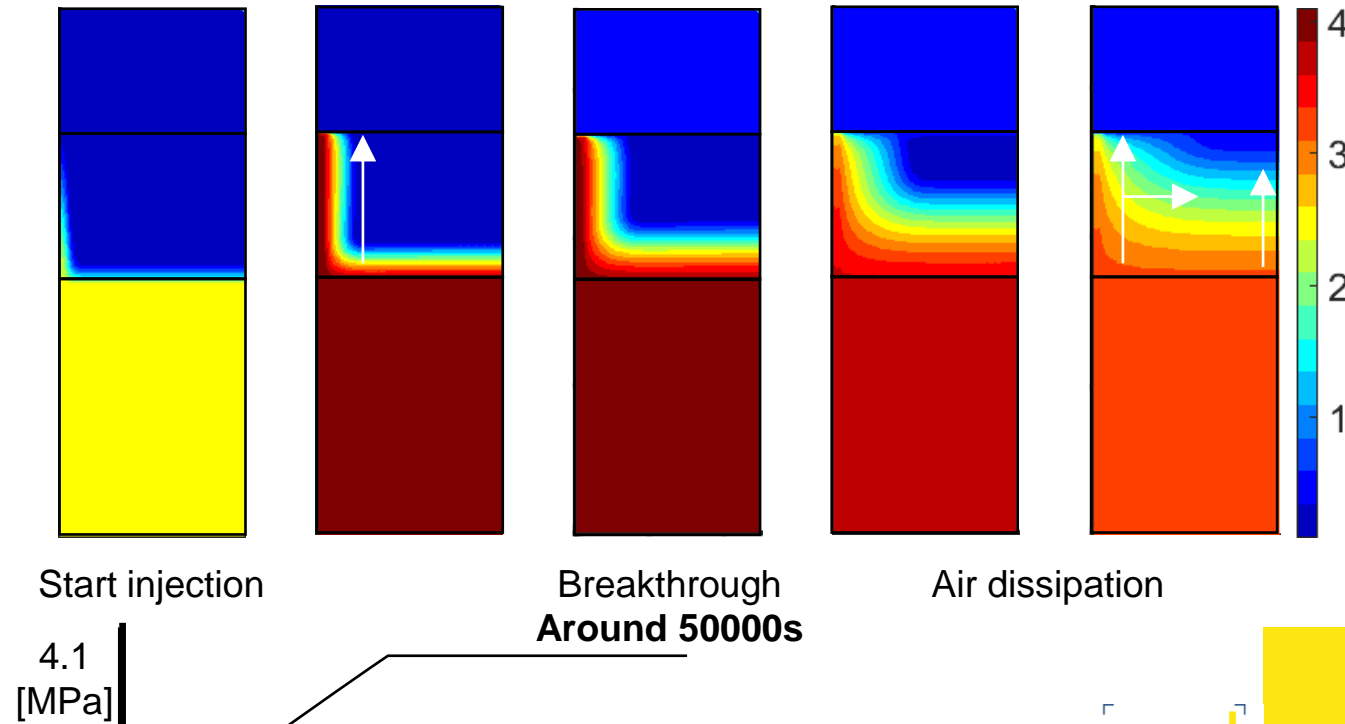
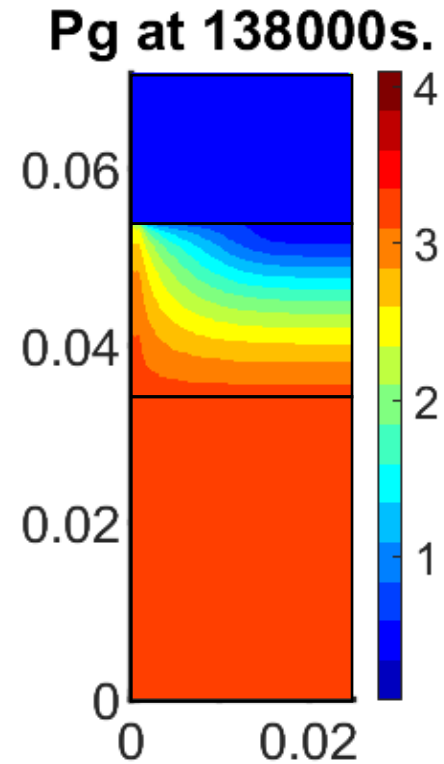
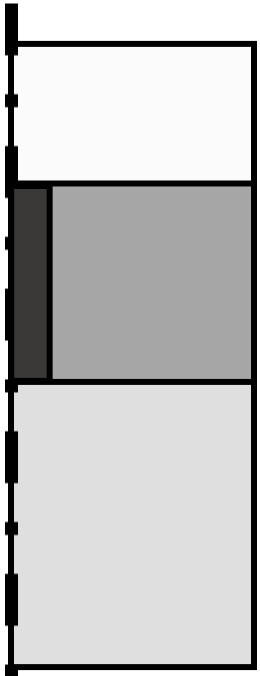
Gas injection experiment

Injection and recovery pressures



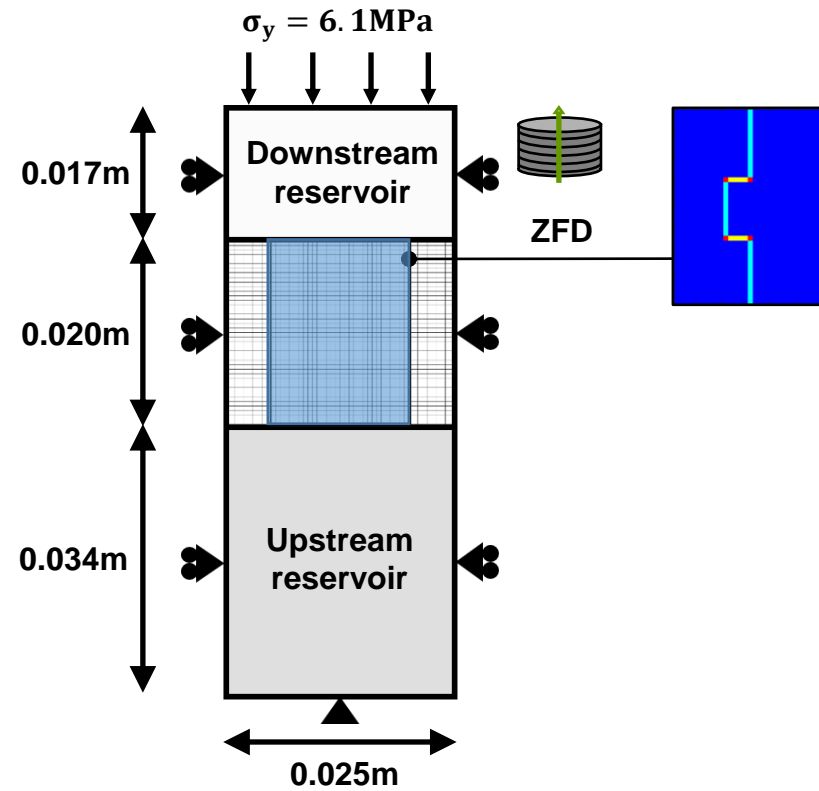
Gas injection experiment

Injection and recovery pressures

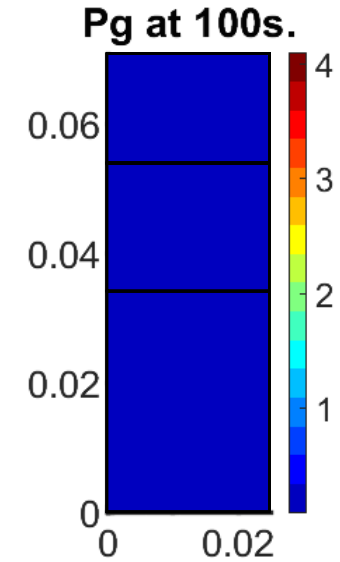


Gas injection experiment

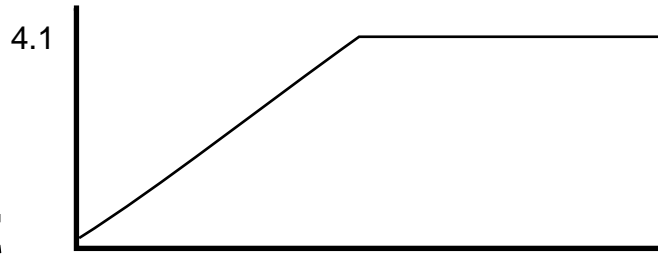
Effect of the connectivity of the planes



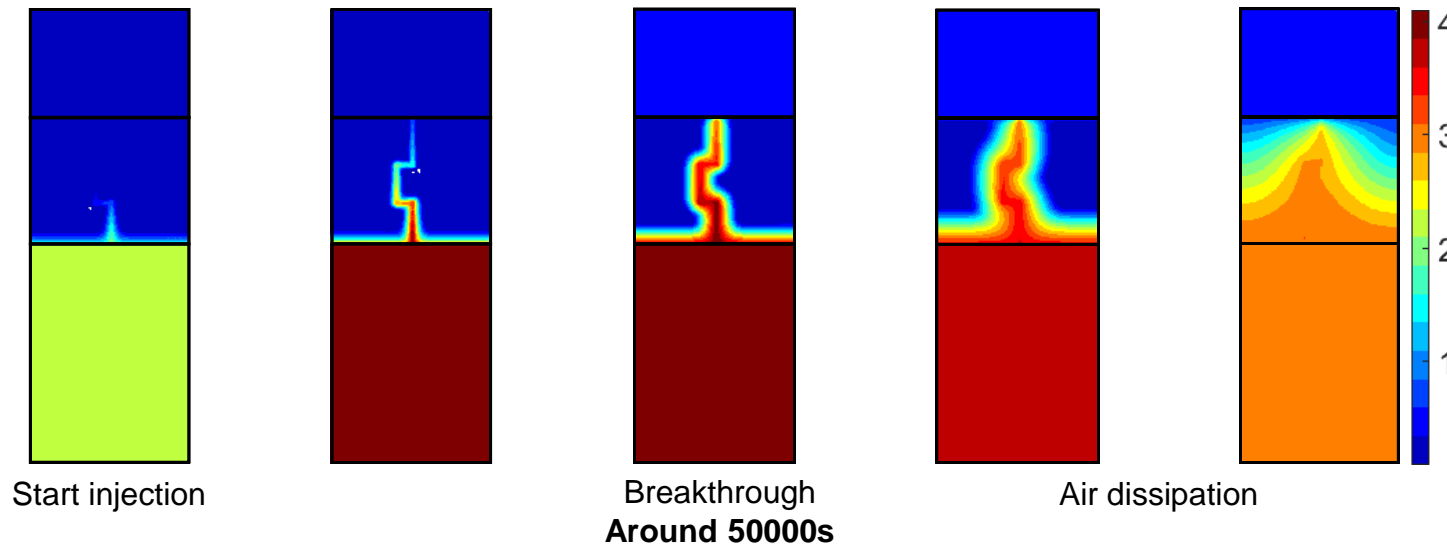
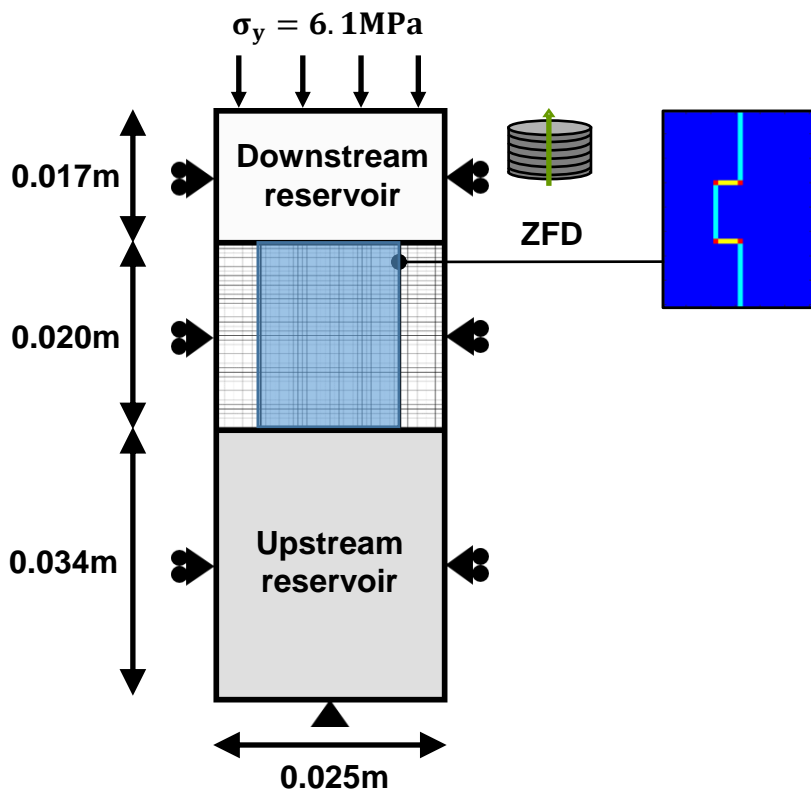
- Undisturbed Boom Clay
- Disturbed bridging planes
- Disturbed bedding and bridging planes
- Disturbed bedding planes



Gas injection experiment

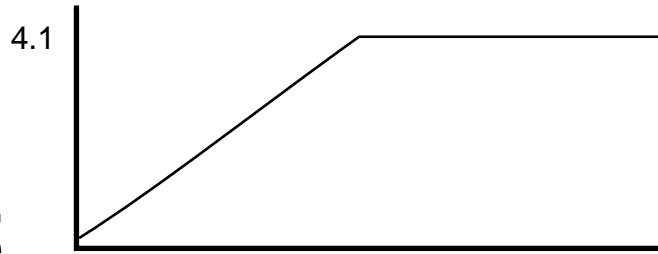


Effect of the connectivity of the planes

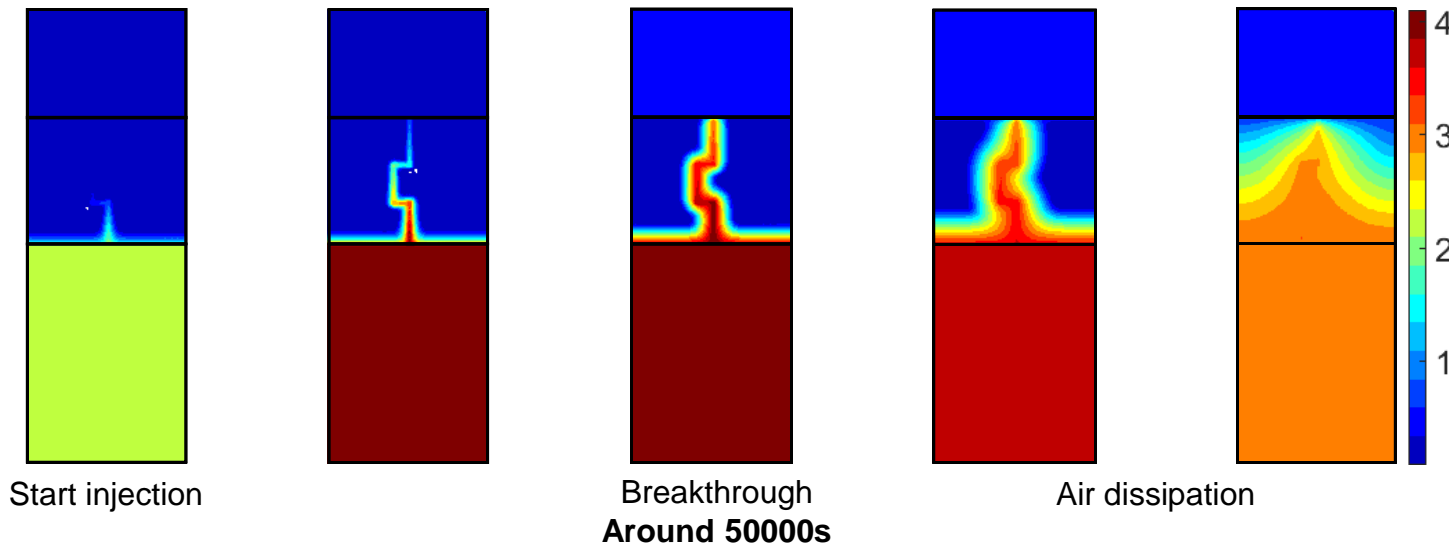
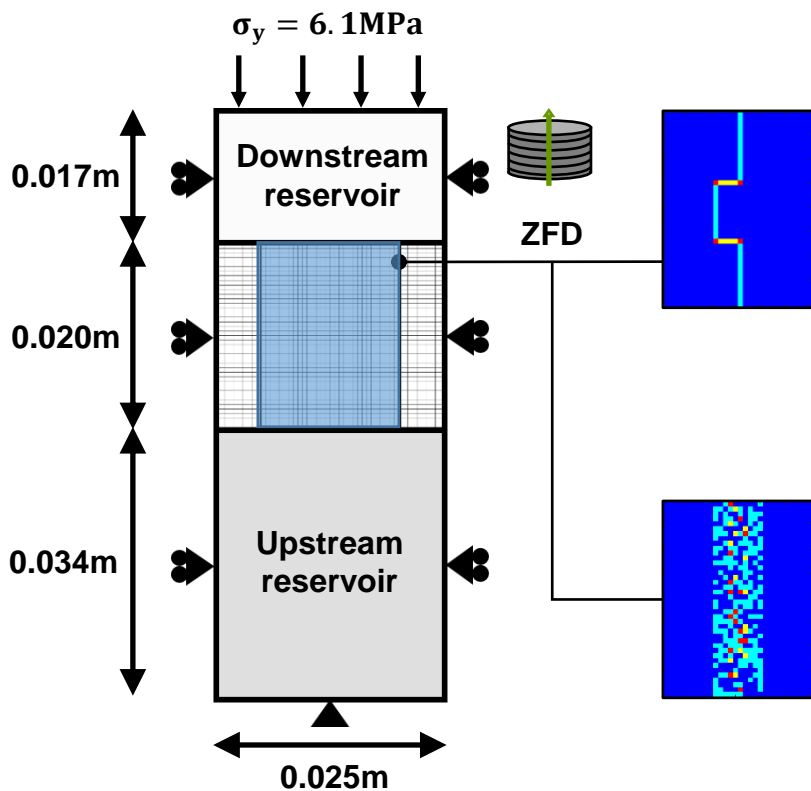


- Undisturbed Boom Clay
- Disturbed bridging planes
- Disturbed bedding and bridging planes
- Disturbed bedding planes

Gas injection experiment

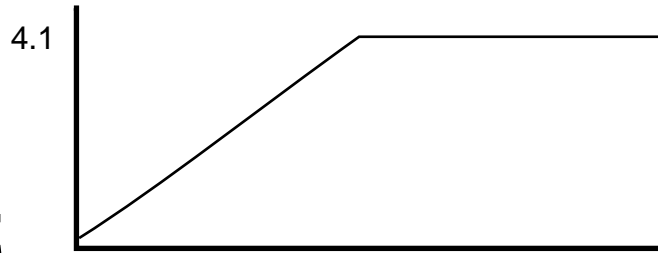


Effect of the connectivity of the planes

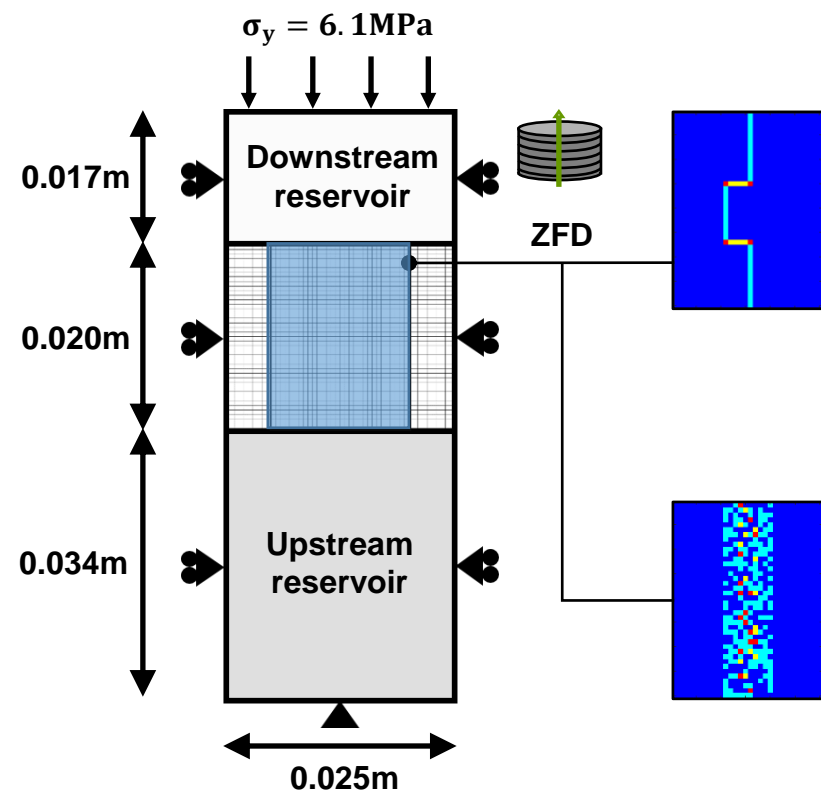


- Undisturbed Boom Clay
- Disturbed bridging planes
- Disturbed bedding and bridging planes
- Disturbed bedding planes

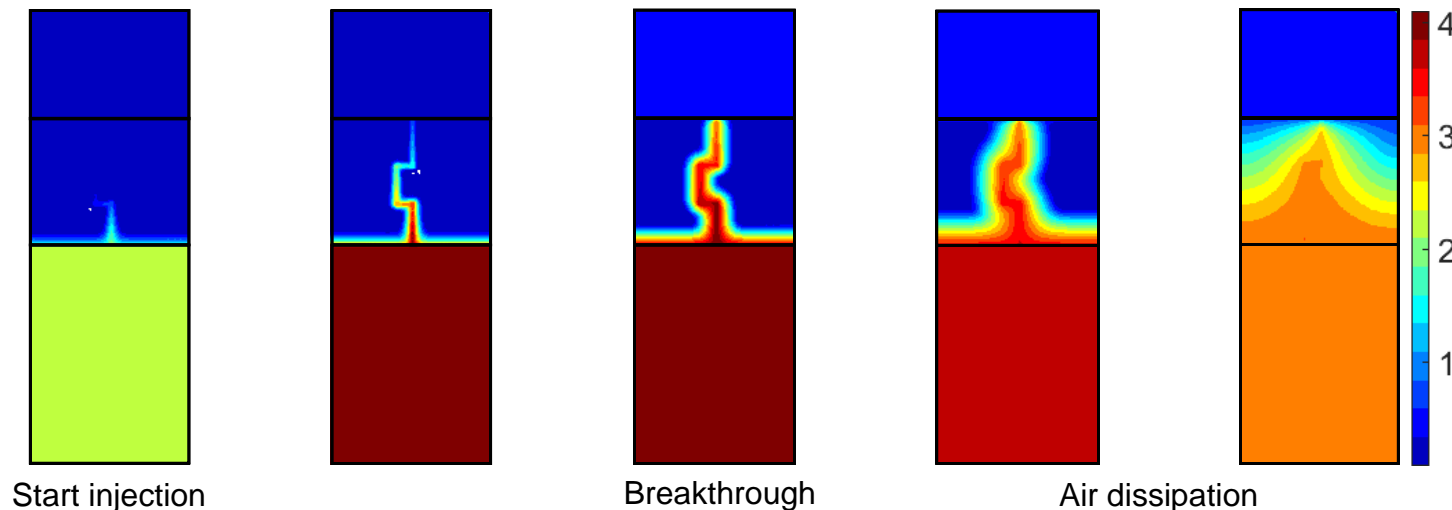
Gas injection experiment



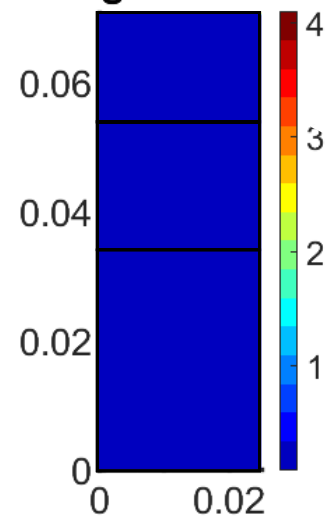
Effect of the connectivity of the planes



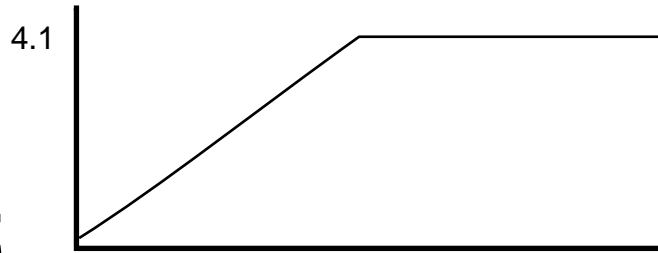
- Undisturbed Boom Clay
- Disturbed bridging planes
- Disturbed bedding and bridging planes
- Disturbed bedding planes



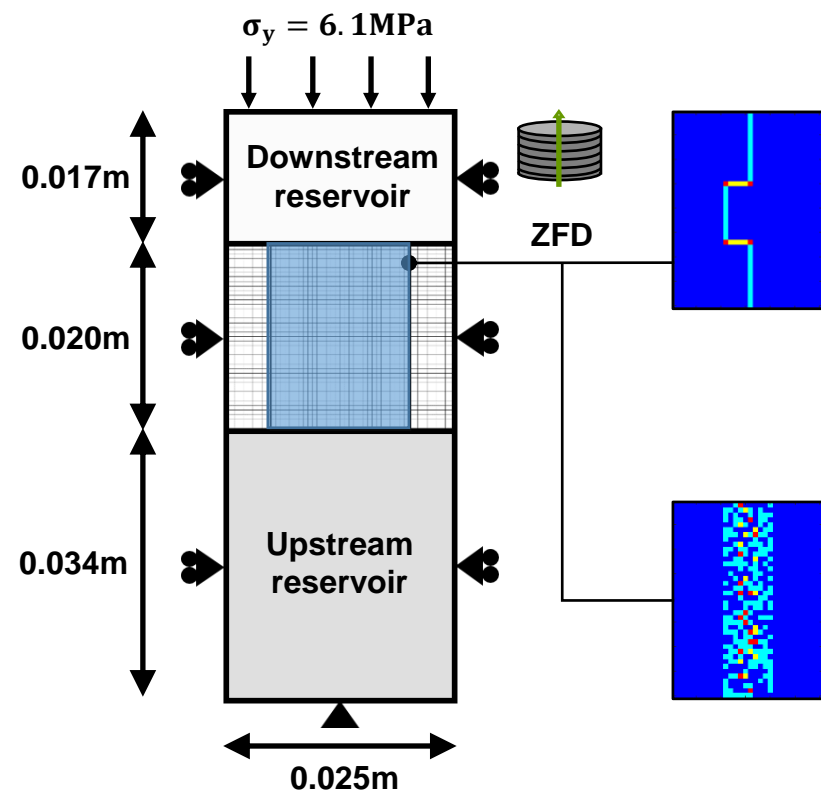
Pg at 100s.



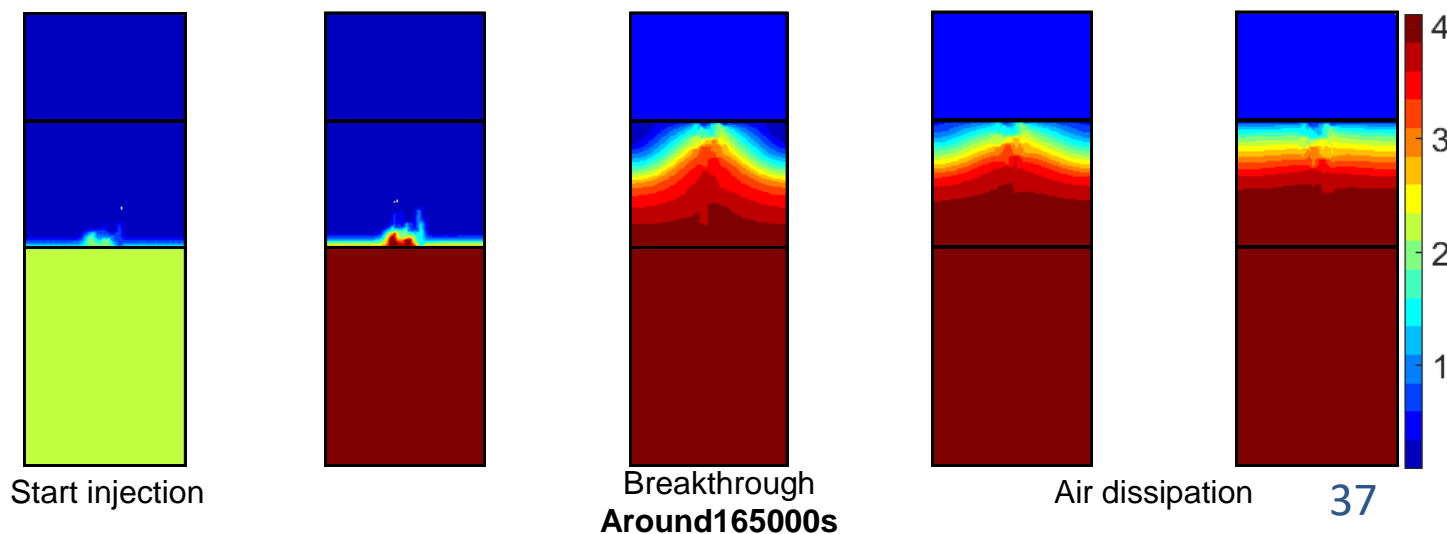
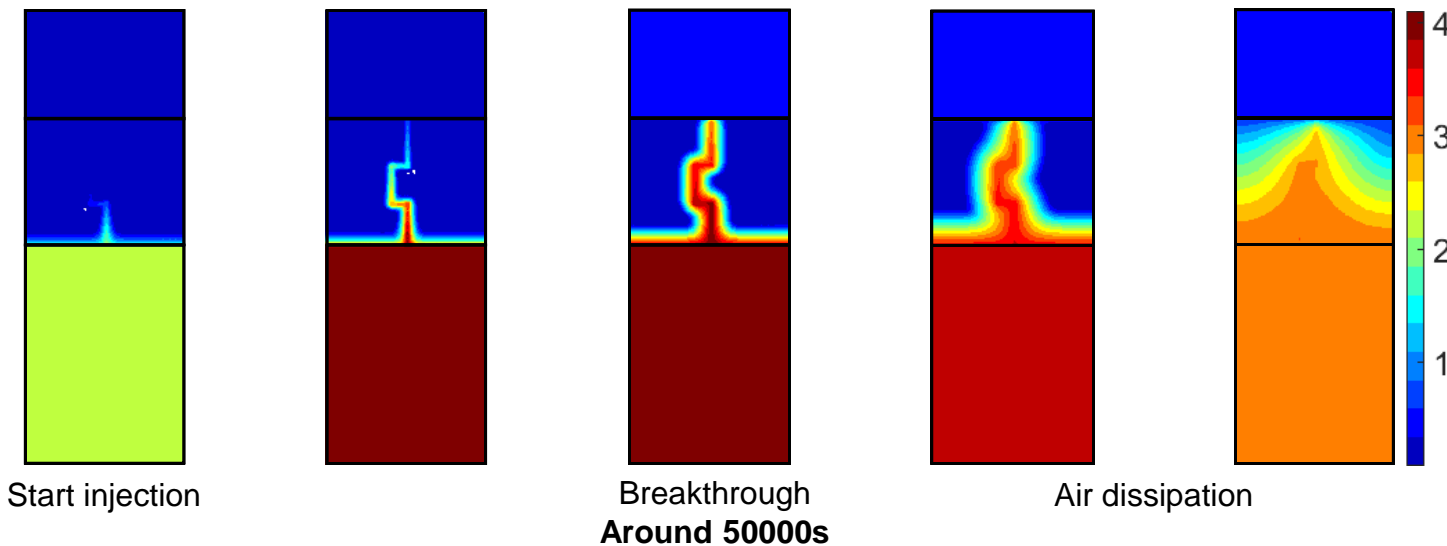
Gas injection experiment



Effect of the connectivity of the planes

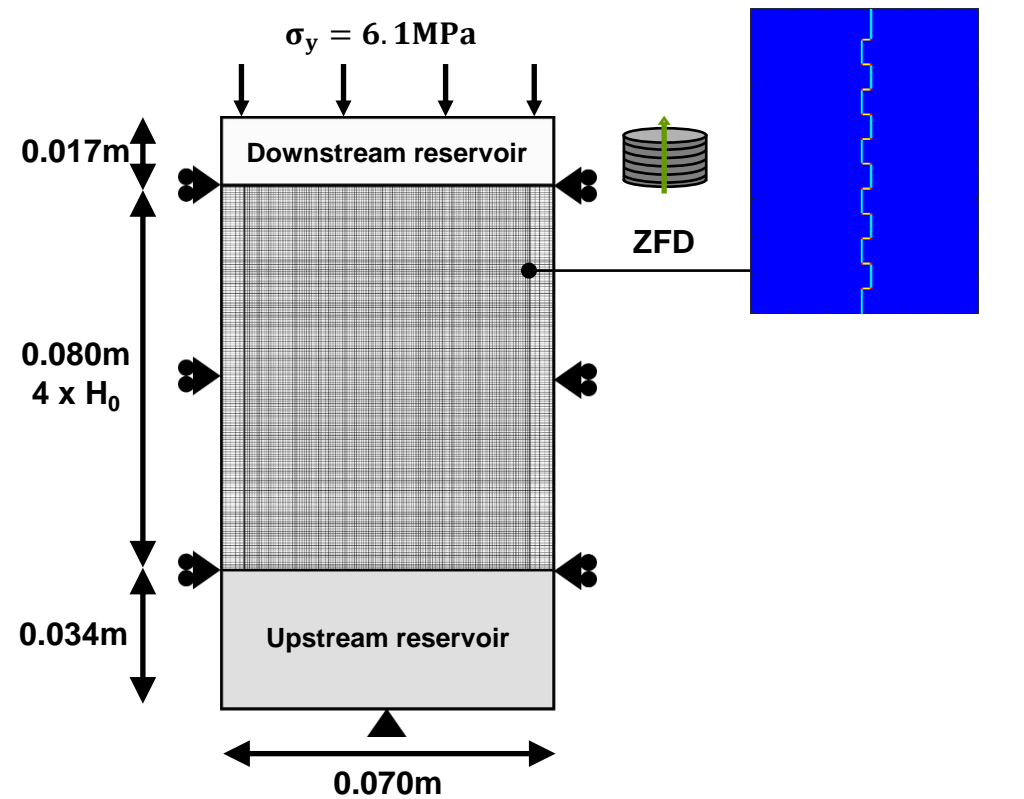


- Undisturbed Boom Clay
- Disturbed bridging planes
- Disturbed bedding and bridging planes
- Disturbed bedding planes



Gas injection experiment

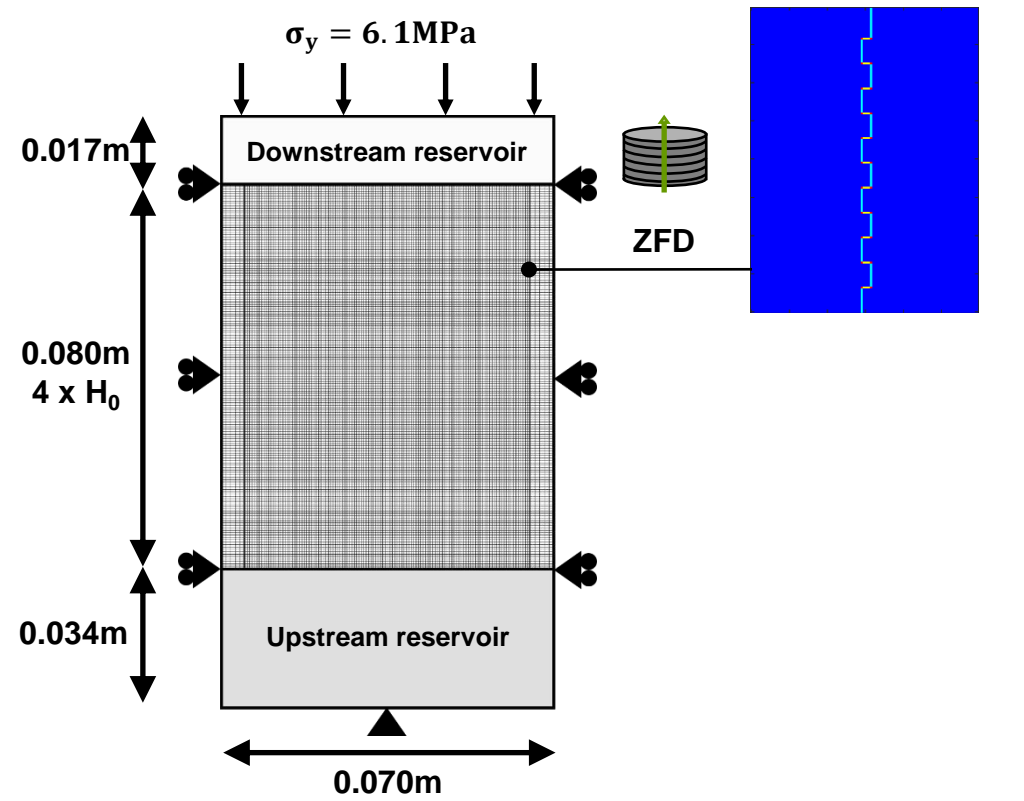
Effect of the connectivity of the planes under up-scaling



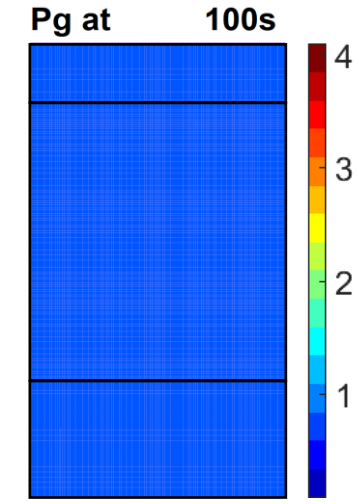
- Undisturbed Boom Clay
- Disturbed bridging planes
- Disturbed bedding and bridging planes
- Disturbed bedding planes

Gas injection experiment

Effect of the connectivity of the planes under up-scaling

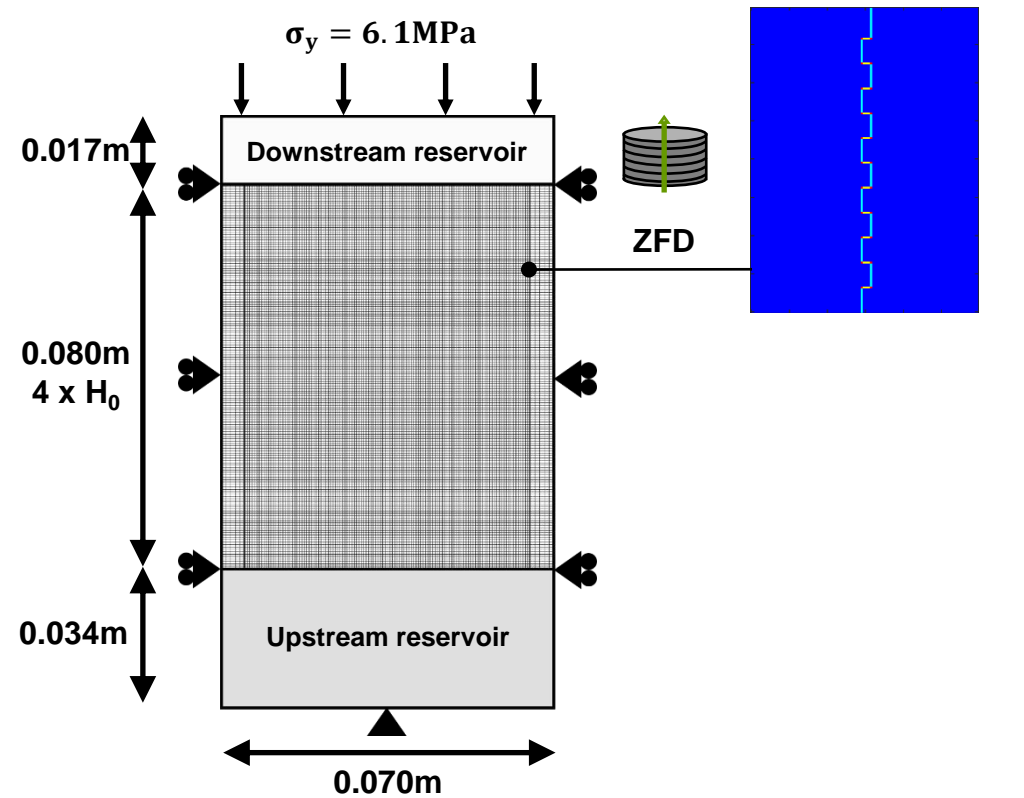


- Undisturbed Boom Clay
- Disturbed bridging planes
- Disturbed bedding and bridging planes
- Disturbed bedding planes



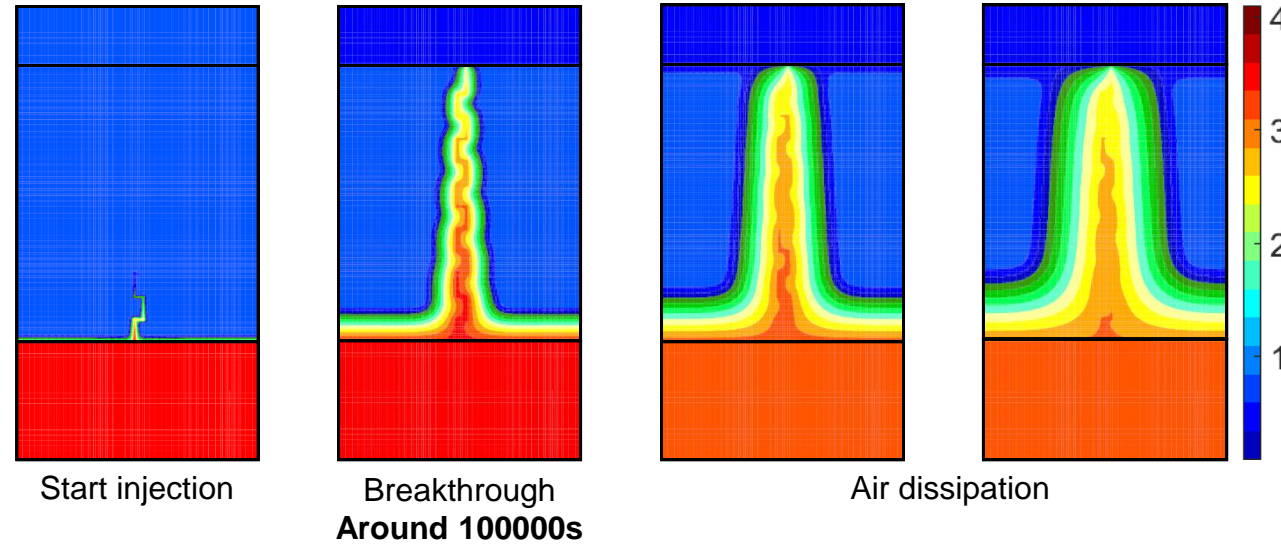
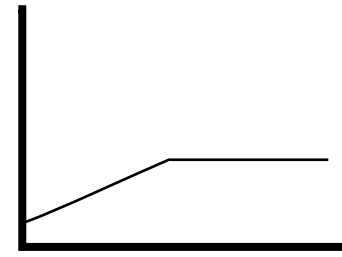
Gas injection experiment

Effect of the connectivity of the planes under up-scaling



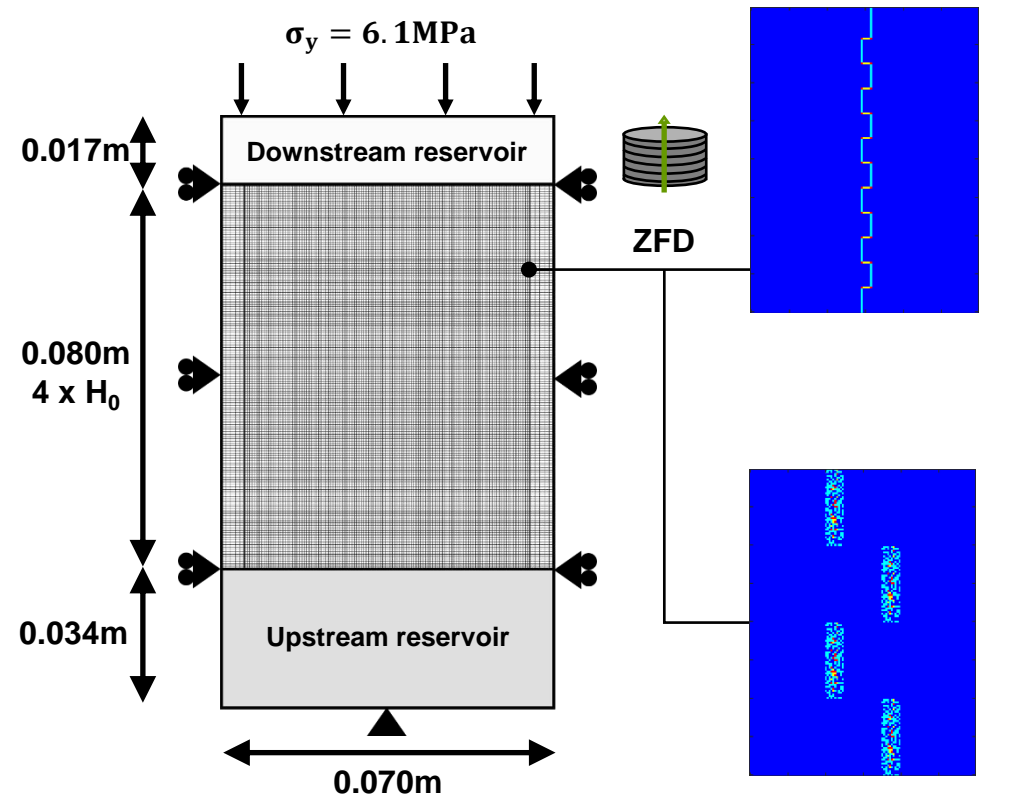
- Undisturbed Boom Clay
- Disturbed bridging planes
- Disturbed bedding and bridging planes
- Disturbed bedding planes

4.1



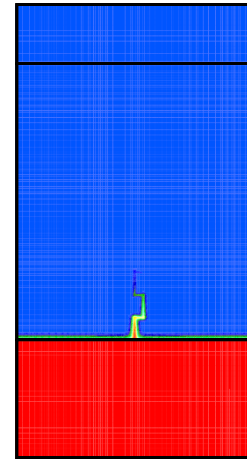
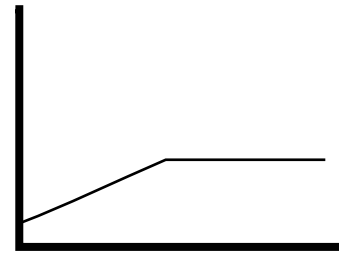
Gas injection experiment

Effect of the connectivity of the planes under up-scaling

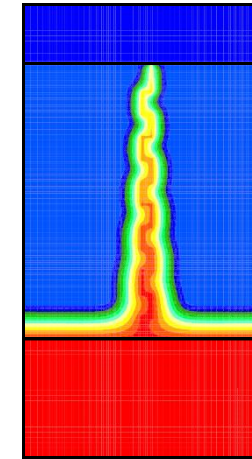


- Undisturbed Boom Clay
- Disturbed bridging planes
- Disturbed bedding and bridging planes
- Disturbed bedding planes

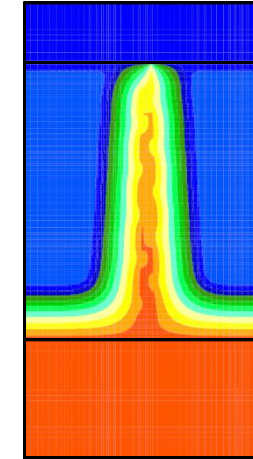
4.1



Start injection



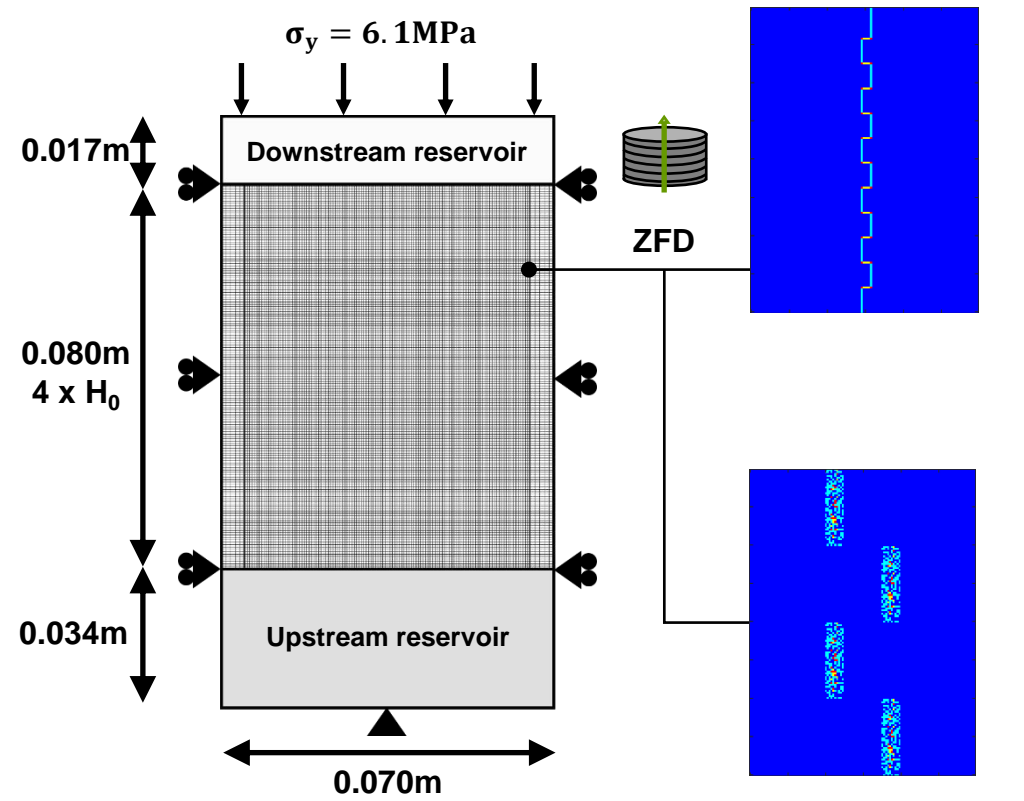
Breakthrough
Around 100000s



Air dissipation

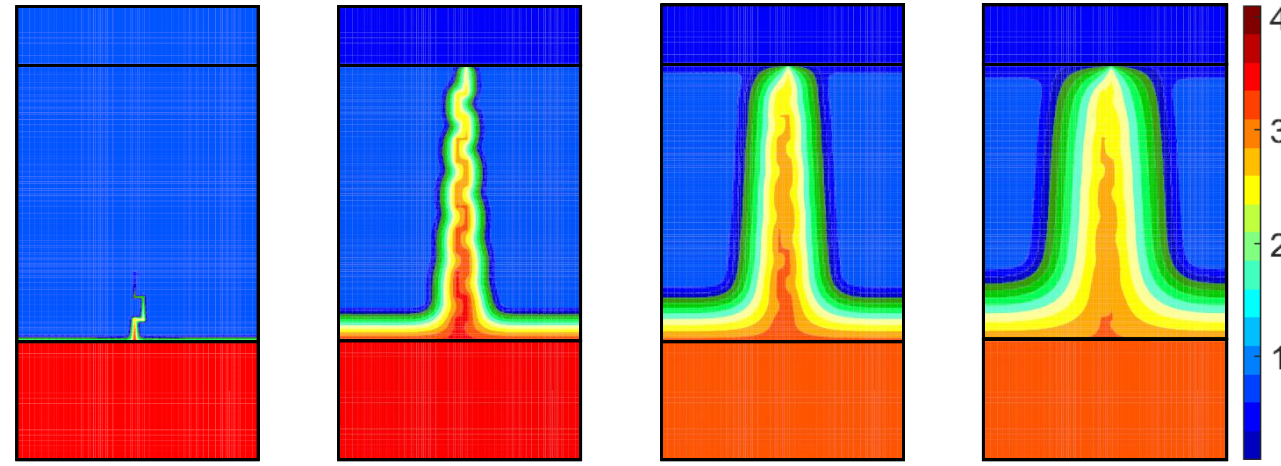
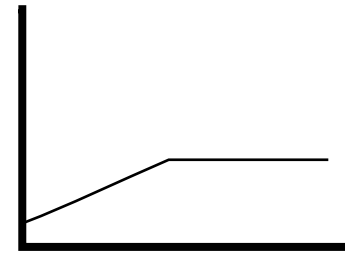
Gas injection experiment

Effect of the connectivity of the planes under up-scaling



- Undisturbed Boom Clay
- Disturbed bridging planes
- Disturbed bedding and bridging planes
- Disturbed bedding planes

4.1

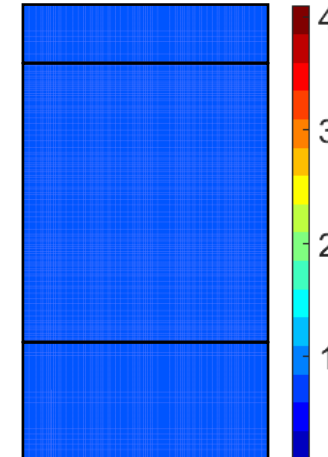


Start injection

Breakthrough
Around 100000s

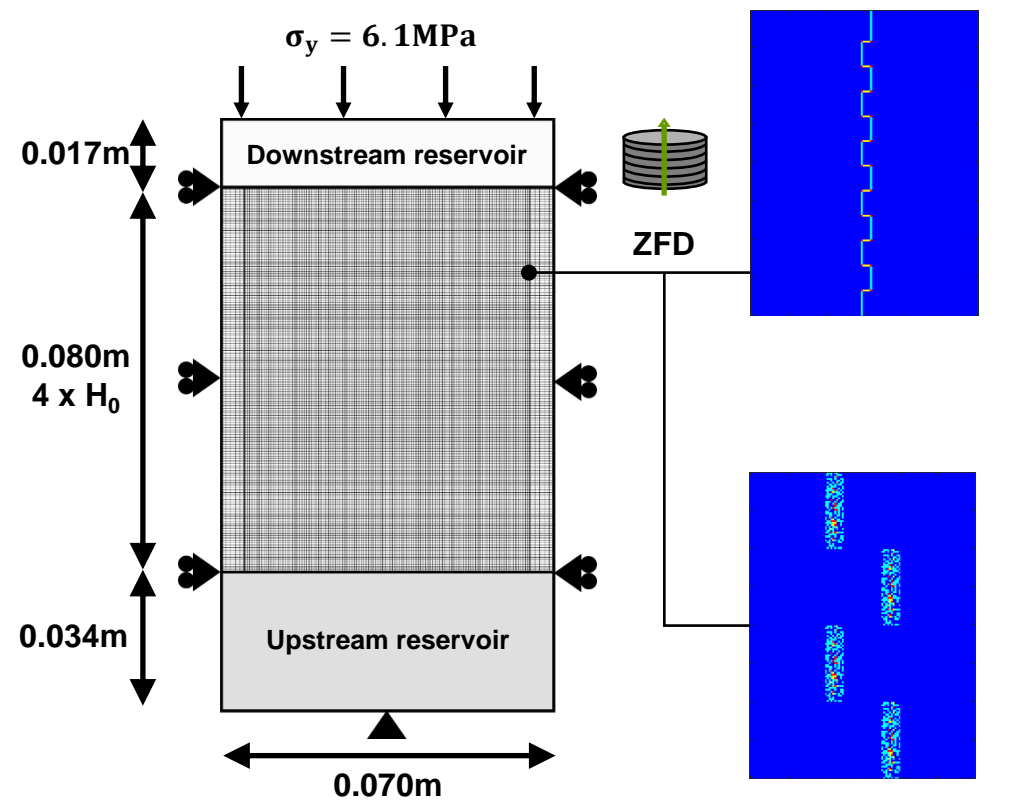
Air dissipation

Pg at 100s

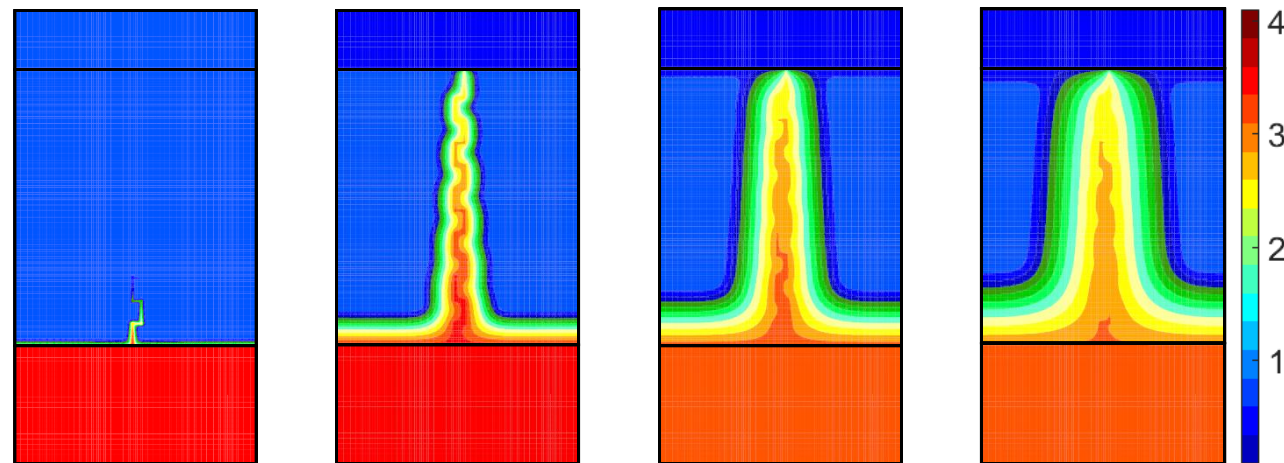
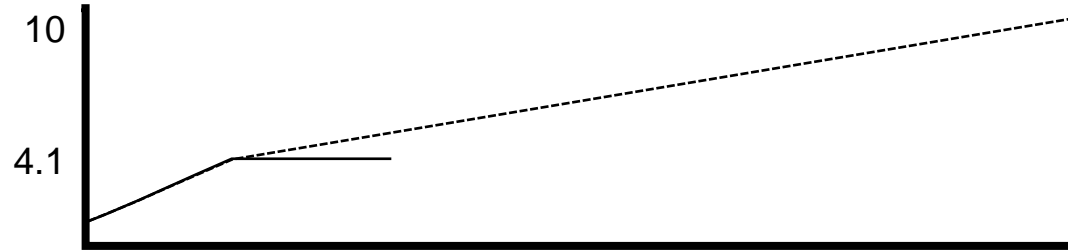


Gas injection experiment

Effect of the connectivity of the planes under up-scaling



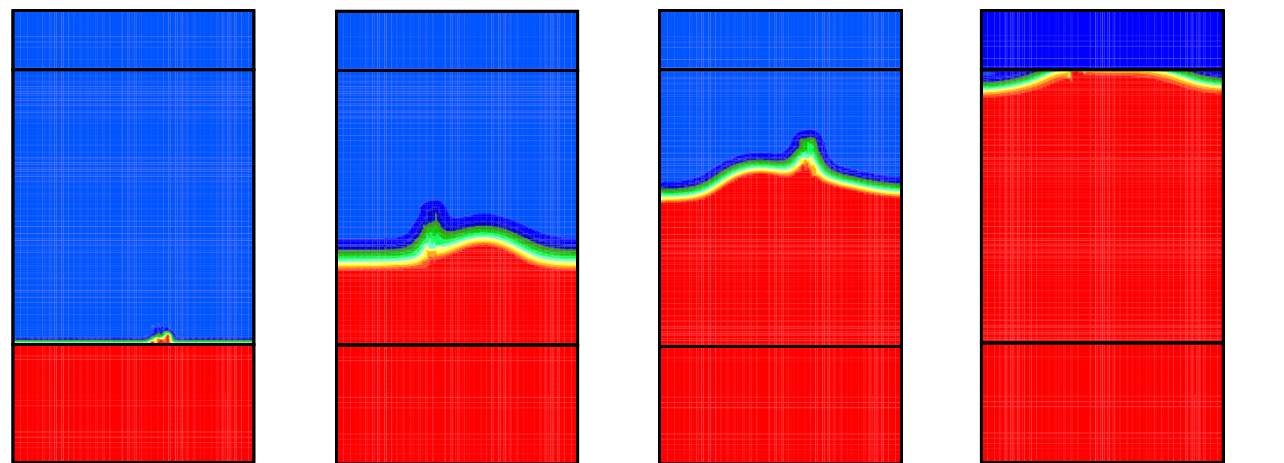
- Undisturbed Boom Clay
- Disturbed bridging planes
- Disturbed bedding and bridging planes
- Disturbed bedding planes



Start injection

Breakthrough
Around 100000s

Air dissipation



Start injection

Breakthrough
Around 325000s



Content

- ① Context
- ② From experimental evidence to modelling
- ③ Multi-scale modelling approach
- ④ Preliminary modelling
- ⑤ Modelling gas injection experiment
- ⑥ Conclusions

Conclusions

We **developed** a multi-scale model able to

1. Simply idealise the microstructure of the rock with fractures and tubes
2. Reproduce mechanisms inherent to gas migrations in sound rock layers

We **showed** that

1. Macro-pores, bedding planes and bridging planes play different roles in gas flows
2. Preferential flow paths can be generated through fractures with weaker properties
3. Different gas mechanisms occur in the presence of weaker bridging planes



Alert Geomaterials



Advanced multiphysics of geomaterials: multiscale approaches and heterogeneities

ALERT OZ / EURAD GAS & HITEC Summer School
28 August – 01 September 2023 • Liège (Belgium)

Pierre BÉSUELLE, Frédéric COLLIN,
Anne-Catherine DIEUDONNÉ, Sebastia OLIVELLA



The project leading to this application has received funding from the European Union's Horizon 2020 research and innovation programme under grant agreement n° 847593.